




REVIEW

[View Article Online](#)
[View Journal](#) | [View Issue](#)Cite this: *J. Mater. Chem. A*, 2019, 7, 22768Silica aerogel composites with embedded fibres:
a review on their preparation, properties and
applicationsTeresa Linhares, ^{ab} Maria T. Pessoa de Amorim ^b and Luisa Durães ^{*a}

Silica aerogels are among the lightest weight solid materials and exhibit other unique properties, in particular an outstanding insulation performance. However, these nanostructured highly porous materials show inherent brittleness that makes their processing and handling difficult and constrains their use in common daily applications. One of the most convincing and effective strategies to reinforce the silica aerogel structure is the manufacturing of aerogel composites with embedded fibres, which significantly contributes to widening their applications. This review encompasses a complete survey on scientific achievements related to silica aerogel composites reinforced with all types of fibres (natural, man-made, organic, inorganic and nanofibres), describing their synthesis approaches and properties. The influence of the embedment of different fibres on the final properties of the composites is thoroughly reported, considering their amount in the matrix and/or their specific characteristics, namely morphology, orientation and optical features. The applications linked to the fibre-reinforced silica aerogel composites are briefly addressed as well, evincing developments in typical functions of aerogels, as thermal and/or acoustic insulators and adsorbents, and also in emerging uses, for example as sensors or technical and protective apparel.

Received 8th May 2019
Accepted 19th September 2019

DOI: 10.1039/c9ta04811a

rsc.li/materials-a

1 Introduction

The aerogel was deemed as the ‘miracle material for the 21st century’¹ due to its highly porous structure, having a network of connected particles resembling a pearl necklace, with an air volume of 80–99.8%.² This unique layout imparts to aerogels the status of the lightest solid materials with the best insulation properties.^{3–7} Other important attributes of this new-generation material are its high specific surface area (100–1600 m² g^{−1}) and a very low refractive index (1.007–1.240).^{2,8}

Adsorbents of harmful compounds,^{9,10} sensors,¹¹ dielectric materials,¹² filtering media,¹³ Cherenkov detectors,¹⁴ kinetic energy absorbers,¹⁵ substrate for catalysts,¹⁶ carriers,¹⁷ extracting agents,^{18,19} protective clothing,²⁰ and even art sculptures²¹ are among the reported end-uses of silica aerogels. Undoubtedly, thermal and acoustic insulation are the most significant applications of silica aerogels,^{22,23} with profuse and detailed published studies.^{24–29}

In spite of the unique properties provided by the nanoscale porosity, the use of silica aerogels in common daily applications has been constrained, mainly due to their inherent brittleness that makes processing and handling difficult.^{30–33} Other intrinsic

drawbacks, such as dust release,^{22,34,35} hydrophilicity,^{9,33,35} volumetric shrinkage,^{30,36,37} time for processing,^{38–41} and ultimately, the prohibitive cost of silica aerogels^{9,34,42,43} (8–20 fold more costly than polyurethane foams),⁵ need to be overcome, in order to broaden the applicability of such auspicious materials.

Strategies for reinforcement of silica aerogels are an effervescent topic of scientific research, either through the use of appropriate additives or by fine-tuning the synthesis conditions.^{44,45} The manufacturing of silica aerogel composites with embedded fibres is one of the most effective techniques to widen their applications.^{37,46–48} However, in terms of scientific reviews, there is a small number of publications on this topic, and generally each review covers a specific type of fibre or nanofibre.^{49–53}

This work intends to highlight the achievements of scientific research on silica-aerogel matrices with all types of fibres, presenting their properties and discussing strategies to encourage their common daily applications. The effect on aerogel composite properties of some parameters related to the fibres (morphology, orientation, amount, and thermal resistance) is analysed. The applications linked to the fibre-reinforced aerogel composites are also briefly addressed.

2 Brief description of silica aerogels:
synthesis and properties

Silica aerogels are synthesised through sol-gel chemistry, defined by IUPAC⁵⁴ as the “Process through which a network is

^aCIEPQPF, Department of Chemical Engineering, University of Coimbra, 3030-790 Coimbra, Portugal. E-mail: luisa@eq.uc.pt; Fax: +351 239798703; Tel: +351 239798737

^b2C2T, Center of Science and Textile Technology of the University of Minho, Campus de Azurém, 4800-058 Guimarães, Portugal

formed from solution by a progressive change of liquid precursor(s) into a sol, to a gel, and in most cases finally to a dry network". The precursors can be either inorganic metal salts or metal alkoxides, but the relatively easy chemistry and versatility of silicon alkoxides make them the most used precursors in sol-gel chemistry of silica,⁵⁵ for example tetramethyl orthosilicate (TMOS) or tetraethyl orthosilicate (TEOS). TMOS is more reactive than TEOS, but the higher price and the associated health hazards of TMOS turned TEOS the most common precursor among silanes.^{6,56,57} The detailed mechanisms of silica aerogel synthesis are widely described in the available literature.^{58–62}

Table 1 summarises the typical properties of monolithic silica aerogels. However, each modified aerogel is unique,⁶³ with specific properties related to the synthesis conditions and used precursors.

2.1 Hydrolysis and condensation/gelation

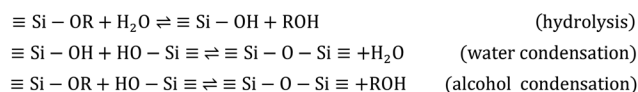
Sol-gel structures start from the hydrolysis of precursors and subsequent condensation into primary particles, evolving through the developing solution, and aggregating to form larger secondary particles, which link in a continuous network with liquid in the interstices.⁵¹

The sol-gel chemical reactions can be summarised according to Scheme 1, where hydrolysis and condensation occur in a parallel way.

The primary particles have diameters less than 2 nm and the secondary particles feature diameters around 10 nm or more. Gelation starts to occur when secondary particles link to each other, resulting in neck-regions between them, and a mesoporous network.^{44,51} These structures are shown in Fig. 1.

The pH value is a decisive parameter for the relative rates of hydrolysis and condensation of alkoxysilanes, as outlined in Fig. 2, for precursors of the type Si(OR)₄. The condensation reaches the minimum rate around pH 1–3, since the isoelectric point of silica is achieved at pH 2, and thus the electrical mobility of silica particles is minimum.^{59,64}

Under acidic conditions, the hydrolysis reaction occurs at higher rate and the condensation/gelation is the rate-determining step, favouring the simultaneous formation of small oligomers with reactive Si–OH groups. This leads to



Scheme 1 Chemical reactions in the sol-gel process of alkoxysilanes.

a polymer-like gel, made from chains with few branches,^{2,64} which are weakly cross-linked, and it easily loses its shape and tends to crush, as the chains impinge on one another due to internal movements. Hence, denser aerogels with small pores are obtained after acid catalysed synthesis.⁷¹ Under acidic conditions the hydrolytic reactions are favoured by proton donors, which readily attack the oxygen atoms due to their partial negative charge, while in a basic medium the slow hydrolysis reaction is the rate-determining step.^{2,58} Under alkaline conditions condensation is faster, due to the slightly positive charge of Si atoms in the presence of proton acceptors,⁵⁸ and the hydrolysed species are readily consumed into larger and denser colloidal silica particles.^{2,58} Such structures are more prone to prevent network dragging and crushing caused by internal pressure, yielding lighter aerogels with higher pore volume.⁷¹

In summary, the porosity of silica aerogels can be tailored through the balance between the hydrolysis and condensation rates, by adjusting the initial pH according to a specific precursor.⁷² As an example, silica aerogel density can be so different as 150 kg m^{−3} or 500 kg m^{−3}, depending on synthesis conditions, respectively, in a basic or acidic medium.⁷³

The gelation or gel point is attained when a continuous network is formed, and the solution no longer flows under the effect of gravity.

2.2 Ageing

Chemical reactions of sol-gel chemistry still exist even after the gel point has been reached. The liquid inside the pores contains small particles, which are able to condense, as well as wandering monomers that will join the network.^{2,74} That continuous process of cross-linking and coarsening due to the additional condensation is the so-called ageing.^{75,76}

Table 1 Typical properties (range of values) of silica aerogels

Property	Units	Range values	References
Bulk density (ρ_b)	kg m ^{−3}	3–500	Hüsing and Schubert; ² Kocon <i>et al.</i> ⁶⁶
Skeletal density	kg m ^{−3}	1700–2100	Hüsing and Schubert ²
Mean pore diameter	nm	10–150	Hüsing and Schubert; ² Han ⁶³
Porosity	%	80–99.8	Hüsing and Schubert; ² Anderson and Carroll ⁶⁷
Specific surface area	m ² g ^{−1}	200–1600	Hüsing and Schubert; ² Boday <i>et al.</i> ⁶⁸
Thermal conductivity (at 25 °C)	mW m ^{−1} K ^{−1}	12–30	Han; ⁶³ Lu <i>et al.</i> ⁶⁹
Refractive index	—	1.01–1.24	Hüsing and Schubert; ² Pierre and Rigacci ⁴
Young's modulus	MPa	0.01–100	Hüsing and Schubert; ² Han ⁶³
Poisson's ratio	—	0.2	Han ⁶³
Sound velocity	m s ^{−1}	20–1300	Han; ⁶³ Groß <i>et al.</i> ⁷⁰

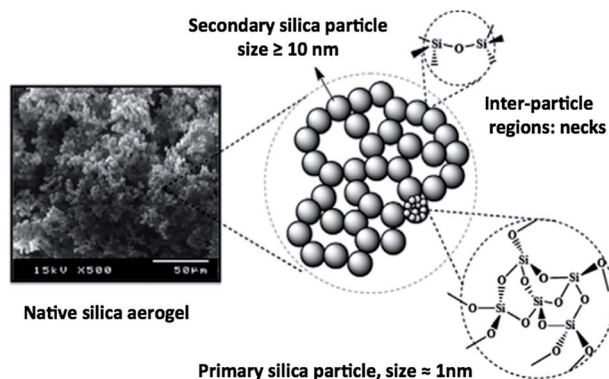


Fig. 1 SEM image of a native silica aerogel with the schematic representation of primary and secondary particles (reprinted from ref. 44, copyright 2014, with permission from Elsevier).

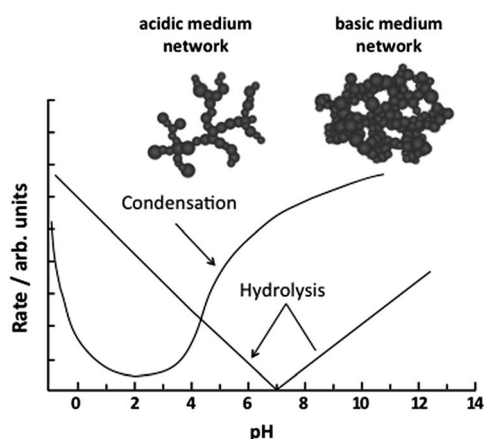


Fig. 2 Rate of hydrolysis and condensation reactions of tetraalkoxysilanes with regard to pH dependency (adapted and reprinted with permission from Springer Nature: Springer-Verlag, Chemistry Spectroscopy and Applications of Sol-Gel Glasses, from ref. 65, copyright 1992).

Ostwald ripening refers to the phenomenon occurring at the micro level during ageing, in which the existing small particles with unreacted sites (OH moieties) tend to dissolve and reprecipitate into larger particles, or condense into more favourable regions of secondary particles, such as pores or crevices, particularly in the necks between them.^{2,77} The micro-level condensation leads to additional stiffness of the gels, which causes contraction of the network and withdrawal of some solvent from the pores; this dimensional change is called syneresis.⁷⁸

The ageing, occurring at pH between 8 and 12, will determine the extent of shrinkage at the drying stage.⁷⁹ A silica matrix strengthened by adequate ageing will better resist the drying capillary pressures,⁷⁹ allowing an improvement of approximately 2-fold in the modulus of elasticity.⁴⁴

2.3 Drying

The ultimate goal of the sol-gel drying process relies on the solvent removal from the matrix by maintaining the gel network, yielding a porous solid with unchanged volume and shape.⁸⁰

During drying, there are two major factors affecting the shape of the solid porous structure of the gel. The first relates to the almost inevitable partial collapse of the network, as even the smallest shrinkage in the interior of the gel body causes a pressure gradient that results in cracks; second, the pore dimensions are different throughout the network, and hence neighbouring pores with different radii show different receding rates of menisci (faster on bigger pores). Thus, the walls between pores of different dimensions endure uneven levels of stress and therefore tend to crack due to the unbalanced forces.^{75,81}

There are several drying techniques, namely, supercritical drying (SCD), freeze-drying, and ambient pressure drying (APD). Along with the gel's composition, the drying of the gels dictates pore dimensions and their overall textural properties, and thus the chosen method is of high relevance.^{80,82} While fibre-reinforced aerogels can be dried under ambient pressure with good results, native silica aerogels are prone to collapse and lose their monolithic shape.⁸³ In fact, the embedded fibres act as a supporting skeleton, preventing the aerogels' shrinkage caused by the drying capillary pressures.^{37,47}

Table 2 highlights the influence of drying conditions on the characteristics of silica aerogels: for a similar fraction of embedded fibres, SCD favours lighter materials (~ 3 to 11%).^{83,84}

APD can be tuned to be a suitable cost-effective alternative: for example, the volume shrinkage of silica aerogel composites reinforced with a micro-glass fibre mat was reduced from $\approx 62\%$ to $\approx 22\%$, following a gradient multi-segment drying process after a surface treatment,⁸⁵ as described in Table 2.

All the composites listed in Table 2 exhibit characteristics of super-insulating materials, designated as such when the thermal conductivity is inferior to $20 \text{ mW m}^{-1} \text{ K}^{-1}$, measured at standard pressure and temperature.⁸⁶

2.3.1 Supercritical drying. SCD is the ideal method for drying the gels, in order to obtain aerogels with lower density.⁸⁷ The technique consists of removing the solvent inside the pores under supercritical conditions in order to avoid capillary pressures, since the liquid-gas interface is suppressed. Therefore, the change in the dimensions of silica gels subjected to supercritical drying is mainly due to the ageing stage.⁸³ The main disadvantages of SCD are the high complexity of the equipment required to operate at high pressure and the significant cost of the process.^{9,39,41–43,46}

In supercritical approaches, the solvent can be removed by two different procedures: (i) the high-temperature supercritical drying, in which the synthesis solvent is vented after surpassing its critical point (first introduced by Kistler in 1931⁸⁸); and (ii) the low-temperature supercritical drying, in which the synthesis solvent is exchanged with a suitable and soluble solvent system, generally supercritical CO_2 (introduced by Tewari *et al.*⁸⁹ in 1985). Since CO_2 features a mild critical point (31.1°C and 73.9 bar ⁹⁰), it is often used for exchanging the synthesis solvent in the pores or dissolving it, allowing SCD to be conducted at low temperature. In this way, the main advantages of SCD in terms of lack of capillary pressures are maintained,⁸⁰ also providing the possibility of drying organic-inorganic matrices without degradation.⁹¹ Yet, solvent exchange can be a rather lengthy process, since it depends on the size of the gel.⁹² So, studies

Table 2 The influence of drying techniques on the final characteristics of silica aerogel composites (obtained from TEOS⁸⁵ and polyethoxydisiloxane (PEDS), a TEOS pre-polymerized solution^{83,84})

Reinforcement	Surface treatment	Drying technique	Volume shrinkage (%)	ρ_b (kg m ⁻³)	Thermal conductivity (mW m ⁻¹ K ⁻¹)	References
Microglass matting, with fibres of 2–4 μ m diameter (9.1 volume%)	HMDZ/ <i>n</i> -hexane (at 50 °C)	APD (five alternatives)	(a) 62.2	(a) 248	(a) —	Jiang <i>et al.</i> ⁸⁵
		(a) 100 °C, 24 h	(b) 55.3	(b) 219	(b) —	
		(b) 50 °C, 5 h + 80 °C, 24 h	(c) 38.3	(c) 171	(c) —	
		(c) 50 °C, 5 h + 100 °C, 24 h	(d) 26.3	(d) 138	(d) —	
		(d) 50 °C, 5 h + 180 °C, 8 h	(e) 22.4	(e) 129	(e) 13 (at 200 °C)	
Tencel® (25 wt%)	HMDZ	(e) 50 °C, 8 h + 80 °C, 8 h + 100 °C, 24 h + 180 °C, 8 h	10	125	17.5 (at \approx 20 °C)	Markevicius <i>et al.</i> ⁸³
		APD	7	121	16.6 (at \approx 20 °C)	
None	HMDZ	APD	Collapsed	—	—	Martinez <i>et al.</i> ⁸⁴
Polyethylene terephthalate (PET) blanket (unknown fraction)	HMDSO	CO ₂ SCD	19	101	14.1 (at \approx 20 °C)	
		APD	3.2	114	16.0 (at \approx 22 °C)	
		CO ₂ SCD	2.3	100	13.9 (at \approx 22 °C)	

were carried out on the development of methods to reduce the time for aerogel manufacturing, based on rapid supercritical extraction. This process (which includes gelation, ageing and drying), carried out in moulds at high-temperature and pressure, yielded aerogels within hours (<5 hours) rather than days.^{93,94} Aerogels with superior mechanical properties were produced, displaying a 3-fold higher elastic modulus compared to the low-temperature SCD aerogels.⁹³ However, this method has a significant impact on the reaction kinetics, leading to the formation of bigger silica particles, with larger necks and, thus, with low specific surface area.^{93,95}

2.3.2 Freeze-drying. Under reduced pressure and temperature, a solvent can be evacuated by lyophilisation, avoiding the liquid-phase meniscus stresses. By a fast freezing of the solvent, using liquid nitrogen, followed by its sublimation under vacuum, it is possible to avoid the skeleton's shrinkage and, consequently, obtain highly porous aerogels.^{25,80} The process is commonly applied to drying hydrogels,⁹⁶ since the solidification of water is more readily accessible than for usual organic solvents.

The lyophilisation cycle encompasses three steps: (a) lowering the temperature of the solvent (inside the pores) below its triple point; (b) evacuation of the system until vacuum; and (c) controlled sublimation under isobaric conditions.⁸⁰ The process is prone to the formation of microcrystalline salt-like structures within the samples, since micro-regions with differences in freezing and sublimation rates can appear.^{80,95} As a result, pore size tends to be augmented, compared to the case of SCD.⁹⁵

Clay based aerogels are generally dried by freeze-drying. It is generally accepted that, during the drying process, a rearrangement of clay layered sheets occurs which leads to lightweight aerogels.^{97,98} This kind of material fulfills the needed features of flame retardant materials.^{99–101}

2.3.3 Ambient pressure drying. The simple evaporation at ambient pressure seems to be the most obvious method to remove the solvent from a porous material, by raising the temperature above the solvent's boiling point and turning it into a gas – this is the basic principle of APD.⁸⁰

The solvent within the system coexists in three states: the liquid filling the pores, the liquid–gas transition phase, and the gas phase. The receding menisci in the pores induce high capillary pressures, reaching hundreds of bars within the nanopores, and cause cracks in the structure.⁸⁰ Often there is a loss of the monolithic shape, when capillary pressures during drying surpass the elastic limit of the solid structure, generating granular aerogels.^{43,83} This is particularly significant with pore sizes smaller than 80 nm. The term “xerogel” defines a shrunken gel. Indeed, APD usually generates xerogels, either in the granular form or as impregnated composites (such as mats or blankets).⁸⁰ The volume of the xerogel is reduced by a factor of 5–10, compared to the dimensions of the gel.¹⁰²

2.4 Strategies to minimize APD shrinkage

APD is an advantageous drying technique when taking into account the involved costs, the low hazard levels and suitability for large-scale commercial applications.^{46,103,104}

In order to prevent irreversible densification or partial collapse due to stresses generated by capillary pressures, the preparation of aerogel-like APD materials requires specific adaptations, consisting of both chemical surface modification and skeleton strengthening.^{37,80}

The condensation of reactive groups in the network surface, mainly Si–OH, causes a gradual shrinkage that leads to the ensuing densification. Those reactions can be prevented after a surface treatment, carried out with reactive alkylsilane compounds, with non-hydrolysable Si–R alkyl groups,^{12,80,105,106} as is the case of HMDZ (hexamethyldisilazane) or HMDSO (hexamethyldisiloxane) (*vide* Table 2).

An increased concentration of hydrophobic moieties directly attached to the silicon atom, such as methyl groups, can lead to reversible shrinkage, the so-called ‘spring back’ effect.^{107–109} It consists of a mechanical expansion of the gel network, which recovers almost to its original volume, as can be seen in Fig. 3. The phenomenon occurs during the last stage of the drying, when the porous structure is able to endure the drying loads, and the spring-back effect is driven by the repelling of hydrophobic functional groups.^{43,109}

The use of precursors with hydrophobic character, such as methyltrimethoxysilane (MTMS), with a non-hydrolysable methyl group, also prevents the collapse of gels during drying and imparts higher flexibility to the matrices.^{35,107}

Hybridization, through the incorporation of polymers in the silica backbone, is another technique of aerogel reinforcement that prevents shrinkage. It consists in the cross-linking of the network by adding monomers (*e.g.*, acrylates and cyanates), leading to increased flexibility and/or mechanical strength of the hybrid material.^{44,110–115} These aerogels are often termed X-aerogels.^{116,117} However, as a consequence of the effective mass addition, the cross-linked gels tend to feature lower porosity, a detrimental outcome that leads to higher density materials, and a decrease of surface area,¹¹⁸ along with the inevitable penalization of the thermal conductivity.¹¹⁵

Another strategy consists in operating with drying control chemical additives, such as glycerol, formamide, dimethyl formamide, or tetramethyl ammonium hydroxide, added during the initial phase of silica gel synthesis. Their function is to promote the uniformity of pore size dimensions, thus minimizing stress asymmetries.⁸⁰

Finally, the embedment of fibres and nanofibres is recognized as an effective method of strengthening silica aerogels,^{46,119–121} since the monolithic shape is preserved due to fibres, in spite of the inevitable fractures (both at micro and macro levels) occurring during evaporative drying.⁸³

The shrinkage and strengthening of wet gels have been, for a long time, a widely researched topic.^{30,44,51,59,122,123} For more details, the pioneering investigation of Phalippou *et al.*,¹²³ the NASA Tech Brief of Paik and colleagues³⁰ and the review work of Maleki and co-workers⁴⁴ are a convenient basis.

2.5 Insulation properties of silica aerogels

The extremely low thermal conductivity and the inorganic nature (non-combustible) of silica aerogels turned them into ideal substitutes for traditional insulating materials, such as polystyrene or polyurethane foams.^{124–127} Currently, rock wool and glass wool are commonly used, and despite their inorganic nature, higher insulation performances are only achieved after increased thickness.^{127,128} Fig. 4 depicts the typical values of thermal conductivity of some insulating materials, along with those for the free air and an aerogel. Additionally, other important aspects have to be considered: while aerogel based thermal insulation materials require less than half of the thickness, when compared to other inorganic-based materials or polymeric foams, aerogels are much more expensive, around 8–9 times more expensive than conventional materials.¹¹⁵

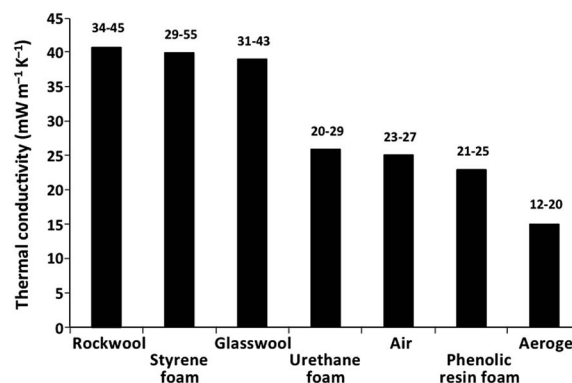


Fig. 4 Average and limit values of thermal conductivity for conventional insulating materials, free air and a silica aerogel (data summarised from ref. 139–141).



Fig. 3 Silica aerogel composites synthesised with polymethylsilsesquioxane precursors and dispersed boehmite nanofibres, under ambient pressure drying conditions: a temporal shrinkage followed by re-expansion can be observed, due to the spring-back effect (reprinted with permission from ref. 138. Copyright 2016, American Chemical Society).

According to a study sponsored by the European Commission, the use of aerogels as building insulation materials was estimated to reduce 30% of overall energy consumption and 25% of CO₂ emissions, yet providing the same comfort level.¹²⁹ Moreover, silica is the most abundant compound on the Earth¹³⁰ and the current environmental issues, such as limited energy resources,¹³¹ emphasize the aerogel application. These materials, being amorphous, have no hazardous effect either for human health or to the ecosystems.^{124,132}

Heat transfer in monolithic non-evacuated aerogels involves three components,^{131,133,134} since the convection heat transfer can be neglected in porous materials where void spaces are smaller than 4 mm.^{135,136} Thus, the total thermal conductivity can be described using eqn (1).

$$k_T = k_s + k_g + k_r \quad (1)$$

where k_T is the total thermal conductivity and k_s , k_g , and k_r refer, respectively, to the solid, gaseous and radiative transfer components of the first.

Aerogels, with a significant fraction of small pores, have also a tortuous silica structure, which minimises both the gaseous and solid conductivities. As an example, an aerogel with a density of 40 kg m⁻³, with *circa* 50% pores over 20 nm in diameter, typically exhibits a thermal conductivity of 18 mW m⁻¹ K⁻¹ at ambient pressure; a denser silica aerogel (*circa* 100 kg m⁻³), with 80% pores with a diameter below 20 nm, displays superior thermal insulation performance, namely 12 mW m⁻¹ K⁻¹ at ambient pressure.⁷⁹ Fricke and colleagues¹³⁷ first established relationships between silica aerogels' bulk density, ρ_b , and the three components of thermal conductivity (eqn (2)–(4)), by varying aerogel density between 70 and 230 kg m⁻³, as follows:

$$k_s \propto \rho_b^{1.5} \quad (2)$$

$$k_g \propto \rho_b^{-0.6} \quad (3)$$

$$k_r \propto (\rho_b e)^{-1} \quad (4)$$

where e is the spectral mass attenuation coefficient, an optical property related to the efficiency of a material to attenuate infrared radiation (IR).¹⁴²

The specific surface area (SSA) of silica aerogels is also useful as an indicator of the thermal insulation performance of aerogels. For a given density, the smaller the size of the pores, the higher the SSA, and the better will be the insulation performance. This evidence was described by Wei *et al.*:¹³⁶ a silica aerogel with a density of 120 kg m⁻³ and a surface area of 400 m² g⁻¹ displayed a thermal conductivity of 20.1 mW m⁻¹ K⁻¹; by increasing the SSA to 1000 m² g⁻¹, the thermal conductivity was reduced to 13.7 mW m⁻¹ K⁻¹. Since the SSA is more easily assessed than the pore size distribution of the aerogels, SSA may be a valuable parameter in this context.

The solid thermal conductivity relates to the solid fraction of aerogels, *i.e.*, it is influenced by the extent of crosslinking and network connectivity.^{133,134} Heat conduction in the solid network occurs through the atomic lattice, due to the excitation

of vibrational energy levels of interatomic bonds or even by free electron transport under thermal gradient.^{143,144}

Heat conduction in the gaseous state exists due to the collisions between molecules, since the faster ones transfer part of their kinetic energy to the slower molecules.¹⁴⁴ However, those movements are of minor relevance in the monolithic native silica aerogels, since the average pore dimensions are typically below 70 nm,¹³³ and the mean free path of air molecules at 1 atm and 23 °C is around 66 nm.¹⁴⁵ The Knudsen effect describes the reduced diffusivity directly linked to the pore dimensions, when each gas molecule collides more frequently with the pore walls than with neighbouring molecules,^{146,147} leading to a reduced energy transfer through the gas molecules.¹⁴⁷

The radiative thermal conductivity relates mainly to the spectral mass attenuation coefficient, e . While the solid and gaseous thermal conduction requires a medium, the radiative thermal conductivity is based on electromagnetic waves, correlated to the photon's mean free path.¹⁴⁸ Therefore, this component is highly temperature-dependent, with a high factor-scaling exponent.¹⁴⁴ According to Fomitchev *et al.*,³ the radiative thermal conductivity of silica aerogels can be computed according to eqn (5):

$$k_r = 16n^2\sigma T^3\varepsilon^{-1} \quad (5)$$

where n is the index of refraction, σ is the Stefan–Boltzmann constant, T is the temperature (K) and $\varepsilon = \rho_b e$, the spectral attenuation coefficient.

Silica aerogels display poor absorptive properties in the near-infrared region, particularly below the wavelength 5–8 μ m.^{124,149} With a rise in temperature from 300 to 1000 K, the radiative thermal conductivity can lead to an increase from 8 to 92% of the total conductivity of native silica aerogels.¹⁵⁰

All the heat conductivity mechanisms within aerogels are sketched out in Fig. 5.

2.6 Mechanical properties of silica aerogels

The mechanical behaviour of native silica aerogels can be understood according to a proportionality that relates the Young's modulus, E , with material's bulk density, ρ_b ,⁶⁵ described using eqn (6).

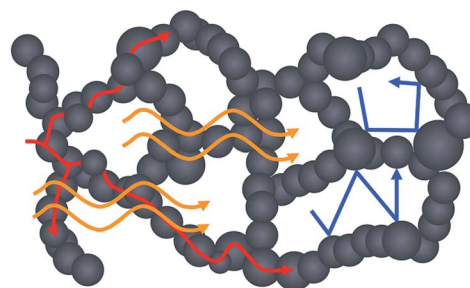


Fig. 5 Different mechanisms of heat transfer in aerogels: solid conduction through the particle's chain (red arrows); radiative conduction (wavy yellow arrows); and gaseous thermal conduction (blue arrows) (colours online).

$$E \propto \rho_b^\beta, \beta \approx 3.2 \dots 3.8 \quad (6)$$

The manufacture technique is somehow relevant, since aerogels synthesised under neutral or mild acidic conditions can be twice stiffer compared to similar density aerogels developed under basic conditions. Suitable ageing and heat treatments can also improve aerogel strength.⁶⁵ Nevertheless, even after optimizing synthesis conditions, silica aerogels are brittle materials, with a friable nature derived from their ionic-covalent bonds and high porosity.^{80,151}

Mechanical characterization of native aerogels is often a difficult task, either in terms of the specimen preparation or precisely measuring the small load forces applied.^{63,117} Therefore, the evaluation is typically performed in compression and flexural modes.^{80,117} Moreover, the tensile strength of aerogels can be deduced from the three-point bending flexural test.¹¹⁷

The compressive response behaviour of aerogels can be quite diverse: at higher densities, they tend to shatter after very little strain, exhibiting glass-like behaviour; at smaller densities, in the range of 80 to 150 kg m⁻³, silica aerogels can withstand compression up to 70% strain and recede back to the original volume.⁸⁰ A silica aerogel of 100 kg m⁻³ subjected to the three-point bending flexural test can sustain a maximum load of 0.02 MPa.¹¹⁷

The integration of fibres has been evidenced as an effective way to improve aerogels' mechanical performance, either during drying or in response to stress loads. As reported by Zhihua and co-workers,¹⁵² after the incorporation of 10 wt% ceramic fibres (Al₂O₃: ≈ 43–45%; SiO₂: ≈ 49–52%; ≈ Fe₂O₃: 0.5–0.8%), the compressive strength of the reinforced aerogel increased six-fold in comparison with the pure silica aerogel, while the thermal conductivity (measured in air at room temperature) just increased from 23 to 29 mW m⁻¹ K⁻¹.

Regarding the effect of fibres on aerogel's properties, a detailed discussion is presented in the next section.

3 Silica-aerogels with embedded fibres

The embedment of fibres in silica aerogels can, to a large extent, prevent the shrinkage during their drying,^{30,47,83} being as well an effective way to improve their mechanical properties.^{30,51,153,154} The challenge is, in spite of the reinforcement, to preserve their inherent insulation properties and high specific surface area.

3.1 Silica aerogel reinforcement strategies: a comparison

Among the current known techniques of silica aerogel reinforcement (previously summarised in Section 2.4), chemical cross-linking with reactive molecules or polymers leads to superior improvement in their mechanical performance.¹⁵⁵ For example, the compressive strength of amine-modified silica aerogels at the breaking point was ~4.1 MPa, with a maximum strain of ~5.7%; after being cross-linked with isocyanate, the mechanical strength at failure became improved by a factor of 45 (~186 MPa, ~77% strain). However, such an extraordinary improvement came at the cost of increased density (190 vs. 478 kg m⁻³).¹⁵⁶ The thermal conductivity of those composites was

estimated from thermal diffusivity data as being 41 mW m⁻¹ K⁻¹,¹⁵⁶ which can yet be considered a good result taking into account the high density of isocyanate cross-linked composites. However, as detailed by Huang and colleagues,¹⁵⁷ when increasing the covalent bonds within a system, its thermal conductivity gets increased as well, since the direct contact between neighbouring particles is augmented.

When lighter materials are sought, by encompassing a balance between moderate mechanical properties and superior insulation performance, this can be better accomplished through silica aerogel reinforcement with fibres, as disclosed in this literature review. Aerogel companies like *Aspen Inc.*, *Cabot Corporation*, and *Nano High-Tech Co., Ltd.* grant further proof by producing aerogel blankets.¹⁵⁸

The appropriate fibre fraction along with their homogeneous dispersion will potentiate improved mechanical and/or insulation properties,⁵⁷ turning this into a versatile route to facilitate aerogel manufacture.^{46,159–161} Additionally, the use of recycled or waste fibres^{23,83} to strengthen silica aerogel composites is being studied at the laboratory scale, paving the way towards sustainable and lower cost materials,⁴⁰ with almost unlimited potential for further development.¹⁶²

There is a broad consensus (either among the scientific community or aerogel industry enterprises) about fibre embedment as being the most versatile and effective method of silica aerogel strengthening.^{30,46,119–121,155,158}

3.2 Techniques for preparation of silica aerogels with fibres

There are several techniques reported in the literature to reinforce silica aerogels with fibres. The pioneering investigation of Wang *et al.*¹³³ consisted of the incorporation of ceramic fibres, to further improve the radiative properties of doped aerogels due to their opacifying effect (mainly for high temperature applications), also providing extra strength to reduce their inherent fragility.¹³³ Such composites were (and still are) accomplished with dispersion of the fibres in the sol prior to the onset of gelation.^{47,163,164} The mixture is then poured into a mould for gelation, and this procedure is typically used to manufacture strengthened and denser materials.^{51,163}

This procedure is briefly sketched out in Fig. 6a. The loading reinforcement limit is imposed by the uniformity of dispersion, since aggregates or bundles due to an excess of fibres might create weakened sites and decrease insulation performance of composites. This is more critical when using inorganic fibres. Some contextual examples are presented in Sections 3.5 and 3.6.

Flexible aerogel composites are generally obtained by pouring the sol over a fibre batting previously placed within a container, as illustrated in the scheme of Fig. 6b. A basic catalyst is added, just immediately before or after pouring the sol, to induce the gelation within a few minutes.^{22,33,165,166} The protocol in which the basic catalyst is added before pouring the sol is preferential, because the fibres may compromise the homogenization of the solution.

There are other versions for this route of composite preparation: (i) alternating the pouring of the sol with deposition of fibres, several times, according to the number of planned

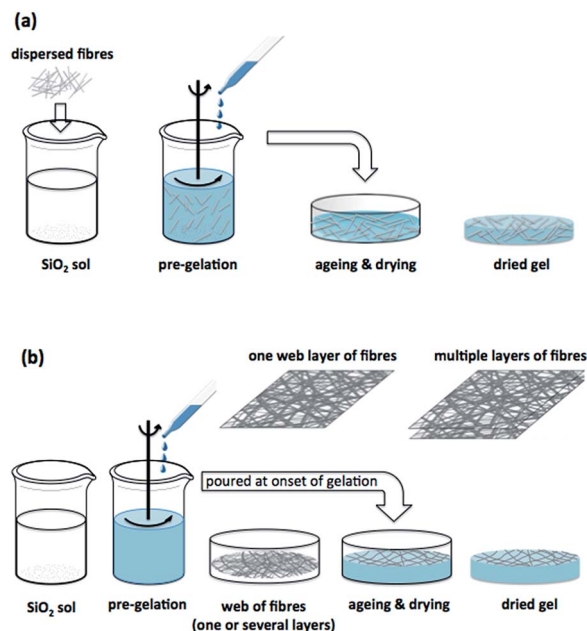


Fig. 6 Schematic procedures of silica aerogel composite syntheses: part (a) shows the addition of dispersed fibres to the silica sol; part (b) refers to the approach where a web or mat of fibres previously fill the mould, over which the sol is poured at the onset of gelation.

layers;¹²⁰ (ii) pouring all the alcosol into the mould and then immersing the fibres layer by layer^{167,168} or (iii) pouring the sol into a container and soaking a fibre matting or entangled fibres at the onset of gelation.^{169,170}

To obtain silica aerogel composites in the form of thin films with extreme flexibility, an ideal technique of reinforcement involves the addition of electrospun nanofibres,^{166,171} since there is an improved integration between the two phases.¹⁶⁶ The embedment procedures can be accomplished by impregnating a web previously formed¹⁷² or electrospinning the fibres *in situ*,¹⁶⁶ fully integrating the sol through precise control of gelation time.^{166,173} A different procedure was described by Mazrouei-Sebdani and colleagues:¹⁷⁴ silica aerogel microgranules were added to an electro-spinning polyethylene terephthalate (PET) solution, yielding a silica aerogel–PET nanofibre composite.

3.2.1 Enhancement of fibre–aerogel interfacial binding.

Chemical interactions between silica sol and the reinforcement materials may occur, depending on their chemical composition, leading to improved mechanical properties of composites. The incorporation of fibres or nanofibres with the ability to react/interact with silanol groups during gelation and ageing steps can prevent the aerogel structure from collapsing during drying.¹³⁸ As reported by Hayase and co-workers,¹³⁸ the hydrolysed MTMS preferentially adsorbs on and reacts with dispersed boehmite nanofibres at an early stage, favouring homopolycondensation on the fibre surface. Chemical interactions were also reported by Bangi and colleagues.¹⁷⁵ They observed silica particles tightly attached to the sidewalls of previously modified carbon nanotubes (CNTs). The modification of CNTs with a surfactant provided OH groups on their surface, which

are responsible for the interaction with silica.¹⁷⁵ In addition, Li *et al.*¹⁶⁴ described the modification of the surface of sepiolite fibres, after immersion in nitric acid aqueous solution, before their dispersion in the sol. Strong composites were produced due to the Si–O–Si chemical bonds between the fibres and silica matrix.

Apart from chemical bonds, other interfacial interactions can also contribute to improving a system's inner adhesion. Fig. 7 shows how, at a fracture (Fig. 7a), protruding aramid fibres were encircled by aerogel fragments (Fig. 7b), revealing the electrostatic attraction between the aerogel matrix and aramid fibres.¹⁶⁷ In another study of the same authors it was better understood how, during gelation, aramid fibre walls acted as nucleation spots of the growing silica network matrix, although FT-IR spectra of the composite revealed no additional chemical bonds.¹²¹

Markevicius *et al.*⁸³ also showed, with a clear SEM image of cellulose–silica aerogel composites, a full detachment between the intact fibre and the fractured aerogel; the cellulosic fibres entrenched within the aerogel matrix sustained the structure and the monolithic shape of composites, and a low thermal conductivity (less than $20 \text{ mW m}^{-1} \text{ K}^{-1}$) was preserved.⁸³

3.3 Inorganic and organic fibres as reinforcement materials of silica aerogels

The type of fibre, its intrinsic features, such as strength, density, length, diameter, length-to-diameter ratio, optical properties, curvature, and orientation angle, as well as the fraction of fibre content contribute to the ultimate features of silica aerogel composites, impacting their mechanical performance and insulation properties.^{176–179} Hence, the accurate selection of the fibre type is essential, in order to create synergies in the conception of composites. For example, a thermal barrier for a high temperature environment must be manufactured with thermally resistant fibres that also have a large spectral complex refractive index throughout the infrared region;¹⁵⁰ if some degree of flexibility would be needed, a flexible fibre should be used in the appropriate fraction.¹²⁷

3.3.1 Inorganic fibres. The thermal stability inherent to inorganic fibres, along with a low thermal expansion coefficient, propels their use as a structural reinforcement material of silica

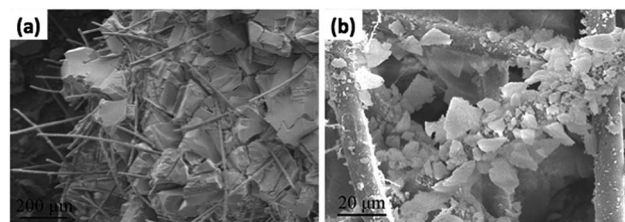


Fig. 7 Interfacial bonding between aramid fibres and a silica aerogel: (a) protruding aramid fibres at the silica aerogel composite's fracture, suggesting the absence of chemical bonds; (b) aramid fibres surrounded by silica fragments, evincing strong attraction between both phases (adapted and reprinted from ref. 167, copyright 2016, with permission from Elsevier).

Table 3 Silica aerogel composites reinforced with inorganic fibres: synthesis, and mechanical and thermal characterization

Reinforcement with inorganic fibres	Synthesis precursor; catalyst; mode of fibre addition; drying	ρ_b (kg m ⁻³)		Compressive strength (MPa)		Thermal conductivity (mW m ⁻¹ K ⁻¹)		References
		Neat	Reinf.	Neat	Reinf.	Neat	Reinf.	
30 wt% TiO ₂ + 20 wt% kaolinite + 10 wt% attapulgite + 10 wt% ceramic fibres ^a	TEOS; acid catalysed by HF; fibres added to the sol; ethanol SCD	112	185	0.018	0.128	14 (100 °C)	22 (100 °C)	Deng <i>et al.</i> ¹⁶³
Individually aligned glass fibres, 5–20 µm diameter, 3 volume%	TEOS; 1st: HCl, 2nd: NH ₄ OH; fibres added layer by layer permeated with sol; APD, 70 °C (12 h) + 100 °C (8 h)	115	163	0.72 (50% strain)	3.70 (50% strain)	22 (25 °C)	24 (25 °C)	Liao <i>et al.</i> ¹¹⁹
Sepiolite fibres, 1.5 volume%	TEOS; 1st: HNO ₃ , 2nd: NH ₄ OH; fibres dispersed in the sol; ethanol SCD	200	210	0.1	1.1	21 (50 °C)	25 (50 °C)	Li <i>et al.</i> ¹⁶⁴
Silica fibres, 10.5 wt%	Sodium silicate ^b /MTES ^c (1/0.3) 1st: cation exchange, 2nd: NH ₄ OH; fibres added to the sol; APD, 50 °C (2 h) + 80 °C (3 h) + 130 °C (4 h)	125	104	— ^d	0.1	36 ^e	22 (RT) ^f	Shao <i>et al.</i> ⁵⁷
Attapulgite fibres, 2 wt%	TEOS; 1st: HCl, 2nd: NH ₄ OH; fibres added to the sol; APD, 50 °C (24 h) + 85 °C (2 h) + 125 °C (1 h)	188	173	— ^d	1.2	21.8 (RT) ^f	19.8 (RT) ^f	Li <i>et al.</i> ³⁷
ZrO ₂ fibers, 4–7 µm diameter, 300–500 µm length, 10 wt%	TEOS; acid catalysed by CH ₃ COOH; fibres added to the sol; CO ₂ SCD	160	290	0.36	0.82	23.5 (25 °C)	26.2 (25 °C)	Hou <i>et al.</i> ¹⁸⁶
Aluminium borate whiskers, 0.5–1 µm diameter, 15–60 µm length, 20 wt%	AlCl ₃ ·6H ₂ O/TEOS (1/0.33) catalysed at 60 °C; whiskers added to the sol; ethanol SCD	150	350	0.26	1.40	27 (RT) ^f	40 (RT) ^f	Hou <i>et al.</i> ¹⁸⁷

^a Mixture of fibres: Al₂O₃, 43–45% SiO₂, 49–52% Fe₂O₃, 0.5–0.8%. ^b 6.2 wt% Na₂O, molar ratio of SiO₂ to Na₂O = 3.13. ^c Methyltriethoxysilane. ^d Compressive strength of unmodified silica aerogels with SCD (ρ_b = 96 kg m⁻³) is ≈ 0.04 MPa.¹⁸⁸ ^e Thermal conductivity of a TEOS derived aerogel, after multiple surface modifications, dried under ambient conditions (pressure and temperature), with an apparent density of 69 kg m⁻³.¹⁸⁹ ^f Room temperature.

aerogel composites, particularly in thermal barrier systems.^{160,164,180,181} For very high temperature insulation, ceramic fibres are the most suitable to embed in aerogel composites, while organic fibres must be excluded; also, carbon-based fibres can't be an option, as they degrade above 300 °C.¹⁸²

Silica fibres are a typical example for demanding environments,⁷⁹ remaining stable under extreme conditions:^{160,180} they exhibit a limit of temperature stability around 1100 °C, being able to surpass that limit for small periods of time.¹⁸⁰ By means of suitable manufacturing conditions, microporous fibres with skeletal densities as low as 1.5 g cm⁻³ can be achieved, allowing a diminished weight of the final composites, a determinant prerequisite in the aeronautics and space engineering fields.^{180,183} An additional and important feature of porous silica fibres is their effective electrical insulation.¹⁸⁰

If silica aerogel composites are envisioned to perform in oxidising atmospheres at temperatures above 1400 °C, the fibre reinforcement material has to be made from oxides with very high melting point, among which α -alumina encompasses all the features, including the advantageous refractory property.¹⁸² Other ceramic fibres, such as Al₂O₃, Fe₂O₃ based, or of alumina-silica type, also incorporate the needed features to integrate high performance thermal barriers, and generally are not sensitive to environmental attack.¹⁸¹ As inorganic fibres are thermally resistant,¹⁸⁴ they are less prone to deteriorate in high temperature environments compared to organic high-performance synthetic fibres.¹⁸⁵ Therefore, a broader operating temperature is allowed when aerogels are reinforced with inorganic fibres.¹¹⁷ When robustness must coexist in tandem with insulation performance, there is an upper limit of inorganic fibre loading in order to attain optimal properties of silica aerogel composites. This issue is better explored in Sections 3.5 and 3.6.

A brief compilation regarding studies of silica aerogel composites reinforced with inorganic fibres, by selecting those in which the differences between them and the native aerogel are disclosed, is presented in Table 3. How the fibres addition affects the mechanical and thermal behaviour can be seen by the comparison of results between "Neat" (refers to a pure silica aerogel) and "Reinf." (refers to a silica aerogel composite reinforced with the indicated fibres).

As a general trend, an increase in the bulk density due to the fibre addition is observed, along with a significant improvement of the composites' mechanical properties compared to the native silica aerogels. On the other hand, the insulation properties tend to become slightly damaged.

However, this is not always the case. According to the results of Shao *et al.*⁵⁷ and Li *et al.*,³⁷ exceptional insulation properties can be achieved in aerogel conception through the composite approach, with thermal conductivity values in the range, or even below those of air. Moreover, lighter materials can be manufactured by fine-tuning of fibres addition.

But, if the reinforcement material is still silica, mechanical performance can only be moderately increased. Shao *et al.*⁵⁷ reported an improvement of compressive strength by a factor of 2, compared to the native and unmodified silica aerogels with

SCD.¹⁸⁸ Nevertheless, lightweight and mechanically robust materials can be developed: reinforced silica aerogels with 2 wt% attapulgite fibres endured a compressive strength of 1.2 MPa³⁷ (an increment by a factor of 12 in comparison to aerogel composites reinforced with 10.5 wt% silica fibres).

According to the work of Li *et al.*,³⁷ appropriate inorganic fibres, even in a small amount, can be able to prevent aerogel densification during ageing and drying, while better insulation and/or mechanical performance can also be achieved.

Recently, Wang and colleagues¹⁹⁰ developed a new technique of manufacturing ceramic nanofibres with controllable diameters, from 47 to 815 nm. In general, the methodology consisted of a solution of solvent/precursor that is pumped and forced out by airflow, through a small aperture, collected in the form of entangled nanofibres. Quite promising results were reported in the synthesis of large-scale 3D sponges composed of titania (TiO₂), zirconia (ZrO₂), or yttria-stabilized ZrO₂ (YSZ), with densities ranging from 8 to 40 kg m⁻³. Moreover, due to the inorganic nature of the blow-spun nanofibres, this web can be used at extremely high operating temperature (the mechanical resilience of the YSZ nanofibre sponge was observed even at 1300 °C).¹⁹⁰

3.3.2 Organic fibres. This type of fibres is mainly used to impart higher flexibility to aerogels^{160,167,172,191} (Fig. 8), yet providing reinforcement/reduced shrinkage during drying.^{42,83}

The high length-to-diameter ratio imparts better flexibility to the organic fibres, compared to the inorganic natural fibres, which is an advantageous feature for the manufacture of flexible aerogel composites.¹⁷²

Natural fibres are viewed as environmentally favourable substitutes of synthetic polymers for reducing the carbon footprint of industrial products.^{83,84,155} Notwithstanding, organic natural fibres are not frequently used as silica aerogel reinforcement materials. Cotton is the most reported one, either used as textile structures^{33,169,192} or as raw cotton.^{44,193,194} Flax and kenaf organic natural fibres are also mentioned in the development of silica aerogel composites.^{195,196}

Several studies demonstrated the versatility of cellulosic fibres (both on the nano- and micro-scale), providing reinforcement of silica-cellulose aerogels for SCD, APD or freeze drying routes.^{38,42,83,169,191,197} The broad availability and low cost

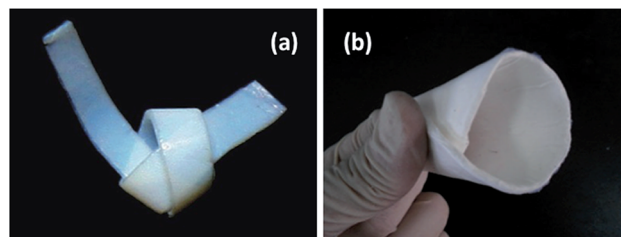


Fig. 8 Examples of flexible silica aerogel composites reinforced with organic fibres. (a) Cellulose-silica nanocomposite aerogel reinforced with regenerated cellulose fibrils (SCD) (reproduced with permission from ref. 191, copyright 2012, John Wiley and Sons); (b) silica aerogel composite reinforced with electrospun polyvinylidene fluoride fibres (APD) (reproduced from ref. 172, copyright 2013).

of cellulose fibres, combined with APD drying, enable a facile way to develop highly efficient composites.

According to the available literature, the first organic fibre embedded in silica aerogels was synthetic polypropylene, in a nonwoven structure reinforcing an adsorbent material.¹⁵⁴ The composite was developed to remove hazardous chemicals from air and sewage disposal, or even for medicine filtering. A surface treatment with trimethylchlorosilane turned the aerogel composite hydrophobic, with a contact angle of 135°. The addition of fibres decreased the aerogel's adsorptive performance but improved the mechanical behaviour of the composite, allowing its use in practical applications. However, according to the authors, these silica-polypropylene aerogel composites performed better than conventional adsorbing materials in the adsorption of benzene, methylbenzene or carbon tetrachloride.^{154,198}

Electrospinning is one of the last developed techniques for aerogel reinforcement by means of organic engineered micro or nanofibres.¹⁶⁰ It is an accessible technique^{172,199} to produce fibres with diameters as thin as 150 nm,²⁰⁰ much smaller than cotton diameter, the most consumed natural fibre,²⁰¹ with an average value of 10 µm.²⁰¹ The technique can be applied to almost any soluble polymer with a molecular weight large enough to form long chains.²⁰²

Briefly, in the conventional nanofibre procedure, the polymer is dissolved in a solvent in order to achieve precise viscosity to yield continuous nanofibres (low viscosity results in droplets that solidify as nanoparticles), then it is jetted through a capillary spinneret under the influence of an electrostatic field, and finally deposited in the form of a web in a collector support or directly into the sol cast.^{166,172}

The diameter of conventional fibres embedded in silica aerogels is significantly higher than the typical dimensions of pores or silica secondary particles, and despite the effectiveness of the reinforcement material, such a difference can lead to unbalanced responses to received stress loads. The smaller diameter of electrospun fibres increases the adhesion between phases, with smooth joints between the aerogel and the fibres, as can be seen in Fig. 9a. The tight adhesion can then potentiate the stability and strength of monolithic aerogels, while enhancing their flexibility.¹⁷² On the other hand, a higher degree of contact can have a detrimental effect in terms of solid thermal conductivity, but the smaller diameter of the nanofibres extends the corresponding specific surface area, which is advantageous to shield heat radiation.¹⁷²

Wu and colleagues¹⁷² developed a flexible silica aerogel composite, with a density of 202 kg m⁻³, reinforced with electrospun polyvinylidene fluoride nanofibres (PVDF) (see Fig. 8b), still maintaining good insulation features (see Table 4). The authors attributed the relatively low conductivity of the material to the diameter of nanofibres, which is between ~20 and 200 nm.

The work authored by Li *et al.*¹⁶⁶ focused on the development of TEOS based aerogel composite films reinforced with polyurethane (PU) electrospun nanofibres (500 nm diameter), in which polydimethylsiloxane (PDMS) was added to the sol prior to the gelation event. The study covered different PDMS

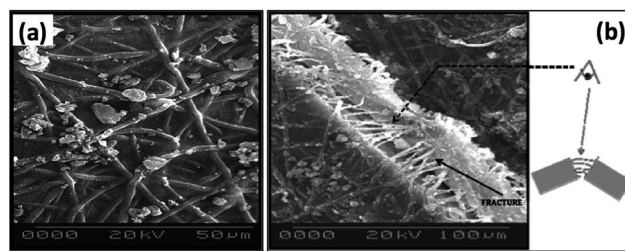


Fig. 9 Examples of fibre-reinforced silica aerogel composite microstructures: (a) with electrospun fibres from PDMS-based polyurethane (reprinted with permission from ref. 166. Copyright 2009, American Chemical Society); (b) appearance after fracture of silica aerogel composites reinforced with PDMS-based polyurethane electrospun fibres (reprinted with permission from ref. 166. Copyright 2009, American Chemical Society).

oligomers, with molecular weights of 538, 1350 and 2973 Da. A film with a thickness of 0.86 mm and a density of 172 kg m⁻³ (50 wt% nanofibres and PDMS M_w of 538 Da) exhibited a very low thermal conductivity of 13 mW m⁻¹ K⁻¹, a typical value of pristine silica aerogels. Another film with a thickness of 0.46 mm and a density of 79 kg m⁻³ (40 wt% nanofibres and PDMS M_w of 1350 Da) featured the worst performance in thermal conductivity, with 51 mW m⁻¹ K⁻¹, around twice the thermal conductivity of air. The difference in thermal conductivity between both materials was attributed to the molecular weight of PDMS, as a higher fraction of PDMS but with lower molecular weight leads to homogeneous mesoporosity, a beneficial feature for insulation performance.¹⁶⁶

The major breakthrough of silica aerogel composites with electrospun fibres is the possibility of producing aerogel composites as thin films with astonishing flexibility and improved response to fracture, as depicted in Fig. 9b. Even when subjected to a stress load that leads to fracture, the morphology of the tiny nanofibre network can to some extent sustain the composites. The cracked aerogel remained bridged by the nanofibres, thus preventing the composite disintegration.¹⁶⁶

Although the pioneering studies on electrospun fibres embedded in silica aerogels need further development to improve insulation efficacy and to scale-up manufacturing processes,^{172,203–205} technical applications such as protective clothing²⁰³ or super-capacitors²⁰⁵ are foreseen and being studied by the scientific community.

Organic man-made and natural fibres are preferentially used in aerogel composites conceived for operating at room temperature, or in moderately high temperature environments, since the low temperature degradation of the embedded fibres imposes such a restriction. For example, unmodified polypropylene fibres' melting point starts at ≈ 150 °C,^{206,207} and these fibres are often used as aerogel reinforcement materials because of their high abrasion resistance²⁰⁷ and hydrophobic properties (surprisingly, a polypropylene-silica aerogel composite dried at 200 °C is reported in the literature¹⁵⁴).

High performance organic fibres can extend the operating temperature of silica aerogel composites. As an example, polybenzimidazole (PBI) is known for its extreme thermal

Table 4 Silica aerogel composites reinforced with organic fibres: synthesis, and mechanical and thermal characterization

Reinforcement with organic fibres	Synthesis precursor; catalyst; mode of fibres addition; drying	ρ_b (kg m ⁻³)		Compressive strength (MPa)		Bending strength (MPa)		Thermal conductivity (mW m ⁻¹ K ⁻¹)		References
		Neat	Reinf.	Neat	Reinf.	Neat	Reinf.	Neat	Reinf.	
Polyvinylidene fluoride (PVDF) electrospun nanofibres, 28 wt% PVDF	TEOS; 1st: HCl, 2nd: NH ₄ OH; PVDF web added to the silica sol; APD, 70 °C (12 h) + 100 °C (12 h)	100 ^a	202	0.75	5.23	0.02 ^b	1.1	24 (RT) ^c	27 (RT) ^c	Wu <i>et al.</i> ¹⁷²
Nanofibrillated cellulose water suspension, 2.28 g L ⁻¹	PEDS ^d NH ₄ OH; nanofibres added to the sol; CO ₂ SCD	75	131	≈ 1	≈ 2	—	—	13.8 (RT) ^c	14.2 (RT) ^c	Wong <i>et al.</i> ¹²⁵
Pectin nanofibres, ≈ 6.7% methoxy groups and 20 wt% pectin content	Sodium silicate solution (26.5% w/w SiO ₂); NH ₄ OH; fibres added to sol (pH 1.5); CO ₂ SCD	110 (at pH 2.5, broke at pH 1.5)	190 (at pH 1.5)	≈ 1.4, 80% strain (at pH 2.5)	≈ 34, 80% strain (at pH 1.5)	—	—	17.4 (25 °C; RH ^e 50%)	16.2 (25 °C; RH ^e 50%)	Zhao <i>et al.</i> ¹⁵⁵
Aramid fibres, KEVLAR®-49, length > 10 cm, ≈ 6.5 wt%	TEOS 1st: HCl, 2nd: NH ₄ OH; fibres added layer by layer, after the sol; APD, 80 °C (8 h) + 100 °C (8 h)	100 ^a	142	1 ^f (E)	≈ 0.14(E)	0.02 ^b	≈ 0.20	17–21 (25 °C)	23.6 (25 °C)	Li <i>et al.</i> ¹²¹
Lyocell fibres (Tencel®), ≈ 8 mm length, ≈ 26 wt%	PEDS ^d NH ₄ OH; sol poured over loosened fibres; APD 140 °C (2 h) & CO ₂ SCD	— ^g (APD), 103 (SCD)	123 (APD), 125 (SCD)	—	—	— ^g (APD), 0.046 (SCD)	0.106 (APD), 0.184 (SCD)	— ^g (APD), 14.2 ^c (SCD)	16.6 ^c (APD), 17.5 ^c (SCD)	Jaxel <i>et al.</i> ⁴²

^a Typical value for bulk density of native silica aerogels. ^b Typical value for bending strength of native silica aerogels with density ≈ 100 kg m⁻³. ^c Room temperature. ^d A solution of pre-polymerized oligomers of TEOS, a SiO₂ content of 20 wt%, in ethanol. ^e Relative humidity. ^f Typical value for elastic modulus (E) of native silica aerogels with a density of 100 kg m⁻³. ^g Pure silica aerogel collapsed during APD drying.

resistance: it does not exhibit melting temperature, and the onset decomposition temperature is 450 °C in air (1000 °C in an inert atmosphere).¹⁸⁴ Remarkably (according to our literature search), PBI hasn't yet been used as an aerogel reinforcement material. On the other hand, *m*-aramid³³ or *p*-aramid¹²¹ fibres, whose melting/decomposition temperature varies from 375 to 560 °C,¹⁸⁴ are already used as silica aerogel reinforcement materials.^{33,121}

A selection of studies on aerogel composites reinforced with organic fibres is summarised in Table 4. Again, it was intended to address a broader perspective of how the fibre addition affects mechanical and thermal behaviour of silica aerogels, observed by comparison of results between "Neat" (refers to a pure silica aerogel) and "Reinf." (refers to a silica aerogel composite reinforced with the indicated fibres).

Regarding the results of those selected studies, the addition of structural reinforcement materials in silica aerogels leads to an increased density. As a consequence, the ability to sustain load is significantly increased after organic fibre addition.

The decreased value of elastic modulus compared to that of native silica aerogels (see the work of Li *et al.*¹²¹) denotes the increased flexibility of reinforced composites. More importantly, silica aerogels can be substantially reinforced without compromising their inherent insulation properties, in light of the presented results of thermal conductivity, before and after the reinforcement. As expected, the best results were achieved after the SCD route (see the work from Wong *et al.*¹²⁵ and Zhao *et al.*¹⁵⁵); the challenge consists of further improvement of silica aerogel composites *via* the APD route, towards cost-effective and efficient materials.

3.4 Influence of fibres on shrinkage and density of silica aerogel composites

Gel shrinkage is a key factor concerning the bulk density of aerogels. In fact, shrinkage or densification starts during crosslinking reactions when silica particles coalesce to form larger necks.⁷⁹ Shrinkage continues during ageing, when the silica matrix develops mechanical rigidity, with clusters restructuring due to the silica dissolution and re-deposition phenomena, which provides better resistance to the drying process,^{79,83} as previously described.

The reported shrinkage values depend on the assessment method. One of the ways consists in the measurement of the initial volume of the mould,^{208,209} or allowing the gelation to occur and measuring the volume of the wet gel,^{42,83} in comparison to the final volume of the dried material; these methodologies will express higher shrinkage values, since the obtained values are cumulative values of ageing and drying shrinkage. The other way consists of carrying out the assessment after the ageing step, expressing solely the shrinkage due to drying.^{57,210} Moreover, some authors report the linear shrinkage (usually in the diameter) and others report the volume shrinkage, the latter leading to significantly higher values. Often, the adopted method is not clearly disclosed.

As reported by Markevicius *et al.*,⁸³ during the ageing process of a pure silica gel, the volume shrinkage (occurring due to the

ageing and drying processes) was around 20%, whereas with the addition of 25 wt% cellulosic fibres, a reduced shrinkage of $\approx 7\%$ was achieved.

During drying, the embedded fibres also act as an effective skeleton frame that hinders shrinkage, since the casting volume is split into sub-volumes defined between two adjacent fibres. The internal movements of silica chains are inhibited, while the drying stresses are limited to small units, instead of one unit comprising the full body of the aerogel. Pure silica aerogels supercritically dried may undergo a linear shrinkage of around 5–10%, while the integration of fibres can reduce the shrinkage to neglectable levels.^{30,83} As an example, the difference in the drying linear shrinkage (gel diameter) between a silica aerogel composite reinforced with silica fibre felt and the pristine counterpart (both supercritically dried in acetonitrile, at 295 °C and 5.5 MPa) was around 13%, and the reinforced aerogel had no apparent shrinkage.³⁰ Shrinkage in silica aerogel composites mainly occurs through thickness (*z* axis),^{79,212} while monolithic non-reinforced aerogels shrink isotropically.⁷⁹

Paik and colleagues³⁰ refer to the composite density as being typically about 10% higher than the density of the corresponding neat aerogel. In general, the mere addition of fibres will lead to increased density, as listed in Tables 3 and 4. Several authors thoroughly addressed this issue, by studying the effect of different fractions of fibres embedded in silica aerogels, and dissimilar outcomes are described below.

Markevicius and co-workers⁸³ developed silica aerogel composites reinforced with Tencel® fibres (diameter of *ca.* 10 μm and length ≈ 2 mm). Tencel® is a commercial designation of a man-made cellulosic fibre, produced through the Lyocell process. The precursor was PEDS (pre-polymerized TEOS), and the gels were subjected to silylation in an HMDZ solution, for 72 h. According to their results, the higher the fibre content, the smaller the shrinkage (Fig. 10a), in contrast to density, which increased with increasing the fibre fraction (Fig. 10b). A similar trend was observed for aerogels obtained both by SCD and APD, but shrinkage also depends on the drying technique. The reported values are the cumulative shrinkage of the ageing and drying steps; while aerogels supercritically dried mostly shrunk during gel ageing, the evaporatively dried gels suffer additional densification due to the capillary pressures during drying (Fig. 10a). Thus, APD yielded generally higher densities than SCD, as presented in Fig. 10b.⁸³

Li and co-workers¹⁶⁴ reported another detailed observation of the range of low % of fibres. They synthesised silica aerogel composites from TEOS, with 0 to 1.5 volume% of sepiolite reinforcing fibres (2–10 μm length) dispersed in the sol, and dried under supercritical conditions. A small amount of fibres (0.5 vol%) prevented part of the shrinkage, resulting in slightly less dense materials (from 200 to 190 kg m^{-3}), in spite of the mass addition; an increase of fibre content led to a denser material (up to 210 kg m^{-3}), since the density of sepiolite fibres (2.0 g cm^{-3})¹⁶⁴ is much higher than the aerogel density.

A similar finding was published by Li *et al.*,³⁷ regarding silica aerogel composites reinforced with attapulgite fibres (a crystalline hydrated magnesium aluminum silicate). TEOS was the used precursor and a surface treatment was performed with

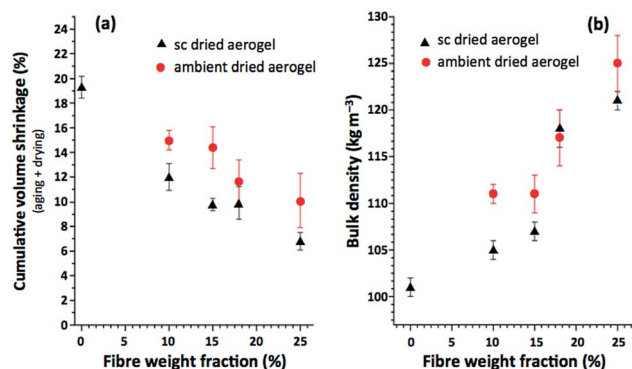


Fig. 10 Silica aerogels' (a) cumulative volume shrinkage (during ageing and drying) and the corresponding (b) final density as a function of Tencel® fibres' weight fraction, for ambient pressure and supercritical drying (aerogels without fibres collapsed during ambient pressure drying) (reprinted with permission from Springer Nature: *J. Mater. Sci.*, from ref. 83, copyright 2016).

trimethylchlorosilane (TMCS/ethanol/*n*-hexane solution), before APD of composites under a multistep temperature gradient. The mass of fibres varied from 0 to 20%, with linear shrinkage gradually diminishing from 32.3 to 10.2%, as depicted in Fig. 11a. Bulk density significantly decreased from 188 to 163 kg m⁻³ after adding 1 wt% fibres, and then gradually rose until 192 kg m⁻³. As claimed by the authors, fibres induced the aerogel matrix to withstand drying stresses, providing lighter materials with a precise addition of fibres.³⁷ It is worth highlighting the higher level of % shrinkage in APD compared to SCD, despite the effectiveness of hydrophobic surface treatments applied to the composites before APD.

In opposition to the monotonic decrease of shrinkage as a function of fibre content, Shao and colleagues³⁷ reported a different pattern, as depicted in Fig. 11b, regarding sodium silicate/MTES (1/0.3) composites reinforced with silica fibres (from 3.5 to 17.5 wt%), with a two-step MTES-TMCS modification. The APD dried composites achieved null volume shrinkage at 7 wt% fibre reinforcement. However, the optimal performance (a balance between insulation and mechanical behaviour) was achieved at 10.5 wt% (*vide* Table 3). With further fibre addition, shrinkage increased and reached ~24%, similar to the native, although two-step modified, silica aerogel. The authors attributed the fact to an incomplete surface modification caused by an excess of fibres that caused the composite densification.⁵⁷

Parmenter and Milstein⁴⁷ reported a different tendency when compared to those presented before. Both the density and shrinkage decreased along with the increase of fibre content.

These authors, who first studied the qualitative correlation between fibre reinforcement and the shrinkage behaviour of silica aerogel composites, used TEOS as the precursor and a mixture of ceramic fibres (68% silica with 3 µm diameter, 20% alumina with 2–4 µm diameter and 12% aluminoborosilicate with 8 µm diameter, all with 1.27 cm length), and the mass percentage of the reinforcement material varied from 0 to 25%. The fibres were added to the silica-based solution, and the composites were

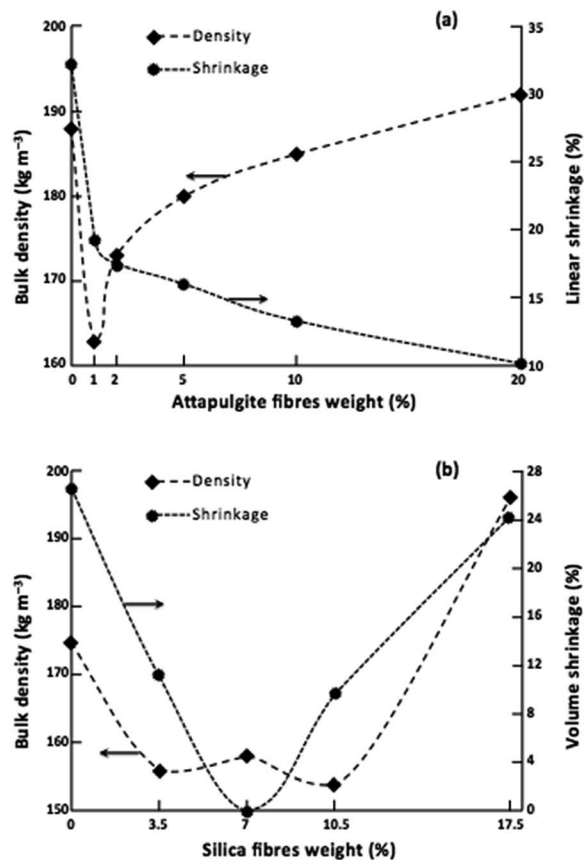


Fig. 11 Density and shrinkage of silica aerogel composites as a function of reinforcement with (a) attapulgite fibres, APD (after surface treatment) (reprinted with permission from Springer Nature: *J. Sol-Gel Sci. Technol.*, adapted from ref. 37, copyright 2017); (b) silica fibres, APD (after two-step surface modification) (adapted and reprinted from ref. 57, copyright 2015, with permission from Elsevier). All sketches were drawn from the published data, with the lines as a guide for the eye, and each arrow pointing to the respective vertical axis.

supercritically dried. They generally concluded that the higher the fibre fraction, the lower the density of aerogel composites. This was attributed to the support of the matrix provided by the fibres, which leads to a decrease of total shrinkage.⁴⁷

The observations reported by Gao *et al.*²¹³ in a subsequent study are in line with those of Parmenter and Milstein.⁴⁷ The aerogel composites were TEOS-based, reinforced with ceramic fibres (mainly composed of SiO₂ and Na₂O) and supercritically dried in ethanol. The fraction of fibres varied from 0 to 11.5 volume%, leading, respectively, to a variation of the composite bulk density between 202 and 142 kg m⁻³, accompanied by a decrease in shrinkage in the *z* direction, achieving a value of only 0.6%.²¹³

In spite of very different findings, there are some notes that can be outlined:

- (1) The bulk density of silica aerogel composites is related to the type and fraction of fibres used for reinforcement;
- (2) As a rule of thumb, the volume shrinkage of silica aerogel composites generally decreases with the increase of fibre content.

3.5 Effect of fibre content on the mechanical performance of silica aerogel composites

The porous nanostructure of silica aerogels can lead to a very low compressive strength, a property that might be critical in the case of load-bearing applications.^{186,214}

Mechanical compressive failures in silica aerogel composites can occur through different mechanisms, such as buckling, delamination, shear deformation and fibre rupture. Buckling is the main cause of fibre break-up, when the stress load is transmitted to the reinforcing fibres, leading to their fracture.²¹⁵

According to the work of Parmenter and Milstein,⁴⁷ both the fibre content and the material density determine the compressive strength behaviour of reinforced composites. These findings are depicted in Fig. 12, in which part (a) refers to the lower densities and part (b) refers to the higher densities. A small amount of ceramic fibre addition, such as 5 wt%, increased the elastic modulus relative to that of the pure aerogel, and this was particularly noticeable in structures with higher density (Fig. 12b), resulting thus in stiffer aerogels. With further increase of the fraction of fibres, the Young's modulus decreased, and hence the composites exhibited a higher degree of flexibility (Fig. 12a, at 10 wt%), which can be advantageous to overcome the inherent brittleness and difficult handling of silica aerogels.

Gao and co-workers²¹³ extended the study of mechanical performance by measuring tensile, bending and compressive strengths as a function of fibre content and density of silica aerogel composites reinforced with ceramic fibres (synthesis conditions and variables previously described). The mechanical strength increased up to 1.2–1.4 MPa with increasing mass of fibres up to 9.4 volume%, and then decreased, in accordance with the results described by Parmenter and Milstein⁴⁷ for the aerogel composites with the highest fraction of reinforcing fibres.

Regarding the results of the different mechanical strength tests as a function of density, Gao *et al.*²¹³ reported an almost linear relationship between tensile/bending/compressive strengths and density.

Boday and colleagues⁶⁸ reported a similar trend for silica aerogel composites reinforced with organic polyaniline

nanofibres, using a three-point flexural compression test. The mechanical strength of composites linearly grew up to 0.06 MPa (the higher strength was recorded at a density of 74 kg m^{-3} , with 3 wt% nanofibres), and then decreased monotonically due to a higher fraction of polyaniline, corresponding to a higher density of composites. The authors conjectured that after the maximum strength, the subsequent decrease was caused by the numerous fibres interfering with the interconnections between silica particles in the network. The best mechanical performance of a polyaniline–silica composite aerogel was 200% higher than that of the pure silica aerogel of the same density. They also reported that the polyaniline–silica aerogel composites supported 8500 times their own weight, in opposition to the 5000–6500 times of the pure silica aerogel counterpart.⁶⁸

Apart from the fraction of reinforcement material, the drying technique also determines the mechanical performance of aerogel composites, since it influences the level of shrinkage and the related density, as previously described. This was evidenced by Jaxel and co-workers,⁴² using the 3 point-bending test performed on aerogel composites of silica–Tencel® (fibre $\approx 14 \mu\text{m}$ diameter and 8 mm length). The fibre volume fraction varied from 0 to $\approx 2\%$; the samples were both ambient pressure and supercritically dried, giving densities of 103 and $\approx 124 \text{ kg m}^{-3}$, respectively, for the neat silica aerogel and the composite with the higher content of Tencel® fibres. The flexural results are presented in Fig. 13a (there are no results for ambient pressure drying with 0% fibre content, due to the loss of the monolithic shape during drying⁴²). The supercritically dried composites displayed higher stiffness, expressed by the higher values of moduli and maximum stress, compared to the ambient pressure dried composites, which showed higher flexibility (Fig. 13a and b). The authors attributed this fact to the gel's partial fragmentation during APD. Under stress loading, the fragmented parts are sustained by the fibres that smoothly move into new rearrangements, while pure silica aerogels tend to break completely.⁴²

Liao and colleagues¹¹⁹ and Hou and co-workers¹⁸⁶ reported similar outcomes, summarised in Fig. 13c and d for: (c) a TEOS-based silica aerogel, reinforced with aligned glass fibres (added to sol in layers perpendicularly oriented), modified by a TMCS/

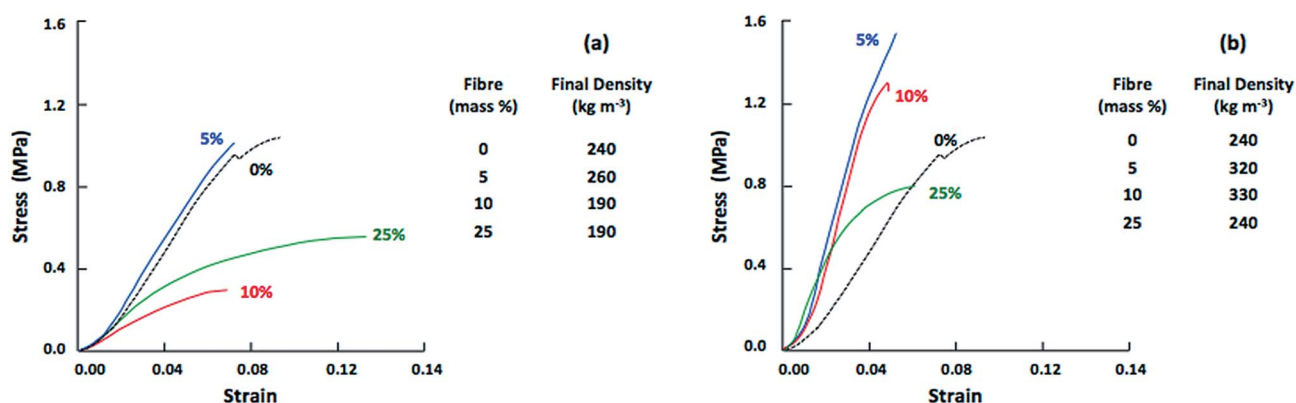


Fig. 12 Stress–strain curves of silica aerogels under compressive load for various degrees of fibre reinforcement and aerogel composites' final densities (adapted and reprinted from ref. 47, copyright 1998, with permission from Elsevier).

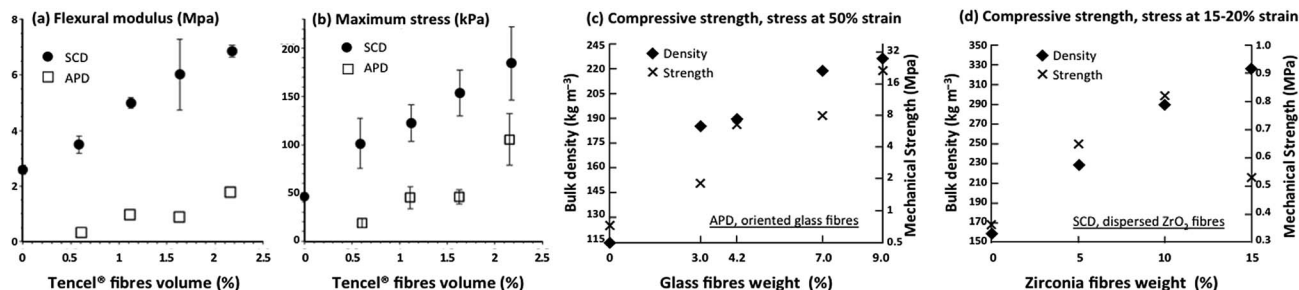


Fig. 13 Mechanical properties of silica aerogel composites: (a) flexural modulus and (b) maximum stress for supercritically dried and ambient pressure dried silica aerogel composites reinforced with Tencel®, as a function of fibre volume (adapted and reprinted from ref. 42, copyright 2017, with permission from Elsevier); (c) and (d) compressive strength and bulk density of silica aerogel composites as a function of fibre weight fraction, with related particularities inscribed (both drawn from the published data, (c) reprinted with permission from Springer Nature: *J. Sol-Gel Sci. Technol.*, adapted from ref. 119, copyright 2012; and (d) adapted from ref. 186, copyright 2018, with permission from Elsevier).

n-hexane solution and subjected to APD;¹¹⁹ (d) a composite developed from a mixture of precursors, TEOS and zirconium oxychloride, reinforced with dispersed ZrO₂ fibres added to the ZrO₂-SiO₂ solution, and subjected to SCD.¹⁸⁶ As depicted in Fig. 13c, the increase of reinforcement material fraction, from 0 to 9 wt% glass fibres, resulted in an increase of compressive strength of the composites, from 0.72 MPa to 21.03 MPa (almost 30-fold), while the bulk density increased from 115 to 227 kg m⁻³ (less than 2-fold).¹¹⁹ The silica-zirconia composites reinforced with zirconia fibres exhibited a positive and almost linear correlation of bulk density and compressive strength with fibre wt%, between 0 and ≈10 wt% (Fig. 13d). Beyond that point, the mechanical strength decreases with the addition of fibre mass. Hou *et al.*¹⁸⁶ explained these results through an excess of fibres that led to clusters (non-homogeneous dispersion), which favoured fibre slip off under stress load and the composite failure.¹⁸⁶

The mechanical response of silica aerogel composites engineered for insulation at high/extreme temperature must fulfill two important requisites: (i) the ability to maintain thermal performance when subjected to a load; (ii) displaying the necessary degree of elasticity under that load.²¹⁶

The loss of integrity of silica aerogel composites under stress load is often the main factor of degradation of their insulation performance due to induced cracks.^{216,217}

3.6 Effect of fibre content on the thermal conductivity of silica aerogel composites

The fraction of fibres reinforcing silica aerogel composites dictates their thermal conductivity, which can also be influenced by the type of fibre.^{85,177} The trend observed for density in the silica-sepiolite and silica-attapulgite composites (Section 3.4) is similar to the trend of thermal conductivity: a small fraction of fibres decreased the thermal conductivity relatively to that of the neat aerogel, while for a higher amount of fibres the thermal conductivity increases. In fact, higher porosity prevailed over a small mass addition of the inorganic fibres, and thermal conductivity decreases due to the increase of voids; but, by increasing the amount of fibres, thermal conductivity

increases almost linearly,^{37,164} as shown in the two examples of Fig. 14.

Other systems of silica aerogels with alumina, silica or silicon carbide fibres were reviewed and explained by Lee & Cunningham.¹⁷⁷ According to their study, a low content of fibres, with residual contact between them, has a negligible effect on the solid heat conduction of the composites.¹⁷⁷

Liao and co-workers¹¹⁹ studied the effect of the fraction content of aligned glass fibres (5–20 μm diameter) on the thermal conductivity of silica aerogel composites. Four layers of fibres were alternately deposited in perpendicular directions and permeated with silica sol. The content of glass fibres was 1, 4.2, 7 and 9 wt%. The increasing mass of fibres led to different thermal performance behaviour: from 1 to 4.2 wt%, there was almost no increase in thermal conductivity, attributed to a low contact between fibres, separated by the aerogel in-between; a further increase in the fibre content, from 4.2 to 7 wt%, increases the mutual contact between fibres due to the nearest adjacent layers of glass fibres, and thermal conductivity rises from 26 to 32 mW m⁻¹ K⁻¹, until full contact of fibres; above 7 wt% fibres, the thermal conductivity increases only slightly.¹¹⁹

Lu and colleagues¹³⁵ evaluated the thermal conductivity using different patterns between adjacent SiC fibres embedded

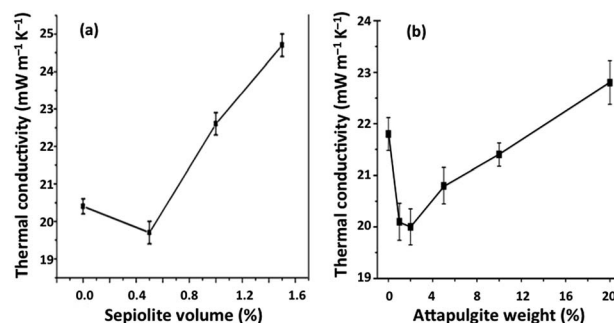


Fig. 14 Influence of fibre amount on the thermal conductivity of silica aerogel composites: (a) volume% of sepiolite fibres (reprinted with permission from Springer Nature: *J. Sol-Gel Sci. Technol.*, from ref. 164, copyright 2013); (b) wt% of attapulgite fibres (reprinted with permission from Springer Nature: *J. Sol-Gel Sci. Technol.*, from ref. 37, copyright 2017).

in a silica aerogel. They assessed three possibilities: (i) strong contact, for effective contact between fibres; (ii) non-ideal contact, with air and cracks between fibres; and (iii) ideal contact, when the space around each fibre was filled by the aerogel. The results are shown in Fig. 15a. The ideal contact leads to the lowest thermal conductivity, suggesting that with lower fibre fraction (with reduced probability of mutual contact) better insulation properties can be achieved.¹³⁵

Dissimilar achievements are also reported in the literature. Jiang and colleagues⁸⁵ developed a silica aerogel composite, reinforced with a microglass fibre mat (2–4 μm diameter), with a volume content of 4.5, 6.8, or 9.1%. The results are depicted in Fig. 15b: the higher the volume of fibres, the lower the thermal conductivity of the composite. According to the authors, the results can be understood in light of the small diameter of the glass fibres, and the consequent high specific surface area. Thus, the higher the fibre content, the higher the ability to suppress the radiative heat conduction. This is supported by the slope of thermal conductivity curves with increasing temperature: the composite with higher fibre content exhibited the lower slope.⁸⁸

In Fig. 15c, corresponding to the work of Yuan *et al.*,²¹⁸ the trend is the opposite: the higher the content of glass fibres, the lower the insulation performance of the silica aerogel composite, which was attributed to an eventual higher connection between fibres, enabling the creation of new paths for heat leaking,²¹⁸ but it can also be related to the higher diameter of glass fibres, which was 12 μm , while Jiang and co-workers⁸⁵ used fibres with a smaller diameter (2–4 μm).

The different trends of thermal conductivity as a function of fibre fraction, by comparing the composites developed by Jiang *et al.*,⁸⁵ Liao *et al.*¹¹⁹ and Yuan *et al.*,²¹⁸ are in accordance with the degree of contact between fibres in the structures; when disposed in layers, the stronger contact between fibres potentiates an increase of conductivity.¹³⁵ Nonetheless, all the composites provided better insulation features than commercial fibre glass insulators, whose typical values of thermal conductivity are around $40 \text{ mW m}^{-1} \text{ K}^{-1}$,⁸³ as shown in Fig. 4.

In the aforementioned development of Markevicius and colleagues,⁸³ cellulosic fibres (Tencel®, 10 μm diameter and 2 mm length) were added to a silica sol at concentrations of 1, 1.5, 2 and 3 wt% (corresponding to 10, 15, 18 and 25 wt% of the dried composite). The influence of APD vs. CO_2 SCD on the insulation performance of composites was also studied. The thermal conductivity of cellulosic fibres is higher than that of the silica aerogel structure, ranging from ~ 0.72 – $5.7 \text{ W m}^{-1} \text{ K}^{-1}$ in cellulose nanocrystals, to lower values of *ca.* 0.22 – $0.53 \text{ W m}^{-1} \text{ K}^{-1}$ in more organized man-made materials, such as cellulosic films.²¹⁹ Therefore, it is expected that the addition of cellulosic fibres, while providing reinforcement of silica aerogels, would have a detrimental effect on their insulation features. In fact, the thermal conductivity of composites slightly increased with the increase in the fraction of fibres, as depicted in Fig. 16.

The SCD composites showed $\approx 7\%$ better performance in terms of insulation, attributed to the reduced shrinkage, thus lower density, compared to the APD composites.⁸³

This group of researchers also assessed the insulation properties of other cellulosic fibres compared to those of Tencel®, namely flax and recycled paper fibres, all with 25 wt% embedded fibres in the silica matrix. According to their results the silica-Tencel® composites performed around 13–14% better.⁸³ Yet, all the composites still exhibit values below the thermal conductivity of free air under standard conditions ($25 \text{ mW m}^{-1} \text{ K}^{-1}$), with insulation performance similar to that of super-insulating materials. This was attributed to the mesoporous structure of the gel, not significantly damaged during drying.

The incorporation of cotton fibres also increases the conductivity of silica aerogels, in accordance with the work of Rezaei and Moghaddas.¹⁹² Even though the structural strength of composites increased, in order to maintain their thermal conductivity below the thermal conductivity of free air, the cotton fibre addition was limited to a maximum content of 60 wt% of the dried aerogel, according to the authors. These composites were obtained from a water glass precursor and APD, after surface modification with TMCS in hexane.¹⁹²

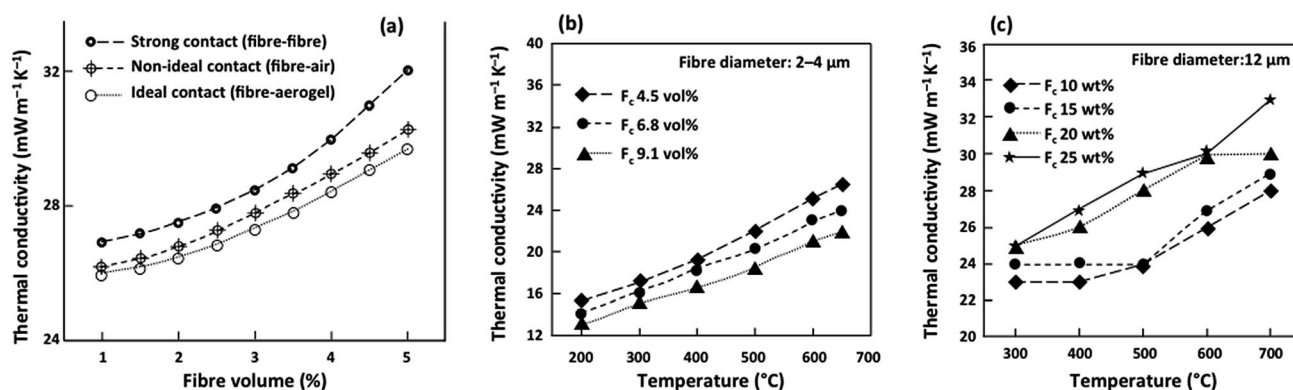


Fig. 15 Thermal conductivity of silica aerogel composites: (a) effect of contact patterns of the reinforcement with SiC fibres (diameter between 2 and 5 μm), measured at 300 K and ambient pressure (adapted and reprinted from ref. 135, copyright 2011, with permission from Elsevier); (b and c) trends of thermal conductivity as a function of fibre content: (b) volume fraction of glass fibres, with 2–4 μm diameter (reprinted with permission from Springer Nature: *J. Sol-Gel Sci. Technol.*, from ref. 85, copyright 2017); (c) mass fraction of glass fibres, 12 μm diameter (adapted and reprinted from ref. 218, copyright 2012, with permission from Elsevier).

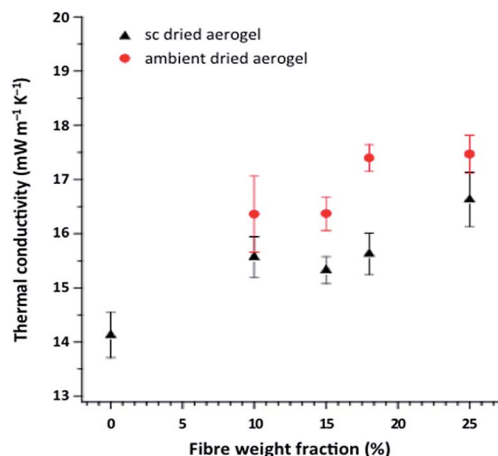


Fig. 16 Thermal conductivity of silica aerogel composites with Tencel® fibres, obtained by APD and CO₂ SCD (no results are shown for the APD-pure aerogel due to its collapse during drying) (reprinted with permission from Springer Nature: *J. Mater. Sci.*, from ref. 83, copyright 2016).

In the development of pectin-silica composite aerogels, by dissolving pectin in water-glass-derived silicic acid solution, the as-prepared high methoxy content pectin nanofibres remained interpenetrated within the silica matrix.¹⁵⁵ The aerogels synthesised at pH 1.5, 3 and 5 and reinforced with 5, 10 and 20 wt% pectin nanofibres exhibited improved insulation properties when compared to the pristine aerogel counterpart. While the pectin-silica composites displayed thermal conductivity values between 14 and 17 mW m⁻¹ K⁻¹, the thermal conductivity of the native silica aerogel was 17.4 mW m⁻¹ K⁻¹.¹⁵⁵ One possible reason for these results may be the smaller dimensions of pores in the hybrid aerogels,³¹ since the diameter of pores in the composites was ≈11 nm, while it was around 14 nm in the native silica aerogel, on average.¹⁵⁵ As revealed by Zhao *et al.*,¹⁵⁵ the composite synthesised at the smaller pH and with a small load of pectin fibres exhibited the lowest thermal conductivity: 14.2 mW m⁻¹ K⁻¹.

Additionally to the size of pores, their relative volume is also a key factor of insulation performance, as demonstrated by Shao *et al.*⁵⁷ while the pristine silica aerogel ($\rho_b = 125 \text{ kg m}^{-3}$, APD), with a mesopore volume of 96.6% displayed a thermal conductivity of ~20 mW m⁻¹ K⁻¹, after the addition of 17.5 wt% silica fibres ($\rho_b = 146 \text{ kg m}^{-3}$, APD) the mesopore volume lowered to 77.7% and the thermal conductivity increased to ~30 mW m⁻¹ K⁻¹ (even so, a very good result was achieved with composites).

3.6.1 Opacified silica aerogels: fibres as a shield for radiative conductivity. The before mentioned eqn (5) highlights the influence of environment temperature on the radiative thermal conductivity of monolithic silica aerogels, which can be dominant over the other two components of thermal conductivity.^{144,177,220}

When exposed to temperatures above 600–700 °C, the structure of native silica aerogels deteriorates due to viscous sintering. This phenomenon can lead to a partial loss of the porous morphology and subsequent densification, imposing restrictions on their applicability as thermal barriers.^{221,222} On the other hand, the spectral mass attenuation coefficient of native silica aerogels is less than 10 m² kg⁻¹ for wavelengths around 3–5 μm, while in the hybrid silica aerogel, heat mitigation in that IR wavelength range can be increased around 100 times,²²³ as shown in Fig. 17.

Actually, an effective way to improve silica aerogels' efficiency for high temperature applications is the attenuation of radiative heat transfer, either by scattering or absorption, which can be accomplished with the embedment of infrared opacifiers, such as soot, TiO₂ particles or inorganic fibres.^{133,177,224,225} Fig. 17a illustrates the effectiveness of a carbon-based additive (soot) in enhancing IR shorter wavelength absorption. Soot is an efficient opacifier, with a mean spectral mass attenuation coefficient of 600 m² kg⁻¹,²²⁶ as described in Table 5, significantly higher than the values of the other typical opacifiers, also presented therein. However, in spite of^{196,197} its broad-band absorption, the carbon black opacifier becomes unstable above 573 K,¹³⁵ and is prone to oxidation reactions in high temperature environments.¹³³

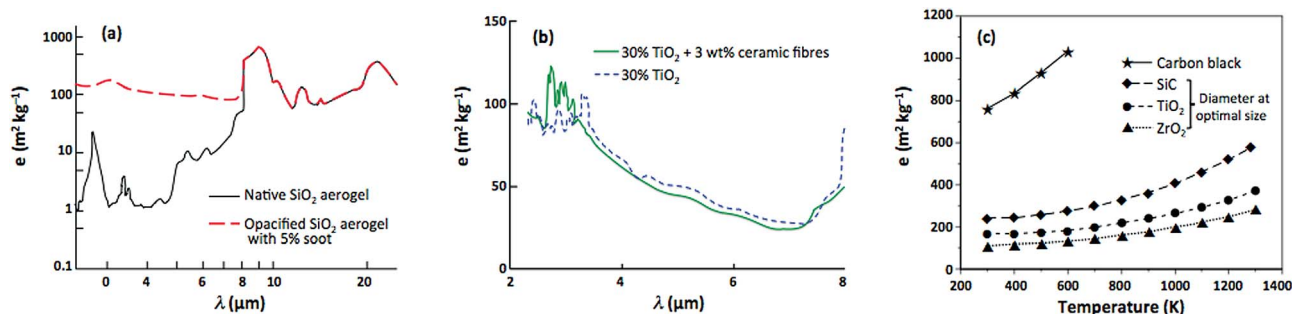


Fig. 17 Spectral mass attenuation coefficient of opacifiers used in silica aerogels: (a) carbon-based, as a function of wavelength (reprinted and adapted from ref. 137, copyright 1992, with permission from Elsevier); (b) spectral mass attenuation coefficient of an opacified silica aerogel with TiO₂ particles and ceramic fibres (adapted and reprinted from ref. 133, copyright 1995, with permission from Elsevier); (c) comparative performance of carbon black and other commonly used aerogel opacifiers, as a function of temperature (adapted and reprinted from ref. 229, copyright 2016, with permission from Elsevier).

Table 5 Spectral mass attenuation coefficients, e , for fibres and opacifiers in the wavelength range 1–50 μm

Material	Particle or fibre diameter (μm)	e ($\text{m}^2 \text{kg}^{-1}$)	References
5% Fe_3O_4 in fumed silica	2	40	Fricke <i>et al.</i> ²²⁶
5% TiO_2 in fumed silica	2.5	40	Fricke <i>et al.</i> ²²⁶
10% TiO_2 in SiO_2 aerogel ($\rho_b = 170 \text{ kg m}^{-3}$)	3.5	14	Kuhn <i>et al.</i> ²²⁷
30% TiO_2 in SiO_2 aerogel ($\rho_b = 220 \text{ kg m}^{-3}$)	3.5	66	Kuhn <i>et al.</i> ²²⁷
Soot	<0.1	600	Fricke <i>et al.</i> ²²⁶
Glass fibre	5	50	Fricke <i>et al.</i> ²²⁶
SiO_2 fibre	10	30	Fricke <i>et al.</i> ²²⁶
AlO_3 fibre	4	50	Fricke <i>et al.</i> ²²⁶
SiC fibre	1.5	160	Wang <i>et al.</i> ²²⁸

TiO_2 combined with inorganic fibres, such as alumina or silica, is often used as an opacifier in silica aerogel composites,^{227,228} with diverse applications, such as in aerospace engineering, high temperature energy storage or even solar energy devices.²²⁴ As the attenuation coefficient of the native silica aerogel decreases with rising temperature and is much smaller than that of inorganic fibres, the silica aerogel with embedded inorganic fibres can be quite effective in suppressing the radiative heat.¹³⁷

Wang and colleagues¹³³ pioneered these studies, by mixing ceramic fibres with TiO_2 particles (mean diameter of 3.5 μm). The strengthened composites were synthesised from TMOS, and had higher absorption of the IR shortest wavelength (see Fig. 17b), widening their applicability for high temperature environments. According to their studies on how doped silica aerogels (with 30% TiO_2 + 3 wt% ceramic fibres, ρ_b as 260 kg m^{-3}) performed in an increasing temperature environment, the total thermal conductivity was 38 $\text{mW m}^{-1} \text{K}^{-1}$ at 800 K, while that value for a conventional insulating material, such as an alumina-fused brick, is around 100 $\text{mW m}^{-1} \text{K}^{-1}$.¹³³ Yet, the thermal stability of SiC fibres leads to improved performance compared to TiO_2 or zirconium fibres, in a range above the service temperature of carbon opacifiers commonly used, with the diameter at an optimal size,²²⁹ as illustrated in Fig. 17c.

Several research studies revealed similar trends regarding the thermal conductivity at high temperature, such as the examples depicted in Fig. 18. Silica aerogels supercritically dried and strengthened with 5% volume of amorphous SiO_2 glass fibres displayed low radiative thermal conductivity with increasing temperature up to 1300 K, compared to the pure silica aerogel,¹⁷⁸ depicted in Fig. 18a.

Another aerogel composite with 10 wt% mullite fibres ($3\text{Al}_2\text{O}_3 \cdot 2\text{SiO}_2$), synthesised in one step from sodium silicate precursors, modified by trimethylchlorosilane and dried at ambient pressure, when exposed to temperature above 300 $^\circ\text{C}$ showed better thermal insulation than the pristine aerogel.²³⁰ This last study was conducted below the sintering temperature of native silica aerogels (Fig. 18b). By selecting a suitable morphology and content, the addition of inorganic fibres is a proven technique to suppress thermal radiation, therefore enabling the decrease of the total thermal conductivity of silica aerogels in high temperature environments.¹⁵⁰ Enhanced results can be achieved with fibres of small diameters.^{85,231}

3.7 Influence of fibre morphology/size

The physical adhesion between the silica phase and the reinforcing fibrous matrices tends to be improved with the roughness of fibres' surface.²³² Other relevant parameters of fibres for the final properties of aerogel composites are mentioned below.

3.7.1 Length-to-diameter ratio. The skeleton structure of monolithic silica aerogels is formed according to the percolation theory: each individual chain constituting the aerogel lattice grows after addition of new particles, randomly occupying available sites, under a certain probability, p . If p is small, only finite clusters are formed; when p exceeds the percolation threshold, a continuous 3D assembly occurs, along with the individual chains.²³³ The theoretical volume fraction of fibres (or particles) above which a continuous network is formed is designated as the percolation concentration.⁴²

There is a correlation between length-to-diameter ratio of fibres and the value of percolation concentration, which can be approximately estimated as being the inverse value of length-to-diameter ratio. As an example, to obtain monolithic aerogels dried at ambient pressure, the minimum amount of cellulosic fibres with a length of 2 mm and diameter of 14 μm has to be $\approx 0.7\%$ volume. However, for easy handling of materials, as well

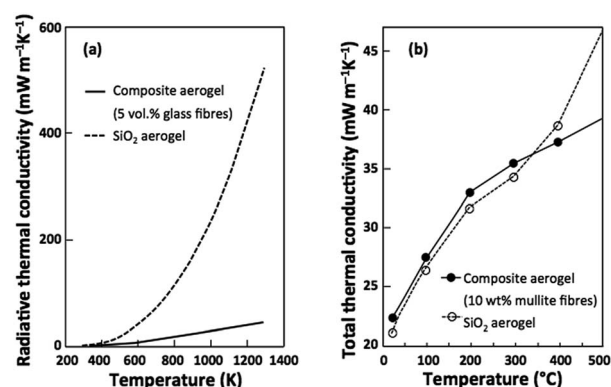


Fig. 18 Effect of increasing environmental temperature on the thermal conductivity of an opacified silica aerogel in comparison to the native silica aerogel: (a) aerogel composites with 5 volume% of amorphous SiO_2 (adapted and reprinted from ref. 178, copyright 2012, with permission from Elsevier), and (b) composites filled with 10 wt% mullite fibres (adapted from ref. 230, copyright 2016, with permission from Atlantis Press).

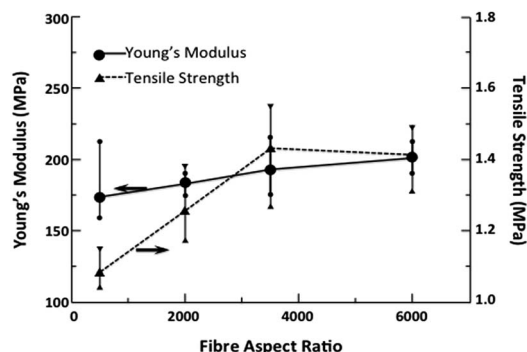


Fig. 19 Effect of fibre length-to-diameter ratio on the mechanical properties of silica aerogel composites (reprinted from ref. 235, copyright 2015, with permission from Elsevier).

as to minimize collapse or shrinkage during drying, the value of % volume of those fibres must be at least twice the value of the percolation concentration.⁴²

The length-to-diameter ratio of fibres also influences the mechanical behaviour of the composites.²³⁴ According to a study carried out by Lu and co-workers,²³⁵ the tensile strength of a silica aerogel, reinforced with 7% volume of ceramic fibres, increased linearly with their increasing ratio, from less than 1.1 MPa (at a ratio of 500) to more than 1.4 MPa with a fibre ratio of 3500. For higher ratios, the tensile strength decreased slightly (Fig. 19).

3.7.2 Length. Monolithic ambient pressure dried silica aerogels can be synthesised without additional chemical treatments, as long as fibres are embedded, in order to prevent their collapse, as aforementioned. Notwithstanding, there is a minimum fibre length to be able to endure the capillary stresses and to sustain the structure. According to the work of Ślosarczyk,²³² in spite of the huge amount of carbon nanofibres with a length of 20 nm (15 vol%), the aerogel composites collapsed into fragmented pieces under ambient pressure drying. In order to obtain monolithic samples, the fibre length had to be around 700 μm .²³² In fact, longer ceramic fibres provided better reinforcement and improved the mechanical performance of the silica aerogel composites.²³⁵

However, an excessive length of the fibres can be detrimental to aerogel's mechanical performance, as explained by Bunsell:²³⁶ as the intrinsic material defects randomly occur at individual units or linkages of the fibres, the bigger its length, the higher the probability of a weakened fibre.²³⁶

The length of fibres can also influence the thermal conductivity of silica aerogel composites. According to a study involving cellulosic fibres with 2, 6, 8 and 12 mm length, the maximum insulation performance was recorded in the composites with 6 and 8 mm fibre length. The researchers hypothesised that higher dimensions of fibres might increase their mutual contact and favour the solid thermal conductivity. On the other hand, short length fibres lead to a higher level of densification during ambient pressure drying.⁴²

3.7.3 Diameter. Some examples had been presented already in this review highlighting the influence of fibre diameter on the final properties of the aerogel composites. Depending on the type of fibre, there is an optimum diameter at which the maximum spectral mass attenuation coefficient is achieved²²⁹ (*vide* Fig. 17c). This is a noteworthy variable in the conception of thermal barriers for high temperature environments. Silica based fibres are often used in those materials.

According to several studies, silicon carbide fibres with diameters around 4–6 μm provide the best insulation properties when embedded in hybrid silica aerogels.^{27,150,229} Tang and colleagues²²⁹ determined more specifically the optimal SiC diameter concerning the intended operating temperature (Fig. 20a). Also, the diameter of amorphous glass fibres, in order to minimize the thermal conductivity for a given service temperature, was assessed by Zhao and co-workers¹⁷⁸ and is presented in Fig. 20b. According to their work, silica aerogels reinforced with fibres with diameters of 4, 6 and 8 μm displayed the highest insulation performance at 1300 K. The study was carried out with composites of density of 110 kg m^{-3} and 94% porosity, with 5% volume of fibres. Tang and co-workers²²⁹ also assessed the optimal reinforcing fibre diameter in order to yield the optimal density of silica aerogel composites, leading to the best insulation performance and covering a broad temperature range. The lightest insulation materials were made with SiC fibres – Fig. 20c. Apart from carbon black, in the lower

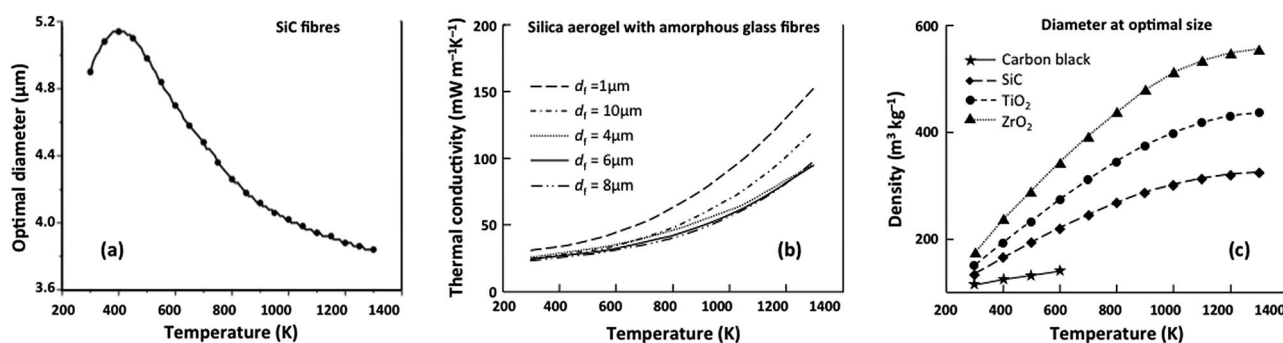


Fig. 20 Fibre diameter for optimal insulation performance as a function of temperature: (a) silicon carbide (reprinted from ref. 229, copyright 2016, with permission from Elsevier); (b) amorphous glass fibres (adapted and reprinted from ref. 178, copyright 2012, with permission from Elsevier); (c) optimal density of silica aerogel composites for a wide range of temperature, reinforced with fibres with optimal diameter (reprinted from ref. 229, copyright 2016, with permission from Elsevier).

temperature range, aerogel composites embedded with SiC fibres displayed the lower thermal conductivity.

With regard to mechanical performance, toughness and flexibility are the features to be assessed during selection of the reinforcement fibres. Bunsell²³⁶ related the fibre flexibility with a function of the reciprocal of the diameter to the fourth power, that is to say, the flexibility of a fibre can be increased 16 times by halving its diameter, as presented in eqn (7):

$$\text{Fibre flexibility} = \frac{64Fl^3}{3E\pi D^4} \quad (7)$$

where Fl is the bending moment produced by the applied force F at the free end of the length l , E is the fibre stiffness or Young's modulus and D is the fibre diameter.

Such a relationship emphasises the prevalent trend of ceramic fibres in silica aerogel reinforcement, since stiff materials can still be flexible materials in the form of fine fibres.

3.7.4 Curvature. The architecture of fibres in the three-dimensional space or in a plane greatly influences the mechanical performance of silica aerogel composites, namely the tensile strength and Young's modulus. As depicted in Fig. 21, the less the curvature of the fibres, the highest is the strength of the composites, since the curved shape inhibits the loading stress to be transferred from the matrix to the fibres, diminishing their role in reinforcement.²³⁵ It should be noted that as the curvature of the fibres increases, there is an improvement in the accuracy of the results.

3.8 Influence of fibre orientation

The absorption and scattering characteristics of each fibre are related to the angle of incidence, defined between the incident radiation and the plane normal to the longitudinal axis of the fibre.^{177,237}

Apart from the optical properties and volume fraction, fibre orientation is an important parameter for the thermal conductivity of aerogel composites. According to the studies of Lee & Cunningham,¹⁷⁷ 25 wt% SiC fibres with 15 μm diameter randomly oriented in a plane normal to the heat flux imparted the lowest conductivity to a silica aerogel composite ($\rho_b = 105 \text{ kg m}^{-3}$), while the fibres randomly oriented in space imparted

the highest value. In order to improve the mechanical properties, mainly the shear strength, the incorporation of fibres randomly oriented in space, along with other fibres in the plane normal to the heat flux, might be an effective solution, despite the increase of the thermal conductivity, especially for high temperature applications.¹⁷⁷

In fact, the total thermal conductivity of silica aerogel composites can be adjusted accordingly to the inclination angle of embedded fibres, either in low or high temperature environments. Zhao and co-workers¹⁷⁸ reported the influence of the orientation of glass fibres, by varying the heat flux incident angle, φ , between 0° and 40° ($\varphi = 0^\circ$ when fibres are perpendicular relative to the heat direction): the thermal conductivity of aerogel composites increased from 20 to 55 $\text{mW m}^{-1} \text{K}^{-1}$, at 250 K, and from 80 to 195 $\text{mW m}^{-1} \text{K}^{-1}$, at 1250 K, as illustrated in Fig. 22a. Lu and co-workers¹³⁵ corroborated and complemented those findings by evaluating the effect of increasing the volume fraction of SiC fibres, oriented in the planes perpendicular and parallel to the heat flux, on the thermal conductivity of aerogel composites, with the perpendicular array being the best option for thermal insulation (Fig. 22b). Moreover, the difference in the plotted curves of the total thermal conductivity between the planes (the perpendicular and the parallel array of fibres) gradually increased along with the volume of fibres, due to the worst insulating properties of SiC fibres compared to the pristine silica aerogel matrix.¹³⁵

Fibre orientation also influences the mechanical properties of silica aerogel composites. The multilayer effect on silica aerogel composites was studied by Wu *et al.*,¹²⁰ using different combinations of glass fibre alignment (5–20 μm diameter and 3% volume). They were deposited longitudinally (L) and transversally (T), in six different designs (LLLL, LTLL, LLTT, LTLT, LTTL, and LTTT), added sequentially and permeated with a silica sol, as depicted in Fig. 23. All the fibre layers in the same direction (LLLL design) imparted to the composite the highest compressive strength, 3.70 MPa at 50% strain, more than two-

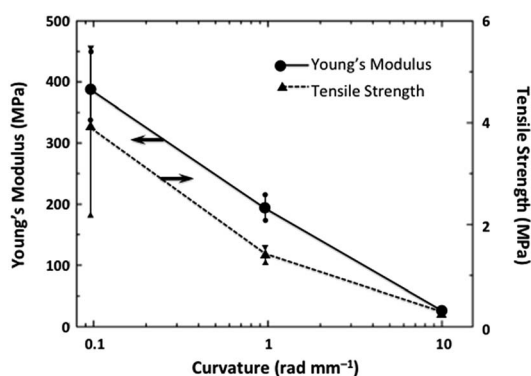


Fig. 21 Effect of the curvature of ceramic fibres on the tensile properties of silica aerogel composites (reprinted from ref. 235, copyright 2015, with permission from Elsevier).

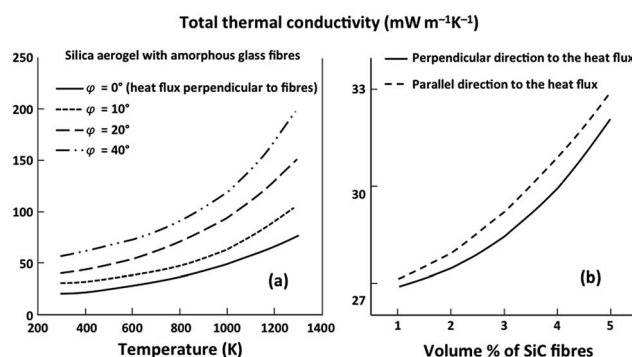


Fig. 22 Effect of fibre orientation on the thermal conductivity of silica aerogel composites: (a) thermal conductivity as a function of increasing temperature and varying the incident angle (φ) of heat flux in aerogel composites with amorphous glass fibres (adapted and reprinted from ref. 178, copyright 2012, with permission from Elsevier); (b) effect of SiC fibre volume fraction and preferential orientation on the total thermal conductivity, measured at 300 K (adapted and reprinted from ref. 135, copyright 2011, with permission from Elsevier).

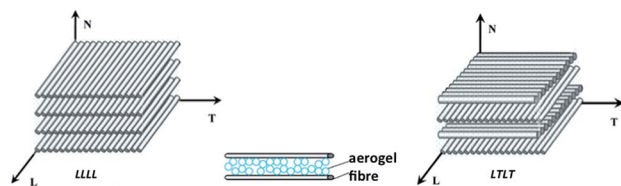


Fig. 23 Two examples of arrangement (LLLL and LTLT) of the six possible combination layers of aligned glass fibres permeated with a sol for the preparation of silica aerogel composites (reproduced and adapted from ref. 120, with permission from Taylor & Francis Ltd, <http://www.tandfonline.com>, copyright 2014).

fold relatively to the composite with alternate directions of fibre layers (LTLT), which withstood a load of 1.71 MPa. According to the authors, the perpendicular direction alignment between two adjacent layers might be prone to create weakened stress points.¹²⁰

As a conclusion of this topic, it can be stated that the thermal and mechanical behaviour of fibre-reinforced silica aerogels can be tailored to the intended application by design of fibre alignment, either to achieve optimal insulation features¹⁷⁷ or improved response in mechanical performance.^{119,120}

4 Applications of fibre–silica aerogel composites

The most important applications of fibre-reinforced silica aerogel composites are presented here.

4.1 Thermal insulation

According to our survey, thermal insulation is the preferred application of silica aerogel composites. Heat barriers must be highly porous materials, in order to display low thermal conductivity. Silica aerogel composites fulfill such a requisite.

Different fibrous matrices were/are used for aerogel reinforcement, which might enhance their applicability as thermal insulation barriers: glass fibres; ceramic fibres, such as xonotlite,¹³⁶ *Cerachrome*®, *Saffil*® or *Q-Fiber*® Felt;³ aramid fibres, such as *Nomex*®,³ or *Kevlar*®;^{121,167} zirconium dioxide;¹⁸⁶ polypropylene;¹²⁷ cellulosic nanofibres;²³⁸ cotton;¹⁹² and even flax.⁸³

Table 6 describes the relevant features of silica aerogel composites, when they have been envisioned for insulation purposes in room temperature environments. Some of the reported values therein were obtained from the graphical results reported in the cited literature. The presentation of the studies is ordered according to the drying technique used (SCD, freeze-drying (FD) or APD). Regarding the thermal conductivity results,

Table 6 Summary of the main properties of fibre–silica aerogel composites developed for insulation purposes at room temperatures

Fibres	Drying technique	ρ_b (kg m ⁻³)	Porosity (%)	Specific surface area (m ² g ⁻¹)	Thermal conductivity (mW m ⁻¹ K ⁻¹)	References
Pectin	SCD	130	92	827	14.2	Zhao <i>et al.</i> ¹⁵⁵
Cellulose nanofibers	SCD	142	—	525	15.3	Hayase <i>et al.</i> ³¹
Sepiolite	SCD	190	3.16 ^a	950	19.7	Li <i>et al.</i> ¹⁶⁴
Cellulose nanofibres	FD/SCD ^b	146	94	454	17.5	Zhao <i>et al.</i> ²⁴¹
Glass	FD	174	1.80 ^a	871	24.8	Zhou <i>et al.</i> ²⁴²
Tencel® (cellulosics)	APD	109	—	600–700	16.0	Jaxel <i>et al.</i> ⁴²
Cotton	APD	125	—	—	17.0	Rezaei <i>et al.</i> ¹⁹²
Aramid	APD	142	84	973	23.6	Li <i>et al.</i> ¹²¹
Glass	APD	142	88	964	23.2	Li <i>et al.</i> ¹⁶⁸
Carbon	APD	153	1.44 ^a	538	26.1	Ślosarczyk ²³²

^a The value refers to the pore volume (cm³ g⁻¹). ^b FD for the cellulose nanofibre scaffold, and SCD for the silica–nanofibre composite.

Table 7 Some properties of fibre–silica aerogel/xerogel composites applicable in high temperature environments

Fibre content	ρ_b (kg m ⁻³)	Upper limit of service temperature (°C)	Thermal conductivity (mW m ⁻¹ K ⁻¹)	Mechanical strength (MPa)	Special remarks	References
Glass (20 wt%) + TiO ₂ (20 wt%)	410	700	30	0.8 ^a	Silica aerogel powder, pressed at 1.5 MPa	Yuan <i>et al.</i> ²¹⁸
Glass (9.1 volume%)	129	650	22	1.4 ^b	Fibre batting; APD	Jiang <i>et al.</i> ⁸⁵
Mullite (20 wt%)	≈ 115	500	39	≈ 12.5 ^c	Mechanical strength > ≈ 4-fold than that of the native aerogel; APD	Liu <i>et al.</i> ²³⁰
Mullite (≈ 70 wt%)	450	1200	182	1.05 ^a	ZrO ₂ –SiO ₂ aerogel; pre-form of bound fibres, with 89% porosity; SCD	He <i>et al.</i> ²⁴³

^a Compressive strength. ^b Bending strength. ^c 3 point bending storage modulus.

it is generally perceived that a better insulation performance is accomplished by SCD, mainly related to the residual shrinkage during drying, thus yielding composites with higher porosity. Good results were as well achieved after freeze-drying. Nevertheless, very good results are disclosed with APD drying, revealing the beneficial effect of fibre embedment on inhibiting the loss of porosity during drying.

There is also a correlation between thermal conductivity and bulk density, as mentioned before: the insulation feature tends to deteriorate with increasing density, which might be attributed to a higher fraction of fibres.

Silica aerogel composites with inorganic fibres, developed under appropriate synthesis conditions (such as low pH, longer ageing times or surface modification), can inhibit extreme temperature heat transfer. These materials can be applied, for example, for protecting building steel frames during fires, thus preventing the structure from softening and collapse, as described by Motahari & Abolghasemi.²⁰⁸

Along with the effective thermal insulation at high temperature, high-tech applications also require efficient mechanical performance,^{135,179} which is affected by the skeletal rearrangement of aerogels induced by increasing temperature (the aforementioned aerogel's sintering). This phenomenon may result, for example, in a partial reduction of the Young's modulus.²¹²

Table 7 highlights some of the properties of aerogel composites developed for high temperature environments.

As previously mentioned, the compressive strength of unmodified silica aerogels (with a density of 96 kg m^{-3}) is approximately 0.04 MPa .¹⁸⁸ The mechanical performance of silica aerogel composites, even when subjected to high temperatures, remained significantly higher, this being a fundamental requisite for such application fields. Also, the bending strength of native silica aerogels with a density of $\approx 100 \text{ kg m}^{-3}$ is around 1 MPa ,²¹¹ which is below that observed by Jiang *et al.*⁸⁵ and Liu *et al.*²³⁰

As reported by Jiang *et al.*,⁸⁵ after reinforcement with glass fibres, and in spite of the temperature (650°C), silica composites can endure high mechanical strength, still being a superior insulating material, with a thermal conductivity of $22 \text{ mW m}^{-1} \text{ K}^{-1}$, which is below the thermal conductivity of free air under standard conditions.

4.2 Adsorption of harmful compounds

Farmer²³⁹ first reported the use of aerogels (carbon-based) in a pioneering technique for continuous removal of ionic

pollutants from aqueous streams, or deionization and electrochemical purification of brackish water ($\leq 5000 \text{ ppm}$). After polarization of the operating cell, through which the salty solution flows, the imposed field deflects anions and cations, which are then electro-sorbed by carbon aerogel electrodes, with surface areas increased up to $2600 \text{ m}^2 \text{ g}^{-1}$.²⁴⁰

Since then, the application of aerogels in environmental remediation has been an increasing practice,^{10,74} and the trend is also valid for silica aerogels with embedded fibres.^{244,245} The chemical versatility of silica aerogels (along with their rough surface and huge surface area) allows them to be tailored for specific adsorption purposes. For example, the grafting of non-polar groups decreases their surface energy, enhancing the interactions of aerogels with other non-polar species, such as polluting oils,^{246–248} as seen in Fig. 24.

That induced hydrophobicity enhances the buoyancy of aerogels in polluted waters, unlike several organic and natural sorbents, which are often used due to their known efficiency (such as low grade cotton, kapok or rice straw).²⁴⁹

In addition, the incorporation of small amounts of fibres in aerogels improves their mechanical performance, allowing the repeatability of adsorption and desorption processes.²⁴⁵

Table 8 summarises some of the available results on removal of organic pollutants from the environment, performed by silica aerogel composites with quite different fibrous materials.

Superhydrophobic materials were successfully developed, after a surface modification with TMCS in *n*-hexane: (i) a polyacrylonitrile–silica aerogel displayed a contact angle of 169° (6 h silylation treatment, at 40°C);²⁴⁵ (ii) an attapulgite–silica aerogel composite exhibited a contact angle of 153° (soaked for 36 h for silylation treatment, at 60°C).²⁴⁴ Additionally, Wei *et al.*²⁵⁰ evaluated the comparative performance of different fibres in terms of their chemical structure, concluding that the adsorption capacity for organic pollutants is around 6 to 8 times the composite weight.²⁵⁰ Slightly better performance was achieved with composites reinforced with hydrophobic fibres, as expected for non-polar pollutants.

In light of the results, fibre-reinforced silica aerogels are remarkable adsorbent materials. Moreover, Shi *et al.*²⁴⁵ stated that diesel oil adsorption/desorption processes could be repeated at least 100 times.

4.3 Acoustic insulation

Noise pollution has become a critical matter in people's daily life, a problem demanding more effective solutions in the prevention of health issues.²⁵¹ Aerogel-based sound attenuation barriers are among the related cutting edge technologies.²⁵²

Noise mitigation is dependent on material's thickness,²⁵³ interrelated with the wavelength: in order to attenuate a sound wave of wavelength λ , the thickness of each discrete insulation layer must be at least $\lambda/2$.¹⁶⁹

Sound wavelength increases with decreasing frequency, and hence, a low frequency range ($100\text{--}2000 \text{ Hz}$) requires thicker insulation barriers,²⁵⁴ diminishing the available and useful space, which can be particularly detrimental in confined spaces. Consequently, aerogel composites are the best-suited materials

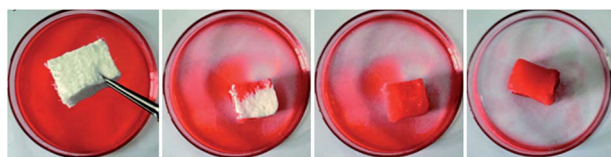


Fig. 24 Sorption of diesel oil by silica aerogels with 0.3 wt\% polyacrylonitrile fibres, within a minute of exposure (reproduced from ref. 245, published by The Royal Society of Chemistry, copyright 2017).

Table 8 Applicability of fibre–silica aerogel composites in environmental remediation

Fibre for aerogel reinforcement	ρ_b (kg m ⁻³)	Surface area (m ² g ⁻¹)	Porosity (%)	Pore volume (cm ³ g ⁻¹)	Pore diameter	Contact angle	Adsorbate	Sorption capacity (g g ⁻¹)	References
Polyacrylonitrile	86	≈ 230	95	5.56	5–20 μm	169°	Diesel oil	9.6	Shi <i>et al.</i> ²⁴⁵
							Acetone	>12	
							Nitrobenzene	>13	
							Paraxylene	>12	
							Tetrahydrofuran	>13	
							N-Methyl-2-pyrrolidone	14.7	
							Toluene	>9	
							N-Hexane	>6	
Attapulgate	550 ^a	594	75	2.15	84.7 nm	153°	Vegetable oil	>9	Zhang <i>et al.</i> ²⁴⁴
							Petroleum hydrocarbons	5.0	
Polyester	625	805	68	1.09	—	—	Benzene	>7	Wei <i>et al.</i> ²⁵⁰
							Toluene	>6.5	
Polypropylene	716	823	63	0.88	—	—	Benzene	>8	
							Toluene	>6.5	
Lignin	678	805	65	0.96	—	—	Benzene	>6	
							Toluene	>6	
Polyacrylonitrile	703	841	64	0.91	—	—	Benzene	>6	
							Toluene	>6.5	

^a Apparent density.

for the insulation of low frequencies, due to their efficiency at reduced thickness.¹⁶⁹

The porous nature of silica aerogels, which hinders heat transfer, is also an ideal feature to achieve effective acoustic insulation.^{4,5} The sound attenuation relies on the fraction of energy loss, since the acoustic waves are successively transferred through the gas and solid phases, gradually reducing their amplitude.²⁵⁵

The acoustic insulation provided by aerogels is a function of several factors, related to the preparation procedures: material's density, interstitial gas pressure and their overall texture.²⁵⁵ For example, surface roughness and larger pores are advantageous features.^{256,257} This was demonstrated by Martin and colleagues,²⁵⁶ in their work on the development of silica aerogels by using polyethylene glycol (PEG) to control pore dimensions. Polymers are known to be used as porogen additives, allowing controlled design of hierarchically porous materials.⁷² For example, by increasing the concentration of high molecular weight PEG in the sol, aerogels with higher pore dimensions can be produced.^{72,256} The sound velocity across native aerogels was reported as 241.0 m s⁻¹, being reduced to 103.2 m s⁻¹ after PEG addition at a concentration of 10.2 mg L⁻¹.²⁵⁶

Similar to the heat transport, there is a relationship between sound propagation and aerogel's density,⁶⁵ according to eqn (8):

$$V_{\text{sound}} \propto \rho_b^\alpha, \alpha \approx 1.0 \dots 1.4 \quad (8)$$

The propagation speed of longitudinal sound waves through native silica aerogels is typically 100 m s⁻¹, for densities around 100 kg m⁻³.^{258–260} In the case of extremely light aerogels, for instance with 5 kg m⁻³, a sound velocity of 20 m s⁻¹ was

reported by Groß and co-workers,⁷⁰ although this value had been achieved after aerogel's evacuation.

In spite of the improvement of acoustic insulation with the decrease of aerogels' density, their inherent fragility poses difficulties for most end applications.²⁵⁹ The incorporation of fibres makes possible easy handling, allowing the applicability of lighter aerogels to be extended, while endowing the materials with a higher degree of flexibility. By using polyethylene terephthalate (PET) nonwoven fabric with 5 mm thickness and a density of 37 kg m⁻³, flexible PET–silica aerogel insulation blankets were manufactured with two different methods: (1) by pouring the silica sol over the nonwoven fibre mat before gelation and (2) by dipping the fibrous mat into a dispersion of ethanol and hydrogel granules that were already aged.²⁶¹ In the last method, the sol was allowed to gel and, after gelation, it was subsequently broken into particles by ultrasonication, which were then aged in an ethanol bath.²⁶¹ The purpose of Oh *et al.*'s²⁶¹ work was to simplify aerogel production processes, mainly in terms of costs, since aerogel granulates can be used to build effective insulator systems,^{115,262} being less expensive than monolithic aerogels.^{262–264} The composites developed with the first method were actually the most effective in acoustic insulation, especially at frequencies between 1000 and 6000 Hz. The analyses were performed in terms of sound absorption coefficient, described as the fraction of sound energy absorbed by a material, with values ranging between 0 and 1 (1 – perfect absorber). At frequencies of 2000 and 5000 Hz, the samples developed with method 2 (ρ_b around 158 kg m⁻³) displayed a value of ≈ 0.2, while in method 1 (composites at ρ_b around 65 kg m⁻³) it was >0.4.²⁶¹

An aerogel composite based on polyacrylonitrile and silica electrospun nanofibres (with apparent density = 9.6 kg m^{-3}), developed under freeze-drying and cross-linked with heat treatment, featured better insulation performance compared to a highly commercial insulating fabric made from polypropylene fibres, adequate to coat the passenger compartment of transport vehicles. This study of Si and colleagues¹⁶⁰ was carried out with aerogel composites of 5 mm thickness and an areal density of 48 g m^{-2} ; the commercial insulating material was twice thicker, with an areal density of 210 g m^{-2} .

Motahari and colleagues¹⁶⁹ used a cotton fibre nonwoven mat (with an areal density of 800 g m^{-2} and 1 cm thickness) as the support matrix to synthesise *in situ* silica aerogels, and assessed the influence of the molar ratio of MeOH/TEOS and ageing time on the composites' sound absorption. The mass of the aerogel in the samples was around 45%. The performance of a composite with a density of 88 kg m^{-3} (molar ratio of 11 and aged for 24 h) was significantly better than that of the original fibrous matting (more than 1-fold, on average), mainly at frequencies below 2000 Hz.¹⁶⁹

Feng and co-workers²³ manufactured silica aerogel composites (1 cm thickness) with cellulose fibres recycled from paper waste. The best performance in sound attenuation was achieved at 2 wt% fibre concentration and 146 kg m^{-3} density. According to the authors, the coefficient of sound absorption reached 0.5, a higher value compared to that of the commercial polystyrene foams. Moreover, researchers claimed that the cellulose-silica composites have the potential to be scaled up for industrial dimensions, with the interest in them relying on cost-effectiveness and higher degrees of flexibility.

In a practical way, silica aerogels embedded with fibres can be tailored to be used as efficient sound barriers with reduced thickness compared to the commonly applied materials, such as rock wool panels or polystyrene foam, broadening the applicability of aerogels where the space for insulation is limited.^{23,265}

4.4 Sensors

The low refractive index of silica aerogels can be harnessed for the development of sensing devices, for example, to be used in waveguides and for supporting the performance of optical fibres.²⁶⁶ Due to the total reflection phenomenon, a light beam can travel long distances within optical fibres, which are known as well for their immunity against electronic interference and ionizing radiation, large bandwidth, signal accuracy and for being light weight and flexible.^{267–269}

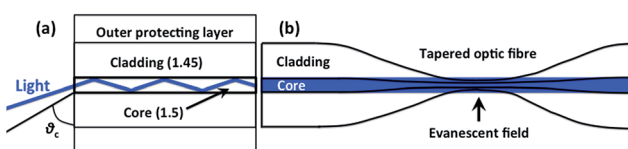


Fig. 25 Optical fibres: (a) total internal reflection within the fibres due to the difference of refractive index between the core and cladding; (b) tapered fibre and the evanescent field.

Conventional optical fibres have thick walls, the cladding, which has a smaller refractive index in comparison to the core. So, light is successively reflected inside the core, providing that the beam refraction angle exceeds the critical angle (θ_c), as sketched out in Fig. 25a. When the light is totally confined to the waveguide region, the optical fibres are the blueprint adequate to the communication field,²⁶⁶ but such a design hinders their application in other sensing mechanisms. On the other hand, if the light would be able to surpass the boundaries of the travelling area, even in a small portion, it could interact with the surrounding environment, for example, by means of scattering, absorption or fluorescence.^{268,270} This is the case of evanescent field sensing performed by tapered fibres, or tapers,²⁷⁰ of which an example is drafted in Fig. 25b. This type of optical fibre is used as a sensor of temperature, external refractive index,^{271,272} optical properties of materials,²⁷⁰ in extended environmental monitoring^{268,272} or clinical diagnosis.²⁶⁸

Tapered fibres are optical fibres stretched over a defined length into thinner diameters, as displayed in Fig. 25b, in which the sensing mechanism occurs through the so-called evanescent field: around the fibre's waist, an oscillating field of released energy is generated, remaining spatially concentrated in the vicinity of the source.²⁶⁶

After the high temperature stretching processes to narrow the waveguide of glass fibres, the inherent fragility of those materials is further increased, as the radial dimensions can be diminished from $125 \mu\text{m}$ to a few hundreds of nanometres.²⁶⁶ The evanescent region can be as thin as less than $1 \mu\text{m}$, and therefore is quite prone to contamination or to be damaged.²⁷⁰ Therefore, a suitable shield is necessary in order to protect the sensing properties of the evanescent field, for example, from the influence of dust or environment water.^{266,270} Silica aerogels provide the ideal protection: their high porosity and absorptive properties, combined with hydrophobic functionalization, are the sought features. Moreover, a hydrophobic aerogel can be used in the evanescent field for detection of dissolved gases in water.²⁶⁶ But the more important related property is the low refractive index of silica aerogels, and hence they do not interfere significantly with light emissions in the evanescent field.^{266,273}

Additionally to the embedment of optical fibres in aerogels,^{266,273} either by sol-gel coating²⁷⁰ or by laying the fibres on aerogel's surface,²⁷⁴ another version of the applicability of aerogels in this technical field is by filling their hollow-core with the sol, allowing *in situ* aerogel synthesis.²⁶⁶ Despite the unusual manufacture of such silica aerogel composites, according to Grogan²⁶⁶ this conception of waveguide allows broader tailoring of the optical sensor properties, such as the control of the flow of light.

The earlier mentioned polyacrylonitrile-silica aerogel composites, developed by Si and co-workers,¹⁶⁰ revealed elasticity-responsive electrical conduction. The electrically conductive carbon fibres were obtained after carbonization of composites, by using the polyacrylonitrile electrospun nanofibres as the precursor for the graphitised carbon, with the electrical conductivity value reported as 0.25 S cm^{-1} . The

flexible composite was connected to a flash light-emitting diode in a 3 V circuit; when subjecting the composites to a stress load up to 50% of compressive strain, the normalized electrical resistance decreased by 70%. The researchers attributed this decrease in electric resistance to temporary contact established between fibres during compression, adding new electrical conduction paths. In spite of the broad availability of pressure sensors, silica aerogel composites may also have a role in this application, as described here.

Chemiresistor gas/vapour sensors were prepared by Boday and co-workers,⁶⁸ by imparting electrical conductivity to a silica aerogel through the addition of polyaniline nanofibres. The work aimed at the application of these silica aerogel composites in the detection of acidic (HCl) and basic (NH₃) gaseous molecules in the environment. The time response accomplished by composites with 9.6 wt% polyaniline nanofibres was similar to that of thin sensor films cast on electrodes, in which the concentration of polyaniline needed to be significantly higher (several orders of magnitude). Moreover, while the time response of thin films decreased with thickness, the performance of polyaniline–silica aerogels was independent of the layer thickness, allowing this way thicker materials, hence easier handling of detection materials. The researchers hypothesized that the speed of response and sensitivity of the polyaniline nanofiber–silica aerogel composites could be attributed to more open mesoporosity and increased surface areas, around two orders of magnitude higher than those of the film of polyaniline fibers. Boday *et al.*⁶⁸ also mentioned that polyaniline–silica aerogel composites, with 16.5 wt% polyaniline nanofibres, displayed higher electrical conductivity values than a polyvinyl alcohol aerogel loaded with 12 mg L^{−1} of carbon nanotubes.

4.5 Technical and protective apparel

The concept of conventional insulation clothing is based on airy textile structures (non-woven fabrics), flexible foams (polyurethane layers) or fibres with a hollow core. Higher thermal insulation performance requires higher thickness (successive layers of fabric or foam), which might restrain the user's movements.¹³⁹

Aerogels are indeed a major breakthrough when applied to apparel, due to their proved efficiency at reduced thickness. Fabrics with integrated aerogels can provide up to six times more insulation performance, with the same fabric thickness, than conventional insulating clothing.¹³⁹ Aerogel based materials encompass the needed features to be used for protection from thermal and electric hazards, to protect workers exposed to molten substances or from flames or radiant heat.³³

Aspen Aerogels Inc. led the manufacturing of aerogel blankets, whose industrial production started around 2003,⁸⁰ with the insulation products resembling textile-like materials.¹²³ The production techniques involve alkoxysilane precursors and CO₂ supercritical drying,⁸³ with the product being around 10 times more expensive than conventional materials with the same level of insulation.¹³² Notwithstanding, when it comes to people operating in an extreme temperature environment, it is quite

important neither to compromise the functional performance of the protective apparel nor hamper the action of users.⁵ Two examples are presented below.

A cold-water diving suit with incorporated aerogel exhibited $\approx 76\%$ improved thermal insulation, compared to a market standard material with a similar thickness, generally used for cold weather clothing (a micro-fibrous polypropylene batting). During the same study, another comparison was made with neoprene foam, which is generally used in wetsuits, revealing a 5-fold improvement for the silica aerogel composite. The solution developed by *Aspen Aerogels* consists in the embedment of the aerogel in a nonwoven fabric in the inner layer of the diving suit, providing a thermal resistance of 12 to 14 clo(†), depending on the measurement under different pressure conditions. Additionally, the thermal performance of this aerogel-based garment did not exhibit a significant loss with a soft laundering maintenance.²⁷⁵

The extreme weather conditions experienced by mountain climbers were also assessed with an *Aspen Aerogels* product, known as *Pyrogel®*. As stated by Ananthan *et al.*,⁵ after three Mont Blanc routes, two climbers reported the unexpected no cold sensation, at severe temperatures of -20 to -25 °C and a wind speed of 70–80 km h^{−1}.

Other studies aimed at better protection of fire fighters during their exigent duties. Aerogel blankets, with applicability in fire fighters' protective clothing, were developed by formation of a silica network within a *meta*-aramid fibrous batting. The composites, dried at ambient pressure, were subjected to silylation treatment with TMCS, imparting hydrophobicity, decreased density and consequently better results in thermal insulation. After a comparative evaluation with conventional non-aerogel blankets, the silica aerogel blankets revealed an increased protection of 58% regarding burn injury hazard.³³

Aerogel based materials prevent heat flux, which is advantageous for inhibiting the incoming heat, but may hinder the necessary heat exchange balance of the human body.^{276,277} Shaid and co-workers²⁷⁸ evaluated the heat stress of fire fighters, when the body temperature rises beyond the safe limits. In their approach, they combined the use of aerogel particles along with phase change materials (PCMs). PCMs have the ability to store and release heat according to the changing environment temperature. A mixture of a dispersion of nanoporous aerogel particles, melted eicosane (an organic PCM with a phase transition temperature around 37 °C) and a coating textile binder was applied to the inner layer of the *Nomex®* fabric(‡), by an impregnation process. The aerogel particles and the binder paste were applied to the outer layer of the *Nomex®* fabric. PCMs absorbed metabolic heat, circumventing the reduction of heat exchange that results from the almost null permeability of

† Clothing insulation can be expressed in clo units. 1 clo is the thermal resistance assigned as $0.155 \text{ m}^2 \text{ K W}^{-1}$, where 1 clo represents the insulation of a suit provided to a resting man to maintain the comfort at 21.1 °C, with a relative humidity of less than 50% and an air velocity of 0.102 m s^{-1} .³⁰⁹

‡ *Nomex®* is the commercial brand of an aramid fibre with *meta*-oriented linkages, stable at a temperature as high as 500 °C for small periods of time; for long term exposure, it can withstand until 220 °C.¹⁸⁵

the aerogel treated fabric. According to the authors, the aerogel/PCM mixture proved to be efficient for fire fighters' equipment, since the time until the pain threshold (when the human body temperature rises up to 44 °C) was delayed by more than 2-fold.²⁷⁸ The advantages of silica aerogel porosity for the infiltration of melt PCMs for textile thermoregulatory applications are thoroughly detailed in other studies.^{279,280}

Another benefit of the aerogel-based fabrics is their relatively reduced thickness, hence less bulky aesthetic appearance, which allows adding design to protective clothing, for example, in ski suits.¹³⁹

4.6 Other applications

According to several authors,^{16,153,281–283} silica aerogels reinforced with ceramic quartz fibre felt can provide a structural frame for the encapsulation of enzymes, allowing their use for repeated cycles.^{153,281} Enzymes were added to the silica sol before gelation and the gel was supercritically dried with CO₂. The aerogel encapsulation technique potentiates a homogeneous dispersion of enzymes,¹⁶ enabling higher concentrations, as well as the enhancement of the catalytic activity per mass of enzyme.¹⁵³ The enzymes studied were lipases, used for the esterification of lauric acid with 1-octanol,^{153,281} transesterification of sunflower seed oil with methyl acetate¹⁶ and methanol,²⁸² and partial transesterification of sunflower oil with ethanol.²⁸³

Karout and co-workers¹⁵³ also tried to use carbon fibre felt in this context, which they claimed to provide extra reinforcement to silica aerogels. In terms of catalytic activity, the results were as good as those obtained by enzyme encapsulation in aerogels reinforced with ceramic fibre felt. However, the authors reported that hydrophobic carbon felt performed better with silica precursors with high ratio of hydrophobic groups, while ceramic felt should be preferentially used to strengthen aerogels synthesised with low proportion of hydrophobic groups.¹⁵³

Other applications of silica aerogels reinforced with fibres are mentioned in the literature as filtering media,^{13,160} corrosion resistant insulators,²⁸⁴ separators of electric charged materials,^{160,285} shock absorbers²⁸⁶ or even tissue engineering scaffolds.^{160,287}

Also, the non-toxic nature of silica aerogels and sufficient biocompatibility with mammals allow them to be used in the pharmaceutical industry, for example as supports of controlled drug delivery.^{287–289}

5 New trends and future perspectives

Apart from the well-established method of fibre embedment, another emerging way to develop flexible and reinforced aerogel composites is through the scaffold concept. It consists of a two-step manufacturing process, starting with the assembly of a macro-porous solid template (either a rigid or flexible structure), which in turn will be dipped in the silica sol that undergoes gelation, filling with a nanostructured matrix the macropores of the template. As an example, Mahadik *et al.*²⁸⁴ used 2-ethylhexyl acrylate for the scaffold synthesis, and MTMS

as the silica precursor. Both networks remained closely adhered, surrounded by each other without additional chemical bonds. Flexible composites were developed, encompassing super-hydrophobicity (165°), low density (123 kg m⁻³) and low thermal conductivity ($\approx 45 \text{ mW m}^{-1} \text{ K}^{-1}$).

Cellulose derived scaffolds, often involving the freeze-drying technique in their manufacture,^{46,241,290} are also being used as silica aerogel reinforcement frameworks. The broad availability of a renewable source might suggest a more sustainable approach of the concept, but among the current drying technologies, freeze-drying is considered too expensive due to its inefficiency in energy consumption.²⁹¹ Nonetheless, in the scientific research domain, good results can be found for silica aerogels reinforced with cellulose templates, both in terms of robustness and thermal insulation (in spite of the unmodified freeze-dried nanofibrous scaffolds typically encompassing high values of thermal conductivity²⁹²). Zhao and co-workers²⁴¹ developed a silylated framework, by adding MTMS to an aqueous suspension of nanofibrillated cellulose (with such a modification, the authors intended as well to further improve the adhesion between the scaffold and the aerogel particles); after that, the silica sol at the onset of gelation was cast into a mould containing the previously prepared scaffold. Additionally, the gels were subjected to a hydrophobic treatment with HMDZ and supercritically dried. The composites displayed super-insulating properties (less than $20 \text{ mW m}^{-1} \text{ K}^{-1}$), and the compressive modulus increased by 55% and maximum tensile strength increased by 126%, compared to the 100% silica aerogel reference sample.²⁴¹

Other researchers were inspired by nature, by mimicking birds' nests.^{243,293} Birds developed the expeditious technique of filling the tree branch structures with highly insulating materials, such as feathers or animal wool, decreasing the lap-branch holes to below the mean free path of air. The aerogel mimic was achieved with mullite fibres, as the macrostructure, and silica–boron²⁹³ or silica–zirconia²⁴³ sols to fill the interstices. High performance materials were then synthesised, able to endure load stress and extreme temperatures. For example, in terms of compressive strength, an increase up to 1.05 MPa was reported, around ten-fold compared to the reference pristine aerogel,²⁴³ or improved flexibility, with the limit of elastic region defined at 2.2 MPa (more than two fold in comparison with silica aerogels), and rebound resilience at 2.0 MPa, still performing at $\approx 86\%$, even when subjected to an environment of 1000 °C.²⁹³ Moreover, it has been recently accepted that ceramic nanocrystalline nanofibres combine the high aspect ratio with a nanometer-sized grain, encompassing the needed flexibility to be used for 3D elastic assemblies.¹⁹⁰

After this exhaustive literature survey, there is absolutely no doubt over the huge potential of silica aerogels, mainly for insulation purposes.²⁹⁴ According to Koebel *et al.*,¹⁴⁰ “buildings are a tremendous market opportunity”, since transport enterprises have been investing in energy efficient systems, mainly for economic motivations. Now, as the climate change protocols demand for diminished CO₂ emissions²⁹⁵ along with EU Directives on building energy efficiency,²⁹⁶ heating, ventilation and air conditioning of buildings remain as the tackling

issues,¹⁴⁰ and so insulating materials with improved efficiency are effervescently sought.^{284,297}

Vacuum insulation panels (VIPs)^{140,298,299} and aerogels^{140,294,298} were accepted as being the cutting edge technology in this context, whose typical values of thermal conductivity are around 4 and 13 mW m⁻¹ K⁻¹, respectively. Both materials are very expensive, but VIPs seem to be more cost-effective,²⁹⁸ with their use being suggested in the retrofit of public historic buildings (even if it was with some restrictions).²⁹⁹ However, the thermal conductivity of VIPs tends to deteriorate with ageing, due to moisture and air penetration by diffusion,^{140,298} while aerogels can be made hydrophobic, with no loss of performance due to ageing.²⁹⁸

Currently, the aerogel market provides high value-added products, in areas that justify their cost,²⁹⁸ mainly in the form of aerogel blankets, as mentioned above (Section 3.1).

It is predicted that, in near future, the decreased costs of aerogels will propel their use as the main insulation resource; in 2008, the cost of an aerogel was \approx £ 3000 m⁻³, and it is estimated that, by 2050, its price will fall below £500 m⁻³.³⁰⁰

Several strategies have been already implemented to improve aerogels' cost-effectiveness:

(1) Cost-effective precursors, as is the case of sodium silicate,^{4,46} or those retrieved from agro-industrial wastes, such as rice hull ash;⁴

(2) Diversification of aerogel reinforcement materials, taking into account their availability and footprint,¹⁶² favouring those obtained from wastes^{23,83} or other industrial by-products;¹⁵⁹

(3) Simplified processes that decrease the manufacturing time and reduce wastes;^{41,46,301}

(4) APD;^{40,300}

(5) For specific needs only accomplished with SCD, the CO₂ fluid might be a sustainable option.^{89,302} This is not, however, a consensual conclusion. According to a life cycle assessment (on the laboratory scale) for silica aerogels synthesized under high and low temperature SCD, the greater environmental burdens (both in energy consumption and in CO₂ emissions) were due to the CO₂ SCD aerogels.³⁰³

A recent successful case of aerogel technology transfer from the laboratory to market, due to a cost reduction of \approx 70% (although in a granular form; brand-named *Quartzene*®), is a material synthesised with affordable precursors and APD. Also, according to the authors, their manufacture is environmentally friendly.³⁰⁴

5.1 Final considerations

Aerogels are viewed as a new class of materials in terms of their chemical architecture,⁵⁸ being some of the most promising nanomaterials for effective insulation barriers, also taking advantage of non-flammable properties of silica.²⁶⁵ However, aerogels' inherent friability derived from the porous structure, and current prohibitive manufacturing costs, impairs their uptake by the market.^{115,294}

Fibre embedment in silica aerogels imparts additional strength to the composites, while acting as starting spots for the development of colloidal networks during the gelation event.⁶⁸ Thus, fibres tend to act as nucleation agents,⁶⁸ diminishing manufacturing time and ultimately the price of aerogels.

However, further research is needed to fully assess the effect of the presence of fibres during gelation and correlate the porous nanostructure features with the type/properties of fibres and the possible chemical interaction between the two phases. This can be performed by using high-resolution microscopy techniques and molecular modelling studies. In fact, the outstanding thermal insulation performance of silica aerogels relies on their nanoporous structure. Thus, any change of the silica network that causes the enlargement of pores may have a detrimental effect on the insulation performance of aerogels, and must be prevented. Their high thermal efficiency at reduced thickness makes them appropriate in cases of space limitation, as can be the case of retrofitting of important old building facades,^{305,306} where the requirements of historical preservation include the maintenance of their appearance.

The production of large-scale silica aerogel monolithic shapes can be better accomplished with extra reinforcement, by following the composite approach, involving the embedment of fibrous materials, mainly in the matt form, but also after fibre dispersion in the initial sol.^{83,307} Besides the already implemented industrial processes (for example, *Aspen Inc.*, *Cabot Corporation*, and *Nano High-Tech Co., Ltd*), novel methodologies are being researched at the laboratory domain to scale-up aerogel manufacture.^{115,241,308}

As already exposed, aerogel syntheses have numerous constraints and are difficult to control, which often cause the lack of a standardised product.²⁹⁴ But there are promising scenarios: a patented process of the French company *SEPAREX S.A.*, involving SCD, allows greater uniformity of the internal structure and better results in terms of thermal conductivity.²⁹⁴ Another solution may be the evacuation and sealing of silica aerogels, which can reduce their thermal conductivity by 50%,¹³⁹ a possible way of circumventing the loss of insulation performance due to fibre addition, considering the composite approach.

The traditional insulation materials, either in the form of mineral fibre panels or polymeric foams, currently account for the largest market shares, due to their relatively accessible costs and high moisture resistance.²³ In line with an European report on aerogels,²⁹⁴ the focus of public-funded research should be geared towards increasing the market attractiveness, capitalising on aerogels' unique features. As referred by Fricke²⁵⁸ (going back to 1992), there is a need for effective environmentally friendly, non-hazardous, non-inflammable thermal insulation materials to replace polymeric foams. The frenetic scientific research in silica aerogels with embedded fibres is in pursuit of those goals.

Also, the successful development of such auspicious materials may provide unexpected insights for new advanced applications, for example, as novel drug carriers, either for agriculture or health applications, tackling the two most important sectors of growing worldwide population.

Disclaimer

The mention to enterprises or market products does not stand for recommendation or endorsement by the authors nor by the Royal Society of Chemistry.

Conflicts of interest

There are no conflicts to declare.

Acknowledgements

The authors acknowledge Professors Maria Helena Gil, António Portugal and Jorge Coelho for their support in the improvement of the text. Funding: this work was funded by Fundação para a Ciência e Tecnologia, I.P., through a doctoral degree grant [SFRH/BD/131819/2017]; this work was also supported by the European Regional Development Fund (ERDF), through COMPETE 2020 – Operational Programme for Competitiveness and Internationalization, combined with Portuguese National Funds, through Fundação para a Ciência e Tecnologia, I.P. [POCI-01-0145-FEDER-006910 (UID/EQU/00102/2013); POCI-01-0145-FEDER-007136 (UID/CTM/00264/2013)].

References

- 1 A. Taher, *The Sunday Times*, 2007.
- 2 N. Hüsing and U. Schubert, *Angew. Chem., Int. Ed.*, 1998, **37**, 22–45.
- 3 D. V. Fomitchev, R. Trifu and G. Gould, in *Engineering Construction and Operations in Challenging Environments Earth and Space 2004: Proceedings of the Ninth Biennial ASCE Aerospace Division International Conference*, ed. R. B. Malia and A. Maji, ASCE, Texas, 2004, pp. 968–975.
- 4 A. C. Pierre and A. Rigacci, in *Aerogels Handbook*, ed. M. A. Aegerter, N. Leventis and M. M. Koebel, Springer Science+Business Media, New York, 2011, pp. 21–45.
- 5 Y. Ananthan, K. Sanghamitra and N. Hebalkar, in *Nanotechnology for Energy Sustainability*, eds. B. Raj, M. Van de Voorde and Y. Mahajan, Wiley-VHC, Weinheim, 2017, pp. 939–966.
- 6 M. A. Hasan, R. Sangashetty, A. C. M. Esther, S. B. Patil, B. N. Sherikar and A. Dey, *J. Inst. Eng. (India): Ser. D*, 2017, **98**, 297–304.
- 7 A. V. Rao, M. M. Kulkarni, G. M. Pajonk, D. P. Amalnerkar and T. Seth, *J. Sol-Gel Sci. Technol.*, 2003, **27**, 103–109.
- 8 S. Henning and L. Svensson, *Phys. Scr.*, 1981, **23**, 697–702.
- 9 S. Yun, H. Luo and Y. Gao, *J. Mater. Chem. A*, 2015, **3**, 3390–3398.
- 10 J. P. Vareda, A. J. M. Valente and L. Durães, *Adv. Colloid Interface Sci.*, 2016, **237**, 1–15.
- 11 M. S. Jalali, S. Kumar, M. Madani and N. F. Tzeng, in *2013 IEEE Sensors Applications Symposium (SAS 2013) Proceedings*, IEEE, Galveston, 2013, pp. 133–136.
- 12 S. S. Prakash, C. J. Sankaran, A. J. Hurd and S. M. Rao, *Nature*, 1995, **374**, 439–443.
- 13 Z. Pakowski and K. Maciszewska, *Inz. Chem. Procesowa*, 2004, **25**, 1435–1441.
- 14 G. Poelz and R. Riethmüller, *Nucl. Instrum. Methods*, 1982, **195**, 491–503.
- 15 K. Ota and J. Inoue, in *Extreme Ultraviolet (EUV) Lithography IV*, ed. P. P. Naulleau, SPIE, San Jose, CA, 2013, vol. 8679, pp. 86792R-1–86792R-10.
- 16 O. Orçaire, P. Buisson and A. C. Pierre, *J. Mol. Catal. B: Enzym.*, 2006, **42**, 106–113.
- 17 C. C. Li, Y. T. Chen, Y. T. Lin, S. F. Sie and Y. W. Chen-Yang, *Colloids Surf., B*, 2014, **115**, 191–196.
- 18 P. C. Thapliyal and K. Singh, *J. Mater.*, 2014, **2014**, 10.
- 19 M. F. Mora, S. M. Jones, J. Creamer and P. A. Willis, *Electrophoresis*, 2018, **39**, 620–625.
- 20 Z. Qi, D. Huang, S. He, H. Yang, Y. Hu, L. Li and H. Zhang, *J. Eng. Fibers Fabr.*, 2013, **8**, 134–139.
- 21 I. Michaeloudis, Can we put the sky into a bottle?, https://www.youtube.com/watch?v=prWpMLB_2Xw.
- 22 Method for production of flexible panels of hydrophobic aerogel reinforced with fibre felts, WO2015016730A2, 2015, 1–7.
- 23 J. Feng, D. Le, S. T. Nguyen, V. Tan Chin Nien, D. Jewell and H. M. Duong, *Colloids Surf., A*, 2016, **506**, 298–305.
- 24 X. Lu, M. C. Arduini-Schuster, J. Kuhn, O. Nilsson, J. Fricke and R. W. Pekala, *Science*, 1992, **255**, 971–972.
- 25 Y. Pan, S. He, L. Gong, X. Cheng, C. Li, Z. Li, Z. Liu and H. Zhang, *Mater. Des.*, 2017, **113**, 246–253.
- 26 H. Liu, X. Xia, Q. Ai, X. Xie and C. Sun, *Exp. Therm. Fluid Sci.*, 2017, **84**, 67–77.
- 27 H. Zhang, W. Z. Fang, X. Wang, Y. M. Li and W. Q. Tao, *Int. J. Heat Mass Transfer*, 2017, **115**, 21–31.
- 28 Y. J. Dai, Y. Q. Tang, W. Z. Fang, H. Zhang and W. Q. Tao, *Appl. Therm. Eng.*, 2018, **128**, 1634–1645.
- 29 X. Hou, R. Zhang and B. Wang, *Ceram. Int.*, 2018, **44**, 15440–15445.
- 30 J. Paik, J. Sakamoto and S. Jones, *NASA Tech Briefs*, 2008, pp. 18–19.
- 31 G. Hayase, K. Kanamori, K. Abe, H. Yano, A. Maeno and H. Kaji, *ACS Appl. Mater. Interfaces*, 2014, **6**, 9466–9471.
- 32 J. Laskowski, B. Milow and L. Ratke, *J. Supercrit. Fluids*, 2015, **106**, 93–99.
- 33 S. Chakraborty, A. A. Pisal, V. K. Kothari and A. V. Rao, *Adv. Mater. Sci. Eng.*, 2016, **2016**, 1–8.
- 34 M. M. Koebel, A. Rigacci and P. Achard, in *Aerogels Handbook*, ed. M. A. Aegerter, N. Leventis and M. M. Koebel, Springer Science+Business Media, New York, 2011, pp. 607–633.
- 35 L. Durães, A. Maia and A. Portugal, *J. Supercrit. Fluids*, 2015, **106**, 85–92.
- 36 M. Sachithanadam and S. C. Joshi, *Silica Aerogel Composites Novel Fabrication Methods*, Springer, Singapore, 2016.
- 37 J. Li, Y. Lei, D. Xu, F. Liu, J. Li, A. Sun, J. Guo and G. Xu, *J. Sol-Gel Sci. Technol.*, 2017, **82**, 702–711.
- 38 A. Demilecamps, C. Beauger, C. Hildenbrand, A. Rigacci and T. Budtova, *Carbohydr. Polym.*, 2015, **122**, 293–300.
- 39 W. Hu, M. Li, W. Chen, N. Zhang, B. Li, M. Wang and Z. Zhao, *Colloids Surf., A*, 2016, **501**, 83–91.
- 40 Z. Shao, X. He, X. Cheng and Y. Zhang, *Mater. Lett.*, 2017, **204**, 93–96.
- 41 X. Wu, G. Shao, S. Liu, X. Shen, S. Cui and X. Chen, *Powder Technol.*, 2017, **312**, 1–10.
- 42 J. Jaxel, G. Markevicius, A. Rigacci and T. Budtova, *Composites, Part A*, 2017, **103**, 113–121.

- 43 J. K. Floess, R. Field and S. Rouanet, *J. Non-Cryst. Solids*, 2001, **285**, 101–108.
- 44 H. Maleki, L. Durães and A. Portugal, *J. Non-Cryst. Solids*, 2014, **385**, 55–74.
- 45 A. E. Danks, S. R. Hall and Z. Schnepf, *Mater. Horiz.*, 2016, **3**, 91–112.
- 46 J. Fu, S. Wang, C. He, Z. Lu, J. Huang and Z. Chen, *Carbohydr. Polym.*, 2016, **147**, 89–96.
- 47 K. E. Parmenter and F. Milstein, *J. Non-Cryst. Solids*, 1998, 179–189.
- 48 M. A. B. Meador, S. L. Vivod, L. McCorkle, D. Quade, R. M. Sullivan, L. J. Ghosn, N. Clark and L. A. Capadona, *J. Mater. Chem.*, 2008, **18**, 1843.
- 49 Z. Qian, Z. Wang, N. Zhao and J. Xu, *Macromol. Rapid Commun.*, 2018, 1700724, 1–16.
- 50 N. Lavoine and L. Bergström, *J. Mater. Chem. A*, 2017, **5**, 16105–16117.
- 51 A. Ślosarczyk, *Nanomaterials*, 2017, **7**, 44.
- 52 K. J. De France, T. Hoare and E. D. Cranston, *Chem. Mater.*, 2017, **29**, 4609–4631.
- 53 O. A. Madyan, M. Fan, L. Feo and D. Hui, *Composites, Part B*, 2016, **102**, 29–37.
- 54 International Union of Pure and Applied Chemistry, *IUPAC Compendium of Chemical Terminology (Gold Book), Version 2.3.3*, Blackwell Publishing, Oxford, 2014.
- 55 P. Innocenzi, *The Sol to Gel Transition*, Springer, Cham-Switzerland, 2016.
- 56 A. Stojanovic and M. M. Koebel, in *Proceedings of CISBAT 2015 International Conference on Future Buildings and Districts - Sustainability from Nano to Urban Scale - Vol. I*, ed. J.-L. Scartezzini, EPFL Solar Energy and Building Physics Laboratory, Lausanne, 2015, pp. 27–32.
- 57 Z. Shao, X. He, Z. Niu, T. Huang, X. Cheng and Y. Zhang, *Mater. Chem. Phys.*, 2015, **162**, 346–353.
- 58 A. C. Pierre and G. M. Pajonk, *Chem. Rev.*, 2002, **102**, 4243–4265.
- 59 C. J. Brinker and G. W. Scherer, *Sol-Gel Science, The Physics and Chemistry of Sol-Gel Processing*, Academic Press, San Diego, 1990.
- 60 V. G. Parale, K. Y. Lee and H. H. Park, *J. Korean Ceram. Soc.*, 2017, **54**, 184–199.
- 61 S. A. Mahadik, F. Pedraza, V. G. Parale and H. H. Park, *J. Non-Cryst. Solids*, 2016, **453**, 164–171.
- 62 V. G. Parale, W. Han, H. N. R. Jung, K. Y. Lee and H. H. Park, *Solid State Sci.*, 2018, **75**, 63–70.
- 63 Y.-L. Han, in *Aerospace Materials Handbook*, ed. S. Zhang and D. Zhao, CRC Press, Boca Raton, 2013, pp. 699–743.
- 64 R. K. Iler, *The Chemistry of Silica—Solubility, Polymerization, Colloid and Surface Properties, and Biochemistry*, John Wiley & Sons, Inc., Hoboken, 1979.
- 65 J. Fricke and A. Emmerling, in *Chemistry, Spectroscopy and Applications of Sol-Gel Glasses*, ed. R. Reisfeld and C. K. Jørgensen, Springer-Verlag, Heidelberg, 1992, pp. 37–87.
- 66 L. Kocon, F. Despetis and J. Phalippou, *J. Non-Cryst. Solids*, 1998, **225**, 96–100.
- 67 A. M. Anderson and M. K. Carroll, in *Aerogels Handbook*, ed. M. A. Aegerter, N. Leventis and M. M. Koebel, Springer Science+Business Media, New York, 2011, pp. 47–74.
- 68 D. J. Boday, B. Muriithi, R. J. Stover and D. A. Loy, *J. Non-Cryst. Solids*, 2012, **358**, 1575–1580.
- 69 X. Lu, P. Wang, M. C. Arduini-Schuster, J. Kuhn, D. Büttner, O. Nilsson, U. Heinemann and J. Fricke, *J. Non-Cryst. Solids*, 1992, **145**, 207–210.
- 70 J. Groß, J. Fricke and L. W. Hrubesh, *J. Acoust. Soc. Am.*, 1992, **91**, 2004–2006.
- 71 A. M. Buckley and M. Greenblatt, *J. Chem. Educ.*, 1994, **71**, 599–602.
- 72 M.-H. Sun, L.-H. Chen and B.-L. Su, in *The Sol-Gel Handbook, Volume 2: Characterization and Properties of Sol-Gel Materials*, ed. D. Levy and M. Zayat, Wiley-VHC, Weinheim, 2015, pp. 987–1030.
- 73 J. Phalippou, T. Woignier and M. Prassas, *J. Mater. Sci.*, 1990, **25**, 3111–3117.
- 74 H. Maleki, *Chem. Eng. J.*, 2016, **300**, 98–118.
- 75 P. B. Wagh, R. Begag, G. M. Pajonk, A. V. Rao and D. Haranath, *Mater. Chem. Phys.*, 1999, **57**, 214–218.
- 76 L. Durães, M. Ochoa, N. Rocha, R. Patrício, N. Duarte, V. Redondo and A. Portugal, *J. Nanosci. Nanotechnol.*, 2012, **12**, 6828–6834.
- 77 N. Leventis and H. Lu, in *Aerogels Handbook*, ed. M. A. Aegerter, N. Leventis and M. M. Koebel, Springer Science+Business Media, New York, 2011, pp. 251–285.
- 78 A. Bisson, A. Rigacci, D. Lecomte, E. Rodier and P. Achard, *Drying Technol.*, 2003, **21**, 593–628.
- 79 R. Trifu, G. L. Gould, K. Qassim and J. L. Clark, in *Engineering, Construction, and Operations in Challenging Environments: Earth and Space 2004*, ed. R. B. Malla and A. Maji, ASCE, Texas, 2004, pp. 976–982.
- 80 S. Zhao, M. S. Manic, F. Ruiz-Gonzalez and M. M. Koebel, in *The Sol-Gel Handbook, Volume 1: Synthesis and Processing*, ed. D. Levy and M. Zayat, Wiley-VHC, Weinheim, 2015, pp. 519–574.
- 81 U. Schubert, in *The Sol-Gel Handbook: Part One Sol-Gel Chemistry and Methods*, ed. D. Levy and M. Zayat, Wiley-VHC, Weinheim, 2015, pp. 3–27.
- 82 M. Shahzamani, R. Bagheri, M. Masoomi, M. Haghgoos and A. Dourani, *J. Non-Cryst. Solids*, 2017, **460**, 119–124.
- 83 G. Markevicius, R. Ladj, P. Niemeyer, T. Budtova and A. Rigacci, *J. Mater. Sci.*, 2016, **52**, 2210–2221.
- 84 R. G. Martinez, E. Goiti, G. Reichenauer, S. Zhao, M. M. Koebel and A. Barrio, *Energy Build.*, 2016, **128**, 111–118.
- 85 Y. Jiang, J. Feng and J. Feng, *J. Sol-Gel Sci. Technol.*, 2017, **83**, 64–71.
- 86 J. Laskowski, B. Milow and L. Ratke, *J. Non-Cryst. Solids*, 2016, **441**, 42–48.
- 87 D. Ciftci, A. Ubeyitogullari, R. R. Huerta, O. N. Ciftci, R. A. Flores and M. D. A. Saldaña, *J. Supercrit. Fluids*, 2017, **127**, 137–145.
- 88 S. S. Kistler, *Nature*, 1931, 741.
- 89 P. H. Tewari, A. J. Hunt and K. D. Lofftus, *Mater. Lett.*, 1985, **3**, 363–367.

- 90 R. T. Toledo, *Fundamentals of Food Process Engineering*, Springer Science+Business Media, New York, 3rd edn, 2007.
- 91 A. White, D. Burns and T. W. Christensen, *J. Biotechnol.*, 2006, **123**, 504–515.
- 92 B. M. Gauthier, S. D. Bakrania, A. M. Anderson and M. K. Carroll, *J. Non-Cryst. Solids*, 2004, **350**, 238–243.
- 93 J. F. Poco, P. R. Coronado, R. W. Pekala and L. W. Hrubesh, *Mater. Res. Soc. Symp. Proc.*, 1996, **431**, 297–302.
- 94 Method and device for fabricating aerogels and aerogel monoliths obtained thereby, *US Pat.* 7384988B2, 2008.
- 95 A. M. Anderson, C. W. Wattlely and M. K. Carroll, *J. Non-Cryst. Solids*, 2009, **355**, 101–108.
- 96 M. V. Dinu and E. S. Dragan, in *Hydrogels Recent Advances*, ed. V. K. Thakur and M. K. Thakur, Singapore, 2018, pp. 51–85.
- 97 M. A. Aegerter, N. Leventis and M. M. Koebel, in *Aerogels Handbook*, ed. M. A. Aegerter, N. Leventis and M. M. Koebel, Springer Science+Business Media, New York, 2011, pp. 893–916.
- 98 Y. Wang, M. D. Gawryla and D. A. Schiraldi, *J. Appl. Polym. Sci.*, 2013, **129**, 1637–1641.
- 99 O. A. Madyan, M. Fan, L. Feo and D. Hui, *Composites, Part B*, 2016, **98**, 314–329.
- 100 L. Wang, L. Cui, M. Sánchez-Soto, W. Shou, Z. Xia and Y. Liu, *Macromol. Mater. Eng.*, 2018, **303**, 1–9.
- 101 L. Wang and M. Sánchez-Soto, *RSC Adv.*, 2015, **5**, 31384–31391.
- 102 L. D. Carlos, R. A. S. Ferreira and V. de Z. Bermudez, in *Hybrid Nanocomposites for Nanotechnology*, ed. L. Merhari, Springer, New York, 2009, pp. 509–586.
- 103 B. E. Yoldas, M. J. Annen and J. Bostaph, *Chem. Mater.*, 2000, **12**, 2475–2484.
- 104 H. Maleki, L. Durães and A. Portugal, *J. Phys. Chem. C*, 2015, **119**, 7689–7703.
- 105 J. L. Gurav, A. V. Rao and U. K. H. Bangi, *J. Alloys Compd.*, 2009, **471**, 296–302.
- 106 R. B. Torres, J. P. Vareda, A. Lamy-Mendes and L. Durães, *J. Supercrit. Fluids*, 2019, **147**, 81–89.
- 107 A. Borba, J. P. Vareda, L. Durães, A. Portugal and P. N. Simões, *New J. Chem.*, 2017, **41**, 6742–6759.
- 108 A. P. Rao, A. V. Rao and G. M. Pajonk, *J. Sol-Gel Sci. Technol.*, 2005, **36**, 285–292.
- 109 K. Kanamori, M. Aizawa, K. Hanada and T. Hanada, *J. Sol-Gel Sci. Technol.*, 2008, **48**, 172–181.
- 110 T. Matias, C. Varino, H. C. de Sousa, M. E. M. Braga, A. Portugal, J. F. J. Coelho and L. Durães, *J. Mater. Sci.*, 2016, **51**, 6781–6792.
- 111 J. P. Vareda, T. Matias, A. C. Fonseca and L. Durães, *J. Sol-Gel Sci. Technol.*, 2016, **80**, 306–317.
- 112 B. N. Nguyen, M. A. B. Meador, A. Medoro, V. Arendt, J. Randall, L. McCorkle and B. Shonkwiler, *ACS Appl. Mater. Interfaces*, 2010, **2**, 1430–1443.
- 113 G. Churu, B. Zupančič, D. Mohite, C. Wisner, H. Luo, I. Emri, C. Sotiriou-Leventis, N. Leventis and H. Lu, *J. Sol-Gel Sci. Technol.*, 2015, **75**, 98–123.
- 114 J. Kehrle, T. Purkait, S. Kaiser, K. N. Raftopoulos, M. Winnacker, T. Ludwig, M. Aghajamali, M. Hanzlik, K. Rodewald, T. Helbich, C. M. Papadakis, J. G. C. Veinot and B. Rieger, *Langmuir*, 2018, **34**, 4888–4896.
- 115 M. M. Koebel, L. Huber, S. Zhao and W. J. Malfait, *J. Sol-Gel Sci. Technol.*, 2016, **79**, 308–318.
- 116 N. Leventis, in *56th International Astronautical Congress*, Fukuoka, Japan, 2005, pp. 1–8.
- 117 H. Lu, H. Luo and N. Leventis, in *Aerogels Handbook*, ed. M. A. Aegerter, N. Leventis and M. M. Koebel, Springer Science+Business Media, New York, 2011, pp. 499–581.
- 118 H. Li, L. Song, Y. Fu, Y. Wei, R. Li and H. Liu, *Compos. Sci. Technol.*, 2017, **138**, 169–178.
- 119 Y. Liao, H. Wu, Y. Ding, S. Yin, M. Wang and A. Cao, *J. Sol-Gel Sci. Technol.*, 2012, **63**, 445–456.
- 120 H. Wu, Y. Liao, Y. Ding, H. Wang, C. Peng and S. Yin, *Heat Transfer Eng.*, 2014, **35**, 1061–1070.
- 121 Z. Li, X. Cheng, S. He, X. Shi, L. Gong and H. Zhang, *Composites, Part A*, 2016, **84**, 316–325.
- 122 S. M. Jones and J. Sakamoto, in *Aerogels Handbook*, ed. M. A. Aegerter and M. M. Koebel, Springer Science+Business Media, New York, 2011, pp. 721–746.
- 123 J. Phalippou, T. Woignier and R. Rogier, *J. Phys., Colloq.*, 1989, **24**, C4-191–C4-196.
- 124 E. Hümmer, X. Lu, T. Rettelbach and J. Fricke, *J. Non-Cryst. Solids*, 1992, **145**, 211–216.
- 125 J. C. H. Wong, H. Kaymak, P. Tingaut, S. Brunner and M. M. Koebel, *Microporous Mesoporous Mater.*, 2015, **217**, 150–158.
- 126 Z. Yu and D. Liang, *Chem. Eng. Trans.*, 2016, **55**, 307–312.
- 127 C. Siligardi, P. Miselli, E. Francia and M. Lassinanti Gualtieri, *Energy Build.*, 2017, **138**, 80–87.
- 128 S. Sattari, R. Lotfi and V. Baharmast, in *Proceedings of the 3rd IASME/WSEAS International Conference on Energy & Environment*, ed. S. Point, World Scientific and Engineering Academy and Society, Wisconsin, 2008, pp. 118–123.
- 129 Aerocoins Project, *Composite/Hybrid Nanomaterials for Cost-Effective Building Super Insulation Systems*, 2011, vol. E2B CASES.
- 130 C. J. Chen, *Physics of Solar Energy*, John Wiley & Sons, Inc., New Jersey, 2011.
- 131 H.-P. Ebert, in *Aerogels Handbook*, ed. M. A. Aegerter, N. Leventis and M. M. Koebel, Springer Science+Business Media, New York, 2011, pp. 537–564.
- 132 B. P. Jelle, R. Baetens and A. Gustavsen, in *The Sol-Gel Handbook, Volume 3: Application of Sol-Gel Materials*, ed. D. Levy and M. Zayat, Wiley-VHC, Washington, D.C., 2015, pp. 1385–1412.
- 133 J. Wang, J. Kuhn and X. Lu, *J. Non-Cryst. Solids*, 1995, **186**, 296–300.
- 134 L. Durães, H. Maleki, J. P. Vareda, A. Lamy-Mendes and A. Portugal, *MRS Adv.*, 2017, **2**, 3511–3519.
- 135 G. Lu, X. D. Wang, Y. Y. Duan and X. W. Li, *J. Non-Cryst. Solids*, 2011, **357**, 3822–3829.
- 136 G. Wei, Y. Liu, X. Zhang, F. Yu and X. Du, *Int. J. Heat Mass Transfer*, 2011, **54**, 2355–2366.
- 137 J. Fricke, P. Wang and U. Heinemann, *Int. J. Heat Mass Transfer*, 1992, **35**, 2305–2309.

- 138 G. Hayase, K. Nonomura, K. Kanamori, A. Maeno, H. Kaji and K. Nakanishi, *Chem. Mater.*, 2016, **28**, 3237–3240.
- 139 M. Venkataraman, R. Mishra, T. M. Kotresh, J. Militky and H. Jamshaid, *Text. Prog.*, 2016, **48**, 55–118.
- 140 M. Koebel, A. Rigacci and P. Achard, *J. Sol-Gel Sci. Technol.*, 2012, **63**, 315–339.
- 141 G. S. Campbell and J. M. Norman, *An Introduction to Environmental Biophysics*, Springer-Verlag, New York, 2nd edn, 1998.
- 142 R. Caps, H. P. Ebert, M. C. Arduini-Schuster and J. Fricke, in *Thermal Conductivity 22*, ed. T. W. Tong, Technomic, Lancaster, PA, 1994, pp. 725–735.
- 143 Y. Bayazitoglu and U. B. Sathuvalli, in *The Engineering-Handbook*, ed. R. C. Dorf, CRC Press, Boca Raton, 1998, p. 49:1–49:28.
- 144 M. F. Modest, *Radiative Heat Transfer*, Academic Press, San Diego, 2003.
- 145 S. Jennings, *J. Aerosol Sci.*, 1988, **19**, 159–166.
- 146 R. P. Schwarzenbach, P. M. G. And and D. M. Imboden, *Environmental Organic Chemistry*, John Wiley & Sons Inc., Hoboken, 2nd edn, 2003.
- 147 B. Notario, J. Pinto and M. A. Rodriguez-Perez, *Prog. Mater. Sci.*, 2016, **78–79**, 93–139.
- 148 J. Fricke, M. C. Arduini-Schuster, D. Biittner, H. P. Ebert, U. Heinemann, J. Hetfleisch, E. Hummer, J. Kuhn and X. Lu, in *Proceedings of the Twenty-First International Thermal Conductivity Conference*, ed. C. J. Cremers and H. A. Fine, Plenum, New York, 1990, pp. 235–245.
- 149 J. Fricke and R. Caps, in *Aerogels - Proceedings of the First International Symposium, 1985, Würzburg*, ed. J. Fricke, Springer-Verlag, Berlin, 1986, pp. 110–115.
- 150 J.-J. Zhao, Y.-Y. Duan, X.-D. Wang and B.-X. Wang, *Int. J. Heat Mass Transfer*, 2012, **55**, 5196–5204.
- 151 T. Woignier, J. Primera, A. Alaoui, P. Etienne, F. Despestis and S. Calas-Etienne, *Gels*, 2015, **1**, 256–275.
- 152 Z. Zhihua, S. Jun, N. Xingyuan, L. Yang, W. Jichao, W. Guangming, Z. Bin, W. Guoqing, W. Peiqing, W. Qingfeng and N. Xixian, in *2008 2nd IEEE International Nanoelectronics Conference, INEC 2008*, Shanghai, 2008, pp. 371–374.
- 153 A. Karout, P. Buisson, A. Perrard and A. C. Pierre, *J. Sol-Gel Sci. Technol.*, 2005, **36**, 163–171.
- 154 Z. Zhang, J. Shen, X. Ni, G. Wu, B. Zhou, M. Yang, X. Gu, M. Qian and Y. Wu, *J. Macromol. Sci., Part A: Pure Appl. Chem.*, 2006, **43**, 1663–1670.
- 155 S. Zhao, W. J. Malfait, A. Demilecamps, Y. Zhang, S. Brunner, L. Huber, P. Tingaut, A. Rigacci, T. Budtova and M. M. Koebel, *Angew. Chem., Int. Ed.*, 2015, **54**, 14282–14286.
- 156 A. Katti, N. Shimpri, S. Roy, H. Lu, E. F. Fabrizio, A. Dass, L. A. Capadona and N. Leventis, *Chem. Mater.*, 2006, **18**, 285–296.
- 157 X. Huang, T. Iizuka, P. Jiang, Y. Ohki and T. Tanaka, *J. Phys. Chem. C*, 2012, **116**, 13629–13639.
- 158 A. Du, B. Zhou, Z. Zhang and J. Shen, *Materials*, 2013, **6**, 941–968.
- 159 M. Li, H. Jiang, D. Xu and Y. Yang, *J. Sol-Gel Sci. Technol.*, 2017, **83**, 72–80.
- 160 Y. Si, J. Yu, X. Tang, J. Ge and B. Ding, *Nat. Commun.*, 2014, **5**, 1–9.
- 161 J. Wang, Y. Wei, W. He and X. Zhang, *RSC Adv.*, 2014, **4**, 51146–51155.
- 162 I. Smirnova and P. Gurikov, *J. Supercrit. Fluids*, 2018, **134**, 228–233.
- 163 Z. Deng, J. Wang, A. Wu, J. Shen and B. Zhou, *J. Non-Cryst. Solids*, 1998, **225**, 101–104.
- 164 X. Li, Q. Wang, H. Li, H. Ji, X. Sun and J. He, *J. Sol-Gel Sci. Technol.*, 2013, **67**, 646–653.
- 165 B. Coffman, J. Fesmire, S. White, G. Gould and S. Augustynowicz, in *Advances in Cryogenic Engineering, Vols 55A and 55B*, ed. J. Weisend, J. Barclay, S. Breon, J. Demko, M. DiPirro, J. Kelley, P. Kittel, A. Klebaner, J. Marquardt, G. Nellis, T. Peterson, J. Pfotenhauer, S. VanSciver, M. Zagarola and A. Zeller, American Institute of Physics, Melville, New York, 2010, pp. 913–920.
- 166 L. Li, B. Yalcin, B. N. Nguyen, M. A. B. Meador and M. Cakmak, *ACS Appl. Mater. Interfaces*, 2009, **1**, 2491–2501.
- 167 Z. Li, L. Gong, X. Cheng, S. He, C. Li and H. Zhang, *Mater. Des.*, 2016, **99**, 349–355.
- 168 C. Li, X. Cheng, Z. Li, Y. Pan, Y. Huang and L. Gong, *J. Non-Cryst. Solids*, 2017, **457**, 52–59.
- 169 S. Motahari, H. Javadi and A. Motahari, *J. Mater. Civ. Eng.*, 2015, **27**, 1–6.
- 170 E. Ul Haq, S. F. A. Zaidi, M. Zubair, M. R. Abdul Karim, S. K. Padmanabhan and A. Licciulli, *Energy Build.*, 2017, **151**, 494–500.
- 171 X. Wang, J. Yu, G. Sun and B. Ding, *Mater. Today*, 2016, **19**, 403–414.
- 172 H. Wu, Y. Chen, Q. Chen, Y. Ding, X. Zhou and H. Gao, *J. Nanomater.*, 2013, **2013**, 1–8.
- 173 S. Batra, W. Zhao, B. Yalcin and M. Cakmak, in *Roll-to-Roll Manufacturing: Process Elements and Recent Advances*, ed. J. Greener, G. Pearson and M. Cakmak, John Wiley & Sons, Inc., Hoboken, 2018.
- 174 Z. Mazrouei-Sebdani, A. Khoddami, H. Hadadzadeh and M. Zarrebini, *RSC Adv.*, 2015, **5**, 12830–12842.
- 175 U. K. H. Bangi, M. S. Kavale, S. Baek and H.-H. Park, *J. Sol-Gel Sci. Technol.*, 2012, **62**, 201–207.
- 176 S. Y. Fu and B. Lauke, *Compos. Sci. Technol.*, 1996, **56**, 1179–1190.
- 177 S.-C. Lee and G. R. Cunningham, *J. Thermophys. Heat Transfer*, 2000, **14**, 121–136.
- 178 J. J. Zhao, Y. Y. Duan, X. D. Wang and B. X. Wang, *J. Non-Cryst. Solids*, 2012, **358**, 1303–1312.
- 179 S. Lyu, X. Yang, D. Shi, H. Qi, X. Jing and S. Li, *Sci. China Technol. Sci.*, 2017, **60**, 1681–1691.
- 180 H.-D. Achtsnit, in *Aerogels - Proceedings of the First International Symposium, 1985, Würzburg*, ed. J. Fricke, Springer-Verlag, Berlin, 1986, pp. 76–81.
- 181 K. K. Chawla, *Composite Materials, Science and Engineering*, Springer Science+Business Media, New York, 3rd edn, 2012.

- 182 A. R. Bunsell and M.-H. Berger, in *High-performance fibres*, ed. J. W. S. Hearle, CRC Press, Boca Raton, 2001, pp. 239–258.
- 183 G. Schuck, W. Dietrich and J. Fricke, in *Aerogels - Proceedings of the First International Symposium, 1985, Würzburg*, Springer-Verlag, Berlin, 1986, pp. 148–153.
- 184 A. R. Horrocks, H. Eichhorn, H. Schwaenke, N. Saville and C. Thomas, in *High-performance fibres*, ed. J. W. S. Hearle, CRC Press, Boca Raton, 2001, pp. 281–324.
- 185 S. Rebouillat, in *High-performance fibres*, ed. J. W. S. Hearle, CRC Press, Boca Raton, 2001, pp. 23–61.
- 186 X. Hou, R. Zhang and D. Fang, *Scr. Mater.*, 2018, **143**, 113–116.
- 187 X. Hou, R. Zhang and D. Fang, *Ceram. Int.*, 2017, **43**, 9547–9551.
- 188 Y. Duan, S. C. Jana, B. Lama and M. P. Espe, *Langmuir*, 2013, **29**, 6156–6165.
- 189 T.-Y. Wei, T.-F. Chang, S.-Y. Lu and Y.-C. Chang, *J. Am. Ceram. Soc.*, 2007, **90**, 2003–2007.
- 190 H. Wang, X. Zhang, N. Wang, Y. Li, X. Feng, Y. Huang, C. Zhao, Z. Liu, M. Fang, G. Ou, H. Gao, X. Li and H. Wu, *Sci. Adv.*, 2017, **3**, 1–10.
- 191 J. Cai, S. Liu, J. Feng, S. Kimura, M. Wada, S. Kuga and L. Zhang, *Angew. Chem., Int. Ed.*, 2012, **51**, 2076–2079.
- 192 E. Rezaei and J. Moghaddas, *Adv. Mater. Lett.*, 2016, **7**, 296–301.
- 193 M. O. Adebajo, R. L. Frost, J. T. Klopogge, O. Carmody and S. Kokot, *J. Porous Mater.*, 2003, **10**, 159–170.
- 194 J. R. Jones, in *The Sol-Gel Handbook, Volume 3: Application of Sol-Gel Materials*, ed. D. Levy and M. Zayat, Wiley-VHC, Weinheim, 2015, pp. 1345–1369.
- 195 G. Markevicius, P. Niemeyer, R. Ladj, J. Jaxel, T. Budtova and E. Al, in *3rd International Seminar on Aerogels: Properties-Manufacture-Applications*, Sophia Antipolis, 2016.
- 196 E. C. Y. Ling and D. L. A. A. Majid, in *Proceedings of Mechanical Engineering Research Day 2017 (MERD)*, ed. M. F. Bin Abdollah, T. B. Tuan, M. A. Salim, M. Z. Akop, R. Ismail and H. Musa, Centre for Advanced Research on Energy, Melaka, 2017, pp. 413–414.
- 197 M. G. Sedighi, M. N. Boone, J. L. Fife, S. Zhao, M. M. Koebel, T. Zimmermann and P. Tingaut, *Compos. Sci. Technol.*, 2016, **124**, 71–80.
- 198 Z. Zhihua, S. Jun and N. Xingyuan, in *2008 2nd IEEE International Nanoelectronics Conference, INEC 2008*, Shanghai, 2008, pp. 366–370.
- 199 A. B. Reddy, G. S. M. Reddy, V. Sivanjineyulu, J. Jayaramudu, K. Varaprasad and E. R. Sadiku, in *Design and Applications of Nanostructured Polymer Blends and Nanocomposite Systems*, ed. S. Thomas, R. Shanks and S. Chandrasekharakurup, Elsevier, Waltham, 2016, pp. 385–411.
- 200 L. Daelemans, A. Cohades, T. Meireman, J. Beckx, S. Spronk, M. Kersemans, I. De Baere, H. Rahier, V. Michaud, W. Van Paepegem and K. De Clerck, *Mater. Des.*, 2018, **141**, 170–184.
- 201 S. M. Burkinshaw, *Physico-Chemical Aspects of Textile Coloration*, Wiley, Bradford, 2016.
- 202 S. Ramakrishna, K. Fujihara, W. E. Teo, T. Yong, Z. Ma and R. Ramaseshan, *Mater. Today*, 2006, **9**, 40–50.
- 203 M. Venkataraman, R. Mishra, J. Militky, J. Marek, K. Kucerova, J. Yao, G. Zhu, J. Militky, J. Marek, K. Kucerova, J. Yao and G. Zhu, *J. Fiber Bioeng. Inf.*, 2017, **10**, 187–199.
- 204 S. Thenmozhi, N. Dharmaraj, K. Kadirvelu and H. Y. Kim, *Mater. Sci. Eng., B*, 2017, **217**, 36–48.
- 205 F. Lai, Y. Huang, L. Zuo, H. Gu, Y.-E. Miao and T. Liu, *J. Mater. Chem. A*, 2016, **4**, 15861–15869.
- 206 H. G. Karian, in *Handbook of Polypropylene and Polypropylene Composites*, ed. H. G. Karian, Marcel Dekker, Inc., New York, 2nd revis edn, 2003, pp. 421–463.
- 207 M. Schwartz, *Encyclopedia of Materials, Parts and Finishes*, CRC Press LLC, Boca Raton, 2nd edn, 2002.
- 208 S. Motahari and A. Abolghasemi, *J. Mater. Civ. Eng.*, 2015, **27**, 1–7.
- 209 H. Maleki, L. Durães and A. Portugal, *J. Mater. Chem. A*, 2015, **3**, 1594–1600.
- 210 Y. Zhang, J. Zhu, H. Ren, Y. Bi, X. Shi, B. Wang and L. Zhang, *J. Porous Mater.*, 2017, **24**, 1303–1307.
- 211 T. Woignier and J. Phalippou, *J. Non-Cryst. Solids*, 1988, **100**, 404–408.
- 212 Y. Jiang, J. Feng, J. Feng and C. Shi, in *Advances in High Temperature Ceramic Matrix Composites and Materials for Sustainable Development*, ed. M. Singh, T. Ohji, S. Dong, D. Koch, K. Shimamura, B. Clauss, B. Heidenreich and J. Akedo, The American Ceramic Society, Hoboken, 2017, vol. 263, pp. 333–339.
- 213 Q. F. Gao, J. Feng, C. R. Zhang, J. Z. Feng, W. Wu and Y. G. Jiang, *Adv. Mater. Res.*, 2010, **105–106**, 94–99.
- 214 A. Liu, L. Medina and L. A. Berglund, *ACS Appl. Mater. Interfaces*, 2017, **9**, 6453–6461.
- 215 D. Shi, Y. Sun, J. Feng, X. Yang, S. Han, C. Mi, Y. Jiang and H. Qi, *Mater. Sci. Eng., A*, 2013, **585**, 25–31.
- 216 J. J. Koravos, T. M. Miller, J. E. Fesmire and B. E. Coffman, *AIP Conf. Proc.*, 2010, **1218**, 921–927.
- 217 X. Yang, Y. Sun, D. Shi and J. Liu, *Mater. Sci. Eng., A*, 2011, **528**, 4830–4836.
- 218 B. Yuan, S. Ding, D. Wang, G. Wang and H. Li, *Mater. Lett.*, 2012, **75**, 204–206.
- 219 J. A. Diaz, Z. Ye, X. Wu, A. L. Moore, R. J. Moon, A. Martini, D. J. Boday and J. P. Youngblood, *Biomacromolecules*, 2014, **15**, 4096–4101.
- 220 Y. Zhao, G. H. Tang and M. Du, *Int. J. Therm. Sci.*, 2015, **89**, 110–120.
- 221 R. Saliger, T. Heinrich, T. Gleissner and J. Fricke, *J. Non-Cryst. Solids*, 1995, **186**, 113–117.
- 222 F. I. Hurwitz, M. Gallagher, T. C. Olin, M. K. Shave, M. A. Ittes, K. N. Olafson, M. G. Fields, H. Guo and R. B. Rogers, *Int. J. Appl. Glass Sci.*, 2014, **5**, 276–286.
- 223 X. Lu, R. Caps, J. Fricke, C. T. Alviso and R. W. Pekala, *J. Non-Cryst. Solids*, 1995, **188**, 226–234.
- 224 H. Liu, X. Xia, X. Xie, Q. Ai and D. Li, *Int. J. Therm. Sci.*, 2017, **121**, 192–203.

- 225 V. G. Parale, H. N. R. Jung, W. Han, K. Y. Lee, D. B. Mahadik, H. H. Cho and H. H. Park, *J. Alloys Compd.*, 2017, **727**, 871–878.
- 226 J. Fricke, D. Büttner, R. Caps, J. Gross and O. Nilsson, in *Materials, Testing and Applications*, ed. D. L. McElroy and J. F. Kimpflen, American Society for Testing and Materials, Philadelphia, 1990, pp. 66–78.
- 227 J. Kuhn, T. Gleissner, M. C. Arduini-Schuster, S. Korder and J. Fricke, *J. Non-Cryst. Solids*, 1995, **186**, 291–295.
- 228 Y. Wang, B. Wang and D. Zheng, in *Advances in High Temperature Ceramic Matrix Composites and Materials for Sustainable Development*, ed. M. Singh, S. Ohji, T. Dong, D. Koch, K. Shimamura, B. Clauss, B. Heidenreich and J. Akedo, The American Ceramic Society, Hoboken, 2017, vol. 263, pp. 19–25.
- 229 G. H. Tang, Y. Zhao and J. F. Guo, *Int. J. Heat Mass Transfer*, 2016, **99**, 192–200.
- 230 G. Liu and Y. Liu, in *Proceedings of the 2016 International Conference on Civil, Transportation and Environment*, Atlantis Press, Guangzhou, 2016, vol. 5, pp. 1300–1304.
- 231 N. L. McKay, T. Timusk and B. Farnworth, *J. Appl. Phys.*, 1984, **55**, 4064–4071.
- 232 A. Ślosarczyk, *J. Sol-Gel Sci. Technol.*, 2017, **84**, 16–22.
- 233 M. Gronauer, A. Kadur and J. Fricke, in *Aerogels - Proceedings of the First International Symposium, 1985, Würzburg*, ed. J. Fricke, Springer-Verlag, Berlin, 1985, pp. 167–173.
- 234 G. Chauve, C. Fraschini and B. Jean, in *Handbook of Green Materials*, eds. K. Oksman, A. P. Mathew, A. Bismarck, O. Rojas and M. Sain, World Scientific, Singapore, 2014, pp. 73–87.
- 235 Z. Lu, Z. Yuan, Q. Liu, Z. Hu, F. Xie and M. Zhu, *Mater. Sci. Eng., A*, 2015, **625**, 278–287.
- 236 A. R. Bunsell, in *Handbook of Properties of Textile and Technical Fibres*, ed. A. R. Bunsell, Elsevier Ltd., Cambridge, 2nd edn, 2018, pp. 1–20.
- 237 S. Lee and G. R. Cunningham, in *7th AIAA/ASME Joint Thermophysics and Heat Transfer Conference*, AIAA, Albuquerque, 1998, p. 2840.
- 238 J. Fu, C. He, J. Huang, Z. Chen and S. Wang, *RSC Adv.*, 2016, **6**, 100326–100333.
- 239 Method and apparatus for capacitive deionization, electrochemical purification, and regeneration of electrodes, *US pat.* 005425858A, 1995.
- 240 J. C. Farmer, J. H. Richardson, D. V. Fix, S. L. Thomsom and S. C. May, *Desalination with Carbon Aerogel Electrodes*, 1996, vol. UCRL-ID-12.
- 241 S. Zhao, Z. Zhang, G. Sèbe, R. Wu, R. V. Rivera Virtudazo, P. Tingaut and M. M. Koebel, *Adv. Funct. Mater.*, 2015, **25**, 2326–2334.
- 242 T. Zhou, X. Cheng, Y. Pan, C. Li, L. Gong and H. Zhang, *Appl. Surf. Sci.*, 2018, **437**, 321–328.
- 243 J. He, X. Li, D. Su, H. Ji and X. J. Wang, *J. Eur. Ceram. Soc.*, 2016, **36**, 1487–1493.
- 244 Y. Zhang, J. Dang, X. Su and H. Jin, *Desalin. Water Treat.*, 2016, **57**, 17463–17472.
- 245 M. Shi, C. Tang, X. Yang, J. Zhou, F. Jia, Y. Han and Z. Li, *RSC Adv.*, 2017, **7**, 4039–4045.
- 246 G. Hayase, K. Kanamori and K. Nakanishi, *J. Mater. Chem.*, 2011, **21**, 17077–17079.
- 247 G. Hayase, K. Kanamori, M. Fukuchi, H. Kaji and K. Nakanishi, *Angew. Chem., Int. Ed.*, 2013, **52**, 1986–1989.
- 248 M. Y. Baktash and H. Bagheri, *Microchim. Acta*, 2017, **184**, 2151–2156.
- 249 A. P. Olalekan, A. O. Dada and O. A. Adesina, *J. Encapsulation Adsorpt. Sci.*, 2014, **4**, 122–131.
- 250 W. Wei, L. Chenwei, X. Jimin, Z. Jianjun, L. Xiaomeng and Y. Changhao, *Mater. Sci. Forum*, 2011, **675–677**, 1035–1039.
- 251 D. R. Chen, X. H. Changy and X. L. Jiao, in *The Role of Colloidal Systems in Environmental Protection*, ed. M. Fanun, Elsevier B.V., Amsterdam, 2014, pp. 573–591.
- 252 S. Malakooti, H. G. Churu, A. Lee, T. Xu, H. Luo, N. Xiang, C. Sotiriou-Leventis, N. Leventis and H. Lu, *J. Non-Cryst. Solids*, 2017, **476**, 36–45.
- 253 A. Hao, H. Zhao and J. Y. Chen, *Composites, Part B*, 2013, **54**, 44–51.
- 254 S. Amares, E. Sujatmika, T. W. Hong, R. Durairaj and H. S. H. B. Hamid, *J. Phys.: Conf. Ser.*, 2017, **908**(1), 012005.
- 255 J. F. T. Conroy, B. Hosticka, S. C. Davis, A. N. Smith and P. M. Norris, *Microscale Thermophys. Eng.*, 1999, **3**, 199–215.
- 256 J. Martin, B. Hosticka, C. Lattimer and P. M. Norris, *J. Non-Cryst. Solids*, 2001, **285**, 222–229.
- 257 Y. E. Lee and C. W. Joo, *J. Appl. Polym. Sci.*, 2004, **92**, 2295–2302.
- 258 J. Fricke, *J. Non-Cryst. Solids*, 1992, **147–148**, 356–362.
- 259 J. Groß and J. Fricke, *Nanostruct. Mater.*, 1995, **6**, 905–908.
- 260 N. Leventis, *Acc. Chem. Res.*, 2007, **40**, 874–884.
- 261 K. W. Oh, D. K. Kim and S. H. Kim, *Fibers Polym.*, 2009, **10**, 731–737.
- 262 J. Fricke, R. Caps, D. Büttner, U. Heinemann, E. Hümmer and A. Kadur, *Sol. Energy Mater.*, 1987, **16**, 267–274.
- 263 A. Hunt and M. Ayers, *A Brief History of Silica Aerogels*, Lawrence Berkeley Laboratories: Microstructured Materials Group, 2000.
- 264 A. V. Rao, G. M. Pajonk, U. K. H. Bangi, A. P. Rao and M. M. Koebel, in *Aerogels Handbook*, ed. M. A. Aegerter, N. Leventis and M. M. Koebel, Springer Science+Business Media, New York, 2011, pp. 103–124.
- 265 E. Moretti, F. Merli, E. Cuce and C. Buratti, *Energy Procedia*, 2017, **111**, 472–480.
- 266 M. D. W. Grogan, *Aerogel and Fibre Optics*, PhD Thesis, University of Bath, 2010.
- 267 B. Lee, *Opt. Fiber Technol.*, 2003, **9**, 57–79.
- 268 A. Leung, P. Mohana Shankar and R. Mutharasan, in *Optical Fibers Research Advances*, ed. J. C. Schlesinger, Nova Science Publishers, Inc., New York, 2007, pp. 15–49.
- 269 L. Mescia and F. Prudenizano, *Fibers*, 2014, **2**, 1–23.
- 270 J. Dakin, K. Hotate, R. A. Lieberman and M. A. Marcus, in *Handbook of Optoelectronics Vol. II*, ed. J. P. Dakin and R. G. W. Brown, Taylor & Francis Group, LLC, Boca Raton, 2006, pp. 1129–1216.
- 271 P. Lu, L. Men, K. Sooley and Q. Chen, *Appl. Phys. Lett.*, 2009, **94**, 2007–2010.

- 272 C. Holmes, A. Jantzen, A. C. Gray, P. C. Gow, L. G. Carpenter, R. H. S. Bannerman, J. C. Gates and P. G. R. Smith, *Opt. Lett.*, 2018, **43**, 791–794.
- 273 L. Xiao, M. D. W. Grogan, S. G. Leon-Saval, R. Williams, R. England, W. J. Wadsworth and T. A. Birks, *Opt. Lett.*, 2009, **34**, 2724–2726.
- 274 L. Tong, J. Lou, R. R. Gattass, S. He, X. Chen, L. Liu and E. Mazur, *Nano Lett.*, 2005, **5**, 259–262.
- 275 M. L. Nuckols, D. E. Hyde, J. L. Wood-Putnam, J. Giblo, G. J. Caggiano, J. A. Henkener and B. Stinton, in *Proceedings of the American Academy of Underwater Sciences 28th Symposium*, ed. N. Pollock, AAUS, Dauphin Island, 2009, vol. 7, pp. 237–244.
- 276 Y. Epstein and D. S. Moran, *Ind. Health*, 2006, **44**, 388–398.
- 277 L. Jin, K. Hong and K. Yoon, *J. Fiber Bioeng. Inf.*, 2013, **6**, 315–324.
- 278 A. Shaid, L. Wang and R. Padhye, *J. Ind. Text.*, 2016, **45**, 611–625.
- 279 Z. Xiangfa, X. Hanning, F. Jian, Z. Changrui and J. Yonggang, *J. Exp. Nanosci.*, 2012, **7**, 17–26.
- 280 A. Shaid, L. Wang, S. Islam, J. Y. Cai and R. Padhye, *Appl. Therm. Eng.*, 2016, **107**, 602–611.
- 281 P. Buisson and A. C. Pierre, *J. Mol. Catal. B: Enzym.*, 2006, **39**, 77–82.
- 282 S. Nassreddine, A. Karout, M. Lorraine Christ and A. C. Pierre, *Appl. Catal., A*, 2008, **344**, 70–77.
- 283 A. Karout and A. C. Pierre, *J. Sol-Gel Sci. Technol.*, 2009, **52**, 276–286.
- 284 D. B. Mahadik, H. N. R. Jung, W. Han, H. H. Cho and H. H. Park, *Compos. Sci. Technol.*, 2017, **147**, 45–51.
- 285 G. Feng, Z. Li, L. Mi, J. Zheng, X. Feng and W. Chen, *J. Power Sources*, 2018, **376**, 177–183.
- 286 M. Shahzamani, R. Bagheri and M. Masoomi, *J. Non-Cryst. Solids*, 2016, **452**, 325–335.
- 287 L. Vazhayal, S. Talasila, P. Mohamed, A. Azeez and A. Solaiappan, *ACS Appl. Mater. Interfaces*, 2014, **6**, 15664–15774.
- 288 R. P. Patel, N. S. Purohit and A. M. Suthar, *Int. J. ChemTech Res.*, 2009, **1**, 1052–1057.
- 289 W. Jin and J. D. Brennan, *Anal. Chim. Acta*, 2002, **461**, 1–36.
- 290 J. Fu, C. He, S. Wang and Y. Chen, *J. Mater. Sci.*, 2018, **53**, 7072–7082.
- 291 J. Milledge, *Energy Balance and Techno-economic Assessment of Algal Biofuel Production Systems*, PhD Thesis, University of Southampton, 2013.
- 292 S. Zhao, O. Emery, A. Wohlhauser, M. M. Koebel, C. Adlhart and W. J. Malfait, *Mater. Des.*, 2018, **160**, 294–302.
- 293 X. Dong, J. Liu, R. Hao, A. Guo, Z. Hou and M. Liu, *J. Eur. Ceram. Soc.*, 2013, **33**, 3477–3481.
- 294 B. I. O. European Commission, *Aerogels, getting their second wind*, 2015.
- 295 G. Erbach, *EU Climate and Energy Policies Post-2020: Energy Security, Competitiveness and Decarbonisation*, 2014.
- 296 European Parliament, *Off. J. Eur. Union*, 2012, 14/11/2012, pp. 1–56.
- 297 Y. Lei, X. Chen, H. Song, Z. Hu and B. Cao, *Ceram. Int.*, 2017, **43**, 10799–10804.
- 298 B. P. Jelle, *Energy Build.*, 2011, **43**, 2549–2563.
- 299 A. Galatioto, R. Ricciu, T. Salem and E. Kinab, *Energy*, 2019, **176**, 58–66.
- 300 E. Cuce, P. M. Cuce, C. J. Wood and S. B. Riffat, *Renewable Sustainable Energy Rev.*, 2014, **34**, 273–299.
- 301 M. V. Khedkar, S. B. Somvanshi, A. V. Humbe and K. M. Jadhav, *J. Non-Cryst. Solids*, 2019, **511**, 140–146.
- 302 M. Habulin, M. Primožič and Z. Knez, in *Modern Biocatalysis Stereoselective and Environmentally Friendly Reactions*, ed. W.-D. Fessner and T. Anthonsen, Wiley-VHC, Weinheim, 2009, pp. 109–121.
- 303 M. Dowson, M. Grogan, T. Birks, D. Harrison and S. Craig, *Appl. Energy*, 2012, **97**, 396–404.
- 304 F. Ghajeri, Z. Topalian, A. Tasca, S. H. M. Jafri, K. Leifer, P. Norberg and C. Sjöström, *Curr. Opin. Green Sustain. Chem.*, 2018, **12**, 101–109.
- 305 M. Sletnes, B. P. Jelle and B. Risholt, *Energy Procedia*, 2017, **132**, 327–332.
- 306 M. Schuss, U. Pont and A. Mahdavi, *Energy Procedia*, 2017, **132**, 508–513.
- 307 Y. Lei, Z. Hu, B. Cao, X. Chen and H. Song, *Mater. Chem. Phys.*, 2017, **187**, 183–190.
- 308 J. He, H. Zhao, X. Li, D. Su, H. Ji, H. Yu and Z. Hu, *Ceram. Int.*, 2018, **44**, 8742–8748.
- 309 D. H. Sweeney and M. J. Taber, in *Protective Clothing Managing - Thermal Stress*, ed. F. Wang and C. Gao, Elsevier Ltd., Waltham, 2014, pp. 39–69.